USE OF BIO-NANO COMPOSITES AS PROTECTIVE COATING ON NATURAL STONE SURFACES

A Thesis submitted to
The Graduate School of Engineering and Sciences of
İzmir Institute of Technology
In Partial Fulfillment of the Requirements for the Degree of

DOCTOR OF PHILOSOPHY

in Chemical Engineering

by
Yılmaz OCAK

June 2013
İZMİR

We approve the thesis of **Yılmaz OCAK**

Examining Committee Members:

_____

Prof. Dr. Aysun SOFUOĞLU
Department of Chemical Engineering, İzmir Institute of Technology

_____

Prof. Dr. Funda TIHMINLIOĞLU
Department of Chemical Engineering, İzmir Institute of Technology

_____

Assoc. Prof. Dr. Fikret İNAL
Department of Chemical Engineering, İzmir Institute of Technology

_____

Assoc. Prof. Dr. Mustafa Muammer DEMİR
Department of Chemistry, İzmir Institute of Technology

_____

Prof. Dr. Mustafa ODABAŞI
Department of Environmental Engineering, Dokuz Eylul University

09 July 2013

_____

Prof. Dr. Aysun SOFUOĞLU
Supervisor, Department of Chemical Engineering
İzmir Institute of Technology

_____

Prof. Dr. Hasan BÖKE
Co-Supervisor, Department of Architectural Restoration
İzmir Institute of Technology

_____

Prof. Dr. F. Seher CAKICIOĞLU-ÖZKAN
Head of the Department of Chemical Engineering

_____

Prof. Dr. R. Tuğrul SENGER
Dean of the Graduate School of Engineering and Sciences

ACKNOWLEDGEMENTS

I would like to acknowledge the people who have helped to make this work possible. I would like to thank to my advisor Prof. Dr. Aysun SOFUOĞLU, Prof. Dr. Hasan BÖKE, and Prof. Dr. Funda TIHMINLIOĞLU for their recommendations, support, and thoughtful advice. I would also like to thank to committee members Assoc. Prof. Dr. Fikret İNAL, Assoc. Prof. Dr. Mustafa Muammer DEMİR and Prof. Dr. Mustafa ODABAŞI for their valuable discussions and contributions.

In this thesis the support of specialist for the analytical analysis from the Centers (MAM and Environmental R&D) of Iztech is also appreciated.

I am also grateful to IYTE MAM research specialists for their help during my material characterization studies.

I would also like to acknowledge The Scientific and Technical Research Council of Türkiye (TUBİTAK) for financial support to 108M335 project.

I would like to appreciate deeply to all my friends for their friendships.

Finally, I would like to express my heartfelt gratitude to my wife Selcan TURUPCU OCAK and my family Cahide OCAK, İsmet OCAK and Yeliz OCAK for their continuous support, patience, affection, encouragement and eternal love which enabled me to overcome difficulties.

ABSTRACT

USE OF BIO-NANO COMPOSITES AS PROTECTIVE COATING ON NATURAL STONE SURFACES

Historical monuments are important heritages to pass cultural values to next generations. Most of the historical monuments were composed of natural stones like marble. SO_2 and NO_x reacts with marble composed primarily of calcite ($CaCO_3$) is a dry deposition process, gypsum ($CaSO_4.2H_2O$) and nitrocalcite ($Ca(NO_3)_2.4H_2O$) are formed after reaction.

The polylactic acid (PLA), 2, 5 and 7 wt.% montmorillonite (MMT) clay added PLA (PLA/MMT2, PLA/MMT5 and PLA/MMT7) bio-nano composites coated and uncoated surfaces were tested for capillary water absorption, water vapor permeability, color alteration, and surface hydrophobicity regarding the nanofiller concentrations before reaction. Results indicated that the bio-nano composite coatings didn't alter the color of the marble, improved the hydrophobicity and barrier properties of the marbles.

The level of layered silicate delamination in the PLA matrix and structural characterizations of PLA nanocomposite coatings were affected the barrier properties of the composites coatings. The X-ray diffraction (XRD), atomic force microscopy (AFM) and scanning transmission electron microscopy (STEM) analysis pointed out that 5% layered silicates were homogenously dispersed in the polymer matrix, exfoliated structures also were observed in some parts of the polymer matrix and nano particles enhanced the nano-composite coating barrier performance.

The protection capabilities of the bio-nano composite coatings were studied in laboratory setup (include nearly 8 ppm SO_2) and ambient city atmosphere (include nearly 8 ppb SO_2 and 64 ppb NO_2). The PLAMMT5 bio-nano composite showed significant reduction (~5 times) in the crust formation after 180 days SO_2-calcite reaction in laboratory and 9-10 times after 20 months ambient city exposures for outdoor conditions. Bio-nano composites also decreased the kinetic parameters such as rate constant (k_s) and effective diffusivity (D_e) values of the marbles. These results indicated that PLA/MMT bio-nano composite coating seems to be significant promising materials as protective coating agents in reducing the effects of atmospheric pollutants on the marble surfaces.

ÖZET

DOĞAL TAŞ YÜZEYLERİNDE BİYO-NANO KOMPOZİTLERİN KORUYUCU KAPLAMA MALZEMESİ OLARAK KULLANILMASI

Tarihi anıtlar kültürel bilgilerimizi gelecek nesillere taşıyan önemli kültürel miraslarımızdır. Tarihi anıtlar büyük çoğunlukla mermer benzeri doğal taşlardan yapılmıştır. Atmosferde bulunan SO_2 ve NO_x gazları su buharı ile birlikte, mermeri oluşturan kalsit kristalleri ile kuru depolanma yöntemiyle reaksiyona girmekte ve alçı taşı ($CaSO_4.2H_2O$) ve nitro kalsiti ($Ca(NO_3)_2.4H_2O$) oluşturmaktadır.

Bu çalışmada mermerler reaksiyona girmeden önce, polilaktik asit (PLA) biyo-bozunur polimeri ve 2, 5 ve 7% montmorillonit (MMT) kil eklenmiş PLA (PLA/MMT2, PLA/MMT5 ve PLA/MMT7) biyo-nano kompozitleri ile kaplanmış ve kaplanmamış mermer yüzeylerinde kılcal su abrorpsiyonu, su buharı geçirgenliği, yüzey kontak açısı ve renk analizleri yapılmıştır. Yapılan bu analizler sonuçunda, kaplama mazlemelerinin, orjinal mermer renginde önemli bir değişikliğe neden olmadığı, mermer yüzey hidrofobisini ve barrier özelliklerini artırdığı belirlenmiştir.

Katmanlı silikatların, PLA polimer anayapısı içerisinde katmanlarına ayrılma düzeyi ve PLA biyo-nano kompozitlerin yapısal karakterizasyonu, kompozit kaplamanın bariyer performansını etkilemektedir. Bu nedenle, biyo-nano kompozitler, X-ışınlarıkırınımı (XRD), atomsal kuvvet mikroskopisi (AFM) ve taramalı geçirimli elektron mikroskopisi (STEM) analizleri kullanılarak incelendi. Bu çalışmalar sonuçunda, özellikle PLA/MMT5 için katmanlı silikatların polimer anayapı içerisinde homojen olarak dağıldığı, bazı kısımlarda ise eksfoliye oldukları görülmüştür.

Kompozit kaplamaların koruyuculuk kapasiteleri, laboratuvarda (8 ppm SO_2) ve şehir atmosferinde (8 ppb SO_2 and 64 ppb NO_2) araştırılmıştır. Laboratuvarda gerçekleşen 180 günlük SO_2-kalsit reaksiyonu sonunda, PLA/MMT5 kompozitleri bozunma ürünleri oluşumunu azaltmıştır (~5 kat). Dış atmosferde gerçekleştiren çalışmalarda ise 20 ay sonunda bozunma ürünleri azalma oranı 9-10 kata çıkmıştır. kompozit kaplamalar mermer yüzeylerinde reaksiyon hız sabiti (k_s) ve efektif difüzyon (D_e) değerlerini azaltmıştır. Sonuç olarak, PLA/MMT biyo-nano kompozit kaplamaların gelecek vaad eden malzemeler olduğu ve mermer yapıların atmosferik kirleticilere karşı korunmasında önemli bir argüman olarak kullanılabileceği belirlenmiştir.

TABLE OF CONTENTS

LIST OF FIGURES

LIST OF TABLES

CHAPTER 1

INTRODUCTION

Historical monuments are the significant cultural heritages to pass cultural information to the next generations. Most of the historical monuments and buildings were made of natural stones like marble, mainly composed of the calcite ($CaCO_3$). Unfortunately, natural stone monuments are subject to degradation due to negative effects of environmental conditions such as relative humidity, water, temperature changes, and air pollutants. Sulfur dioxide (SO_2) is a well known environmental pollutant and has reactive and corrosive effects on the building materials. In the presence of the water or water vapor (Gauri and Bandyopadhyay, 1999; Böke et al., 2002) SO_2 reacts with calcite crystals on the stone and forms gypsum ($CaSO_4.2H_2O$) as a final sulphation product. Gypsum is a soluble compound, and has occupies more volume than the calcite. Therefore the marble surface is eroded in rain-washed at unsheltered areas and disintegrated at sheltered places (Böke et al., 1999; Gauri and Bandyopadhyay, 1999; Böke and Gauri, 2003). In addition, coexisting presence of SO_2 and NO_2 in the atmosphere leads to reactions with carbonate stones through dry deposition results in crusts formation as a mixture of gypsum and nitrocalcite ($Ca(NO_3)_2.4H_2O$). Presence of NO_2 in the air accelerates the gypsum formation. Since, NO_2 increases the oxidation of SO_2 to sulfur trioxide (SO_3), which reacts with calcite and converts to the gypsum. Gauri and Bandyopadhyay (1999) pointed out that gypsum formation predominates over nitrocalcite formation in the carbonate rocks.

In order to reduce decaying or deterioration of historical monuments, many protection methods were developed to convert the formed gypsum back by using potassium carbonate to calcium carbonate (Skoulikidis and Beloyannis, 1984), and decrease the solubility of calcium carbonate with the addition of some water soluble organic and inorganic compounds (Böke et al. 2002, Böke and Gauri 2003, Thompson et al. 2003). Unfortunately, formed $CaCO_3$ remained in the form of powder on the surface and deformation of stone was not inhibited (Skoulikidis and Beloyannis, 1984). While the use of synthetic polymers such as polyacrylonitrile and polyacrylic acid as coating agents (Gauri et al., 1973; Atlas et al., 1988; Elfving et al., 1994; Striegel et al., 2003; Thompson

et al., 2003) showed short term inhibition on the SO_2-calcite reaction, however, stone degradation increased exponentially in the long term due to water vapor entrapment under the coating. Reduction in the gypsum formation was achieved with 10% reduction (Böke et al., 2002) with decreasing of solubility studies. Calcium carbonate surface was also coated to oppose a resistance to acidic conditions by using anionic surfactants such as phosphate, oxalate ($C_2O_4^{-2}$), oleate ($C_{17}H_{33}COO^-$) (Böke and Gauri, 2003). When these solutions were used on the calcium carbonate surfaces, calcium oxalate, oleate or phosphate layer formed on the surface and formation of reaction products on the surface were reduced approximately 15% (Böke and Gauri, 2003). Inferentially, these studies either enhanced the gypsum formation or did not supply enough protection on the stone surfaces. On the other hand, use of synthetic polymers created more problems in terms of renewability of the coating. Polymer adhesion on the surfaces did not allow easy removal for reapplication. Mechanical removal requirement led to extra physical damages on the surface.

Some biodegradable polymers such as polyhydroxybutyrate (PHB), high and low molecular weight poly-L-lactide (PLA) were used as coating agents to slow down SO_2-calcite reaction on the marble surfaces (Ocak et al., 2009). The researchers indicated that the use of high molecular weight PLA polymers on marble surfaces provided significant protection up to 60% for 90 days of exposure to SO_2 and water vapor (Ocak et al., 2009). It could be said that high molecular weight PLA polymer can be used as a promising protective coating agent for reduction of gypsum formation on marble surfaces in polluted environment.

Nanoparticle addition to the polymer matrices has been gaining attention due to improvements on barrier, optical, electronic, magnetic, catalytic, mechanical, chemical and tribological properties of the coating materials. Especially silicone containing polymer matrices (Zielecka and Bujnowska, 2006), nano silica added flouroalkylsilane coatings (Su et al., 2006), silica added Polymethyl methacrylate (PMMA) and perflouroether (PFPE) polymer matrices (Manoudis et al., 2007), nano silica added siloxanes (Manoudis et al., 2009), organoclay added epoxy and silane (Christopher et al., 2008) coatings have been studied to investigate the additional effects of nano particles on the polymers for the protection of the surfaces. The results showed that nanoparticle addition into polymer matrix increased the surface hydrophobicity and decreased the water action effects on coated surfaces.

International Conservation Community of Historic Monuments and Building suggests that the coating agents applied on the stones surfaces should not change their transparency and they should be reversible which allows the renewability of coatings. Reversibility is defined as a vital condition for conservation products since the applied treatment applied to an object intended to last for a while and should allow renovation without leaving any damage on the original surfaces. Reversibility is inherently available for biodegradable polymers. Therefore the main purpose of this study was designed to investigate the effectiveness of clay nanoparticle addition into high molecular weight PLA biodegradable polymer for the protection of Marmara marble in extremely acidic atmosphere in the reaction chamber and ambient air. Specific purposes of this thesis are:

- To determine bio-nano composite film properties.
- To investigate coated marble surface properties such as: hydrophobicity, water vapor permeability, capillary water absorption, and color variation.
- To test the protection effectiveness of the coated surfaces under extreme acidic conditions in reaction chamber and outdoor conditions.
- To estimate the mass transfer coefficient (h_d), the kinetic rate constants (k_s), and the internal diffusion (D_e) on the coated and uncoated marble surfaces by using the shrinking unreacted core model (SUCM).
- To determine surface morphology, formation of sulphation products and characterization of microstructure before and after SO_2-calcite reactions in the laboratory and outdoor conditions on the coated and uncoated marble surfaces.

This thesis consists of seven chapters. An overview and objectives of the study were presented in Chapter 1. Chapter 2, Chapter 3 and Chapter 4 reviews the concepts and previous studies related to this work. Experimental work is summarized in Chapter 5. Results and discussions are presented in Chapter 6. Chapter 7 includes conclusions and suggestions drawn from this study.

CHAPTER 2

AIR, POLLUTANTS, REACTIONS AND EFFECTS

2.1. Atmospheric Properties of Air

With a molecular weight of 28.96 g/mol, air is mainly composed of atmospheric substances such as particles, aerosols and gases. Main components of air which are practically the same throughout the globe are nitrogen (78.08 volume per cent) and oxygen (20.95 v.%). Along with them air contains 0.94 v.% of inert gases and 0.03 v.% of carbon dioxide. In the lower atmosphere strata, the air contains also water vapor, where its concentration is substantially variable depending on the partial water vapor pressure at the appropriate temperature and relative humidity. For example, air contains about 0.02 v.% of water vapor at 20°C and relative humidity of 80%. In the air layers close to the earth surface, other components may be present being in most cases of anthropogenic origin. These substances can be carried in the atmosphere depending upon their form. For instance, small size particles or aerosols can be suspended in the air and transported over long distances in the atmosphere (Torfs and Grieken, 1997). Therefore it is known that atmosphere is the main pathway for the transport of the gases, particles, etc. When gas or particle enters the atmosphere until removal process depending upon the properties of particles they travel. If a substance is not in the natural composition of air, it could be called as a contaminant or a pollutant based on the negative impact on materials or living organisms.

2.2. Pollutants

Pollutant is a word used for the substances stay in the atmosphere for either a time duration or concentration where a detrimental effect could occur due to presence of the substances in that air on anything. Though atmospheric pollutants cover a wide range of substances, this thesis will cover mostly the precursors of acidic deposition or precipitation as pollutants.

Air pollution is explained the increase in the background level of the any kind of atmospheric substances. Air pollution causes many harmful effects on living organisms and materials. The pollutants are generally classified into two groups: primary and secondary air pollutants. Primary pollutants are emitted directly from stationary or mobile sources to the atmosphere. The carbon compounds, such as carbon monoxide (CO), carbon dioxide (CO_2), methane (CH_4), and volatile organic compounds (VOCs); nitrogen compounds, such as nitrogen oxide (NO), dinitrous oxide (N_2O), and ammonia ($NH_{3)}$; sulfur compounds, such as hydrogen sulfide (H_2S) and sulfur dioxide ($SO_{2)}$; halogen compounds, such as chlorides, fluorides, and bromides and particulate matter (PM or "aerosols") can be classified as primary pollutants. On the other hand, secondary pollutants are formed as a result of atmospheric chemical reactions of primary pollutants. The main secondary pollutants are nitrogen dioxide (NO_2), nitric acid (HNO_3) sulfuric acid droplets, nitric acid droplets, sulfate and nitrate aerosols (Daly and Zanetti, 2007).

Sources of these pollutants can be either human-related or natural (Botkin and Keller, 1995). In the polluted atmosphere, 50% of the total sulfur oxides (SO_x) present in the atmosphere is emitted from natural sources, and the remaining as a result of human-related activity such as combustion of fossil fuels and industrial processes. Contrarily, nearly all of the nitrogen dioxide (NO_2) is caused from the human-activity such as transportation (mostly automobiles) and combustion of fossil fuels. When all the sources considered, human activity produces emissions of sulfur and nitrogen oxides exceed natural inputs of these compounds (Botkin and Keller, 1995).

2.2.1 Concentrations of Pollutants in Atmosphere

High concentrations of the sulfur oxides (SO_x) and nitrogen oxides (NO_x) in the urban atmosphere may cause harmful effect on living organisms and materials. For instance, SO_2 causes eye irritation, wheezing, chest tightness, shortness of breath and lung damage on the human health, while NO_2 causes susceptibility to respiratory infections, irritation of the lung and respiratory symptoms (USEPA, 2000). Moreover, SO_2 and NO_2 are also known as the main reasons for the deterioration of the marble monuments causing a crust composed of gypsum ($CaSO_4.2H_2O$) and nitrocalcite ($Ca(NO_3)_2.4H_2O$ via dry deposition on marble surfaces (Yerrapragada et al., 1994; Yerrapragada et al., 1996; Pedrazzani et al., 2006). In the last decade, concentrations of

these pollutants were increased in the atmosphere due to increased industrial activities. SO_x and NO_x are the pollutants whose concentrations are monitored at the monitoring stations all around the world, due to their hazardous effects on the human health and materials. The examples of these monitoring stations in some European cities and regions in 2010 were given in Table 2.1 (Kreindl and Hager, 2011). The results showed that NO_2 concentrations generally were higher than the SO_2 concentrations in the most of the European cities because of better control of SO_x emissions.

Table 2.1. SO_2 and NO_2 concentrations and monitoring stations numbers of the European cities and regions (Source: Kreindl and Hager, 2011)

Cities	Pollutants	Number of monitoring stations	Annual mean values, [$\mu g/m^3$]
Barcelona	SO_2	5	2
	NO_2	5	47
Munich	SO_2	1	5
	NO_2	6	57
Stockholm	SO_2	1	1
	NO_2	3	43
Vienna	SO_2	9	3
	NO_2	17	31
London	SO_2	6	4
	NO_2	14	51
Madrid	SO_2	9	10
	NO_2	22	44
Milan	SO_2	1	3
	NO_2	8	58

The concentration values of these pollutants have been also monitored in some cities of Turkey since 1997 (TUIK, 2009). The concentrations were reported (Table 2.2) in environmental information report (TCDR, 2011) which pointed out that SO_2 levels were higher than European countries.

Table 2.2. Annual SO_2 mean concentration values of the cities of Turkey (Source: TCDR, 2011)

Cities	SO_2, [μg/m^3]				
	2007	2008	2009	2010	2011
İstanbul	13	8	15	7	9
İzmir	71	14	17	12	15
Ankara	--	19	14	14	15
Hakkari	138	199	156	117	137
Manisa	20	12	18	7	15
Trabzon	24	11	23	11	8

Izmir is an highly industrialized area, situated in the west coast of the Turkey. It is surrounded by industrial regions (especially petroleum refineries, petrochemical industries, iron and steel factories in Aliağa and Kemalpaşa) that affect the urban air quality (Odabaşı et al., 2008). The combustion of fuels (mostly coal), industrial activities and increase of mobile sources increase the air pollutants and adversely affect the urban air quality in Izmir. Odabasi et al. (2008) measured SO_2 and NO_2 concentrations at 16 different regions in Izmir from January 2007 to April 2008. Guzelyali, Alsancak and Bornova Profesorler Sitesi regions were selected as urban atmosphere and average NO_2 values were as 29.36 μg/m^3, 41.29 μg/m^3 and 30.65 μg/m^3 respectively, while the average SO_2 values measured as 53,37 μg/m^3, 60.94 μg/m^3 and 28.35 μg/m^3. They concluded that NO_2 concentrations increased with increasing traffic density. Additionally they observed similar trend for SO_2 seasonally, but SO_2 concentration increased in January and February, 2008 in Alsancak and Guzelyali (Odabaşı et al., 2008) as a result of residential heating.

The Environmental Protection and Control Department (EPCD) of the Izmir Metropolitan Municipality established monitoring stations on some sites in Izmir. The daily, monthly and annual SO_2 concentrations were measured in the all monitoring stations, and NO, NO_2 concentrations were available in only Alsancak station from 2010 to 2012 (Table 2.3 and Table 2.4). The measured annual SO_2 concentrations were 15, 19, and 7μg/m^3 for 2010, 2011 and 2012 respectively. These results pointed out that SO_2 concentrations usually increased in the winter season due to residential heating. Generally NO_2 concentrations were reported to be higher than the SO_2 concentrations in the Izmir metropolitan area.

Table 2.3. Monthly SO_2 mean concentration values of the Izmir
(Source: EPCD, 2013)

		Mean concentration values [µg/m^3]											
		January	February	March	April	May	June	July	August	September	October	November	December
2010	Karşıyaka	21	29	32	16	11	22	10	11	10	9	10	15
	Güzelyalı	13	10	22	17	16	13	13	12	15	15	30	35
	Bornova	14	21	25	12	13	25	30	23	7	6	--	7
	Alsancak	17	13	9	8	10	8	19	16	6	9	11	9
	Şirinyer	9	7	15	5	7	5	3	4	4	5	11	9
	Çiğli	6	8	8	10	27	25	27	17	22	15	11	11
	Bayraklı	13	15	36	29	20	15	9	10	7	9	26	33
	City Average	13	15	21	14	15	16	16	13	10	10	16	17
2011	Karşıyaka	42	38	34	14	10	13	13	13	17	17	14	4
	Güzelyalı	58	32	22	15	7	17	12	17	25	21	25	21
	Bornova	15	22	26	47	34	26	39	33	26	7	8	7
	Alsancak	10	5	4	1	3	8	3	3	3	4	4	4
	Şirinyer	9	9	10	11	12	13	13	13	14	10	11	12
	Çiğli	10	10	12	11	12	13	22	26	26	21	6	6
	Bayraklı	50	40	15	4	4	4	9	4	4	3	4	3
	City Average	32	24	15	18	19	36	16	16	16	11	11	9

(Cont. on next page)

Table 2.3. (Cont.)

		Mean concentration values [µg/m^3]											
		January	February	March	April	May	June	July	August	September	October	November	December
2012	Karşıyaka	4	5	6	9	8	12	13	7	7	7	7	7
	Güzelyalı	20	22	17	5	8	4	8	8	7	7	10	14
	Bornova	7	7	7	6	6	5	5	5	5	7	7	7
	Alsancak	5	5	5	9	6	6	6	6	7	2	4	3
	Şirinyer	8	8	9	9	9	9	9	9	9	8	8	8
	Çiğli	4	4	4	4	4	7	9	4	6	7	5	5
	Bayraklı	9	13	12	6	6	6	2	9	10	8	11	28
	City Average	8	9	9	7	7	7	6	7	7	7	8	11

Table 2.4. Monthly NO, NO_2 and NO_x mean concentrations values of the Izmir (EPCD, 2013).

		Mean concentrations values [µg/m^3]											
		January	February	March	April	May	June	July	August	September	October	November	December
2012	NO	20	21	39	69	107	106	99	111	126	23	3	5
	NO_2	26	33	39	37	35	38	40	47	63	201	243	144
	NO_x	46	55	78	106	138	143	139	143	189	217	246	149

2.2.2. Atmospheric Chemistry of SO_2 and NO_x

Acid rain arises from the oxidation of SO_2 and NO_2 in the troposphere to form sulfuric and nitric acids which are eventually deposits on the earth surface either in dry or wet form. The process can proceed at either short or long distances far from the sources. Some of air pollutants are emitted to the atmosphere undergo chemical reactions and forms some other compounds such as sulfuric acid and ozone. Therefore it is essential that the chemical processes taking place in the atmosphere to be understood. In this section the conversion of gaseous SO_2 to sulfuric acid aerosols and sulfates and gaseous NO_x to nitric acid and nitrates will be examined. Mostly the oxidation of both SO_2 and NO_2 is initiated by hydroxyl radicals in the gas phase. Meanwhile, in the case of SO_2 oxidation aqueous phase chemistry should be considered due to the presence of SO_2 in the form of aerosol particles, clouds, and fog.

2.2.2.1 Atmospheric Chemistry of SO_2

It is known that SO_2 have a strong tendency to react with oxygen in air. The rate of gas phase reaction under catalyst free condition referred as slow. SO_2 reacts with oxygen and forms of SO_3 which rapidly react with vapor to form sulfuric acid. Homogenous gas phase reactions could occur in the any compounds such as O_3 or with labile species as OH, HO_2, CH_3O_2, NO_3 radicals, the Criegee biradical R_1R_2COO and O (^3P) atoms (Seinfeld, 1986). But among them the fastest and efficient reaction occurs via OH radical with the following reaction:

$$OH^{\bullet} + SO_2 \rightarrow HOSO_2 \qquad (2.1)$$

The presence of aqueous droplets in the form of aerosols, clouds, fogs and rain in the troposphere makes another phase important for the oxidation of SO_2. In this pathway, SO_2 gas dissolves in water. Due to equilibrium, three species of SO_2 (hydrated SO_2, the bisulfite ion (HSO_3^-) and the sulfite ion (SO_3^-)) forms atmospheric droplets in the pH range of 2-6. Later the SO_2 either H_2O_2 or O_3 may be oxidized to form sulfuric acid.

2.2.2.2. Atmospheric Chemistry of NO_x

Inorganic and organic nitrogenous compounds play a significant role in the chemistry of clean atmosphere as well as polluted atmosphere. Especially inorganic nitrogenous compounds such as nitric oxide (NO), nitrogen dioxide (NO_2), nitrate radical (NO_3), dinitrogen pentoxide (N_2O_5), dinitrogen trioxide (N_2O_3), nitrogen containing acids (nitrous acid (HONO), nitric acid (HNO_3) and peroxynitric acid (HO_2NO_2)) and ammonia (NH_3) are mainly related to organic oxidation as well as to acid deposition. Furthermore, these nitrogenous compounds reacted with each other and convert NO_x to HNO_3 which affects the natural stone and converts $CaCO_3$ to calcium nitrate (Ciferri et al., 2000).

In the atmosphere, NO_x is usually assumed to comprise NO and NO_2 (Corvo et al., 2010). NO and NO_2 are the most significant pollutants emitted both mobile and stationary sources. Johansson et al., (1988) pointed out that gasoline-powered automotive exhaust include 100-1000 ppm NO, and 10-100 ppm NO_2. However, NO_2/NO ratio was increased in the atmosphere due to oxidation of NO to NO_2. Therefore the kinetic and mechanism of gas phase reactions of NO and NO_2 have an importance for degradation of the carbonate stones.

In the atmosphere, NO conversion to NO_2 is as (Finlayson-Pitt and Pitt, 1986).

$$2NO + O_2 \rightarrow 2NO_2 \qquad (2.2)$$

There are also other reactions related to the oxidation of the NO to NO_2 in the atmosphere. The peroxy radicals are the other components responsible for NO oxidation. The conversion of NO to NO_2 in ambient air involves the chain oxidation of organics initiated primarily by the free radical of OH. The propyl radical reacts with O_2 to form an alkylperoxy radical and this oxidizes NO to NO_2. The RO_2 radical reacts with the NO and oxidize it to NO_2 and alkoxy radical (RO) is formed (eqn 2.3). Then, the HO_2 can oxidize NO in a second to NO_2 (eqn 2.4). NO also reacts rapidly with O_3 and convert to NO_2 (eqn 2.5). NO reacts very rapidly with NO_3 (eqn 2.6) (Finlayson-Pitt and Pitt, 1986). All these oxidation reactions of the NO indicated that NO_2 concentration is effected by the NO concentration in the atmosphere,

$$RO_2^{\cdot} + NO \rightarrow RO + NO_2 \qquad (2.3)$$

$$HO_2 + NO \rightarrow OH + NO_2 \qquad (2.4)$$

$$NO + O_3 \rightarrow NO_2 + O_2 \quad (2.5)$$

$$NO + NO_3 \rightarrow 2NO_2 \quad (2.6)$$

2.3. Acid Rain and Deposition

Rain with pH 4-5 is quite common in Europe and in the northeast of US. Acidic precipitation with pH<4 could be seen all around the world. It is not only rain but also some of the fog could have pH value smaller than 2 (Seinfeld, 1986). It is known that in the pristine atmosphere, water vapor in the atmosphere is in equilibrium with atmospheric CO_2 has pH value of 5.6 which can be referred slightly acidic. The chemical reactions that help for the conversion of SO_2 and NO_x to sulfate and nitrate are the major precursors to determine the relationship between them and acidic deposition. Once the gaseous SO_2 is oxidized in the plume or in ambient atmosphere to sulfuric acid aerosols or sulfates by the reactions could occur in the gas phase, in the liquid phase, or on the surfaces of solids or combination of all three. Therefore both gas-and aqueous–phase reactions would be important in the step. It is known that for the gas-phase reaction of SO_2 and NO_x occurs through the OH radical involvement (Seinfeld, 1986). The atmospheric pathway of acidic deposition is presented in Figure 2.1 in detail.

$$SO_2 + {}^{\cdot}OH \rightarrow H_2SO_4 \text{ (after several steps)} \quad (2.7)$$

$$NO_2 + {}^{\cdot}OH \rightarrow HNO_3 \quad (2.8)$$

The reaction rates in the gas phase depend on the OH radical concentrations. The reaction rates are faster in summer than winter. In the gas phase reactions, nitrate conversion has higher rate measured in the urban plume, therefore nitric acid production in the vicinity of source would be higher compared to sulfuric acid, but the ratio of sulfate to nitrate would increase with distance from a source-rich region. Even though conversion of SO_2 to H_2SO_4 aerosol in the gas phase is explained directly with OH dependency, indirectly it is related to

the levels of NO_x, hydrocarbon and sunlight intensity as well. There is complex relationship in the formation of H_2SO_4 (Seinfeld, 1986).

Absorption of SO_2 by droplet could be another pathway of sulfate formation. After absorption of SO_2 by droplet aqueous phase oxidation occurs through H_2O_2 and O_3.

Once acid formed, the acid can be deposited onto earth surface either by gas or particle deposition called as "dry deposition" under the gravity, or these pollutants could be dissolved in fog, rain or snow and return to earth surface in these forms called as "wet deposition". Dry and wet depositions are the major ways of removal of the pollutants from atmosphere. Dry deposition is one of the removal processes of atmospheric pollutants in the absence of precipitation in arid or semi-arid environments. Dry deposition is mostly characterized by a deposition velocity or rate V_d which is the ratio of flux and concentration of pollutant (Seinfeld, 1986).

2.3.1. Dry and Wet Deposition of Pollutants on Calcareous Stones

SO_2 and NO_2 react with the calcite crystals of the natural stones and most abundant pollution products such as gypsum ($CaSO_4.2H_2O$) and nitrocalcite ($Ca(NO_3)_2.4H_2O$) are formed (Gauri and Bandyopadhyay, 1999). SO_2 and NO_2 or its oxidizing products such as SO_3, H_2SO_4 and HNO_3 reach the stone surface either by "dry" or "wet" deposition. The interactions of the gaseous pollutants with the surface by turbulence and winds are basically called as dry deposition. "Wet deposition" is the precipitation of oxidized or derived species of the pollutants dissolved in the atmospheric moisture (Garland, 1978). Atmospheric pollutants are diffused in the tiny liquid droplets and tiny solid particles suspended in the air and deposited on directly to rain protected surfaces. "Dry deposition" is one of removal pathways of pollutants from atmosphere to surfaces such as soil, water, vegetation or stone (Gauri and Bandyopadhyay, 1999). In the literature, time averaged dry deposition rate or velocity (in $cm.s^{-1}$) V_d was used to describe deposition velocity on the materials. The meteorological conditions, surface characteristics and particle properties affect the dry deposition rate (Wesely and Hicks, 2000; Nho-Kim et al., 2004). SO_2 and NO_2 dry deposition rate on the carbonate stones were studied in the literature by many researchers (Gauri et al., 1982/1983; Johansson et al., 1988; Johnson et al., 1990; Haneef et al., 1992; Cobourn et al., 1993; Yerrapragada et al., 1994; Grossi and Murray, 1999; Gauri and Bandyopadhyay, 1999).

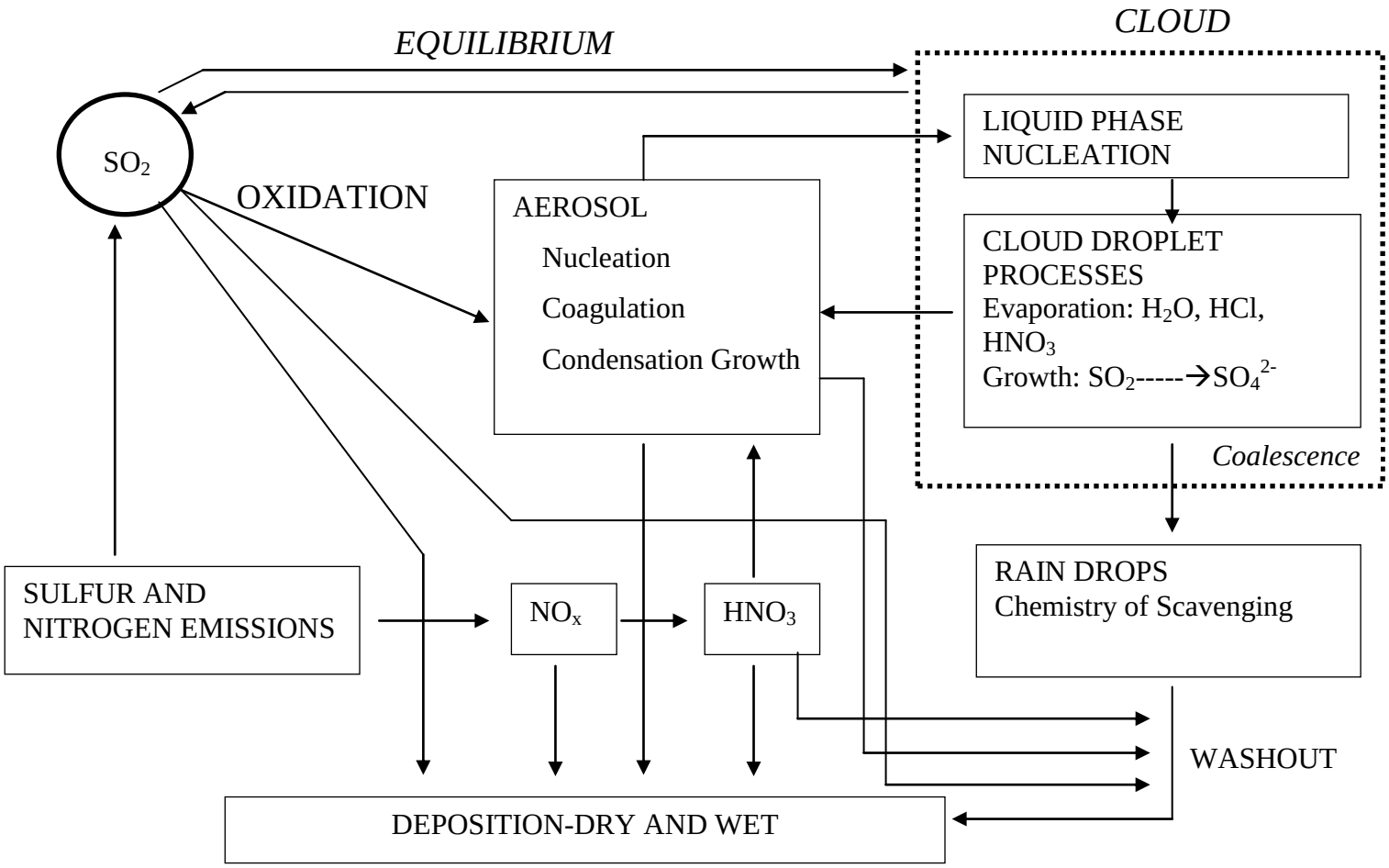

Figure 2.1. Atmospheric pathways of acid deposition
(Source: Seinfeld, 1986).

Grossi and Murray (1999) investigated the effects of dry deposition on the carbonate buildings with stone characteristics such as pore distribution, porosity, specific surface area, and impact of water sorption as well. The higher the porosity was resulted in the higher the absorbed water on the stone surface. The increased pore distribution and specific surface area enhanced the uptake of the moisture from air. The accumulation of dissolving salts as well as gypsum, originated from the dry deposition, increased these deliquescent salts in the water content of the stones. Grossi and Murray (1999) also mentioned that these salts allowed more acidic gases absorption until they washed away with rain, otherwise they stayed there indefinitely. Johansson and coworkers (1988) pointed out SO_2 absorption rate increased on depending on pore size. For example large porosity of limestone increased the effective surface area and enhanced SO_2 absorption rate. Spiker et al. (1992) also investigated the parameters which affected the SO_2 deposition on the stones and SO_2 deposition velocity on Salem limestone and Shelburne marble by using computerized controlled environmental chamber. They found out that surface moisture, roughness and porosity increased the absorbed water as well SO_2 deposition on the surface, and the SO_2 deposition velocity of limestone was twenty six times greater than marble due to greater porosity and surface roughness of limestone.

SO_2 deposition velocity on marble and dolomite surfaces were also measured by using quantitative analysis of formed gypsum and epsomite (Cobourn et al., 1993). The deposition velocities varied between 0.02 and 0.10 cm s^{-1} for dolomite, and 0.02-0.23 $cm.s^{-1}$ for marble respectively. This study also pointed out that deposition velocity increased significantly when condensed moisture was observed on the stone surface for both type of stones (Cobourn et al., 1993). Grontorft and Raychaudhuri (2004) gathered NO_2 and SO_2 deposition velocities on the indoor different surfaces from literature, and compared the experimental results from the experimental chambers (20 ppb SO_2 and NO_2 concentration and relative air humidity ranging from 0% to 90%) (Table 2.5). The increase in humidity increased the deposition velocity and changes with the surface properties.

Stone surface can be affected from water in different ways. One of them is that gases, aerosols dust or dirt particles in water can be converted to the form of aerosol particles by condensation on stone surfaces. The pollutants can also be concentrated in the mist or fog form of the water which may be carried over long stretches and discharged on the surface of buildings. Besides, the increase of water capillary content

which includes soluble salts in the porous building materials like calcareous stones can result in severe damages on the stone surfaces, since the salts can be found in the sulfate form of calcium, magnesium, sodium, and potassium (Torfs and Grieken, 1997; Kucera and Fitz, 1995). As a result, the water in atmosphere reaches the building surfaces in the form of rain. The acidity of rainwater can be enhanced by the increase of sulfate and nitrate concentrations. All form of the precipitation such as rain, fog and snow called as wet deposition, but, rainfall can be considered as the dominant pathway for the wet deposition of pollutants on stone surfaces. The acidity of rainfall may lead to direct attack on mineral compounds of a stone material (Torfs and Grieken, 1997).

Table 2.5. Humidity-dependent SO_2 and NO_2 surface deposition velocities (V_d) on different materials (Source: Grontorft and Raychaudhuri, 2004).

Material Surface	V_d **(cm/s)**	**Relative Humidity (%)**				
		0	**30**	**50**	**70**	**90**
Hard dense stone -Alkaline (Marble)	SO_2	0.009	0.0011	0.010	0.014	0.015
	NO_2	0	0	0	0	0
Hard dense stone -acidic (Granite, slate)	SO_2	0.0045	0.0053	0.0060	0.0070	0.0076
	NO_2	0	0	0	0	0
porous stone - alkaline (limestone)	SO_2	0.88	0.11	0.13	0.15	0.17
	NO_2	0	0	0.02	0.025	0.025
porous stone - acidic (silicate sand stone)	SO_2	0.044	0.055	0.065	0.075	0.085
	NO_2	0^{-4}	0^{-4}	0.01	0.013	0.013
Gypsum wall board, Untreated	SO_2	0.11^{-15}	0.12^{-15}	0.14^{-15}	0.15^{-15}	0.18^{-15}
	NO_2	0^{-15}	0.025^{-15}	0.054^{-15}	0.065^{-15}	0.084^{-15}

2.3.2. Effects of Air Pollutants on Carbonate Stones

The detrimental effects of the air pollutants have accelerated the decay rate of the carbonate rocks due to logarithmic increase in industrialization in the last century. Carbonate stones, like marble, limestone and dolostone mostly contain calcite ($CaCO_3$)

and dolomite ($CaMg(CO_3)_2$ minerals, are commonly used building materials for historical monuments (Gauri and Bandyopadhyay, 1999). The oxidation reactions of SO_x and NO_x with water give rise to formation of acidic sulfates, nitrous and nitric acids in the atmosphere. These aerosols can be easily transported to the washed out or sheltered surfaces as acid solution droplets by acid rain or fog. The penetration of sulfates by nitrous and nitric acids into the calcite lead to the formation of sulfates and nitrates salts that finally cause deterioration, exfoliation, detachment and loss of material on the stone surfaces (Pedrazzani et al., 2006). Bernal and Bello (2003) indicated that especially gypsum formation are responsible approximately 30-50% losses of materials on the stone surfaces due to solubility of gypsum in water. Marble has a nonporous and homogeneous composition and entirely composed of calcite minerals (Gauri and Bandyopadhyay, 1999). Gypsum is a sulfation reaction product, being more soluble and inherently occupies more volume than the calcite. This type of erosional loss of material from the stone surfaces was explained by the solubility of gypsum in rain-washed areas and sheltered places (Böke et al., 1999; Gauri and Bandyopadhyay, 1999).

SO_2, NO_2 and acid aerosols react with carbonate stones by dry deposition in sheltered places and produce crust made of gypsum ($CaSO_4.2H_2O$) and nitrocalcite ($Ca(NO_3)_2.4H_2O$). Gauri and Bandyopadhyay (1999) pointed out that gypsum formation pre-dominated over nitrocalcite formation for the carbonate rocks, since NO_2 presence in the air accelerates the gypsum formation and NO_2 increases the oxidation of SO_2 to sulfur trioxide (SO_3) in the sulfating reaction. Detection of nitrocalcite in the form of crystals under humid atmosphere is difficult due to its highly deliquescent salt properties. Previous studies indicated that nitrocalcite easily absorbs moisture or water vapor from the air and converts nitrocalcite to liquid form under 50% relative humidity (R.H) at 25°C (Amorosso and Fassina, 1983; Yerrapragada et al., 1996; Gauri and Bandyopadhyay, 1999).

It is also reported that not only SO_2, but also SO_3 in the air accelerates sulfation of calcite and deterioration of carbonate stones (Nord and Holenyi 1997; Gauri and Bandyopadhyay, 1999). When relative humidity ranges from 40-90 % at room temperature, SO_2-calcite, SO_3-calcite, NO_2-calcite reactions and gypsum and nitrocalcite formations can be summarized by the following equations (eqns 2.9-22). SO_2-calcite reaction proceeds and gypsum formation is occurred in two steps. SO_2 reacts with calcite ($CaCO_3$) in the presence of water (H_2O) and converts it into calcium

sulfite hemi-hydrate ($CaSO_3.1/2H_2O$) (eqn 2.9). Calcium sulfite hemi-hydrate is known as an unstable product and it can easily be oxidized to gypsum ($CaSO_4.2H_2O$) by the oxygen in the presence of water (eqn 2.10) (Gauri et al., 1989; Yerrapragada et al., 1996; Böke et al., 1999). Nord and Holenyi (1997) pointed out that soot and iron particles can serve as catalyst and accelerate the reaction as well.

$$CaCO_3 + SO_2 + 1/2\ H_2O \rightarrow CaSO_3.1/2H_2O + CO_2 \quad (2.9)$$

$$CaSO_3 . 1/2H_2O + 1/2O_2 + 3/2H_2O \rightarrow CaSO_4 . 2H_2O \quad (2.10)$$

SO_2 conversion to SO_3 is a gas-phase reaction which also includes catalytic oxidation in the crust formation (eqn 2.11). The presence of NO_2 gas in the atmosphere may cause the conversion of SO_2 to SO_3 (eqn 2.12). Finally, the formed SO_3 gas reacts with calcite in the presence of water, and gypsum crust occurs without differently formation of the sulfite (eqn 2.13) (Yerrapragada et al., 1996; Gauri and Bandyopadhyay, 1999).

$$SO_2 + 1/2\ H_2O \rightarrow SO_3\ (g) \quad (2.11)$$

$$SO_2 + NO_2 \rightarrow SO_3\ (g) + NO \quad (2.12)$$

$$CaCO_3 + SO_3\ (g) + H_2O\ (g) \rightarrow CaSO_4.2H_2O + CO_2 \quad (2.13)$$

In some instances, surface reactions cause crust formation which prevents the marble surface – atmosphere interface. Condensed water vapor and droplets may occur on the crust surfaces and hydrogen (H^+), nitrous (HNO_3^-) and sulfurous (HSO_4^-) ions are formed (eqns 2.14-16) and, formed hydrogen ion passes through the crust and separate calcium ions (Ca^{2+}) from the calcite in the underlying the marble. Besides, separated calcium ions pass from the underlying marble to surface and react with nitrous and sulfurous ions and finally gypsum and nitrocalcite appear on the surface (eqns 2.17-19) (Yerrapragada et al., 1996; Gauri and Bandyopadhyay, 1999).

$$SO_2 + H_2O + 1/2\ O_2 \rightarrow H_2SO_4 \quad (2.14)$$

$$H_2SO_4 \rightarrow H^+ + HSO_4^- \quad (2.15)$$

$$NO_2 + H_2O \rightarrow H^+ + HNO_3^- \quad (2.16)$$

$$CaCO_3 + 2H^+ \rightarrow Ca^{2+} + H_2O + CO_2 \quad (2.17)$$

$$Ca^{2+} + HSO_4^- + 2H_2O \rightarrow H^+ + CaSO_4.2H_2O \quad (2.18)$$

$$Ca^{2+} + 2HNO_3 + 4H_2O \rightarrow 2H^+ + Ca(NO_3)_2 \cdot 4H_2O \quad (2.19)$$

Bernal and Bello (2003) defined another gypsum formation as the adsorption of sulfur dioxide in rain water, liquid atmospheric aerosols, or moist film supported on a stone surface where it is oxidized to form a sulfuric acid solution that dissolves the calcium carbonate and gypsum formation takes place (eqns 2.20-21).

$$SO_2 + O_2 + H_2O \rightarrow H_2SO_4 \quad (2.20)$$

$$CaCO_3 + H_2SO_4 + H_2O \rightarrow CaSO_4 \cdot 2H_2O \quad (2.21)$$

2.3.3. Protection Studies of Stone Surfaces

Due to detrimental effects of weathering caused undesirable alterations in the physical and chemical characteristics of the historical monuments and facades, protections of the marble monuments have been gained attraction by academics all around the world in the last century.

The damage results in the formation of gypsum, product of sulfation reaction, arises from combination pollutant gases, relative humidity, porosity of stone, temperature and sorption of organic and inorganic matters on the surface. For instance, Johansson et al. (1988) showed that high porosity increased the SO_2-stone reaction due to the wide surface area. Gauri and Gwinn (1982/1983) was also proved enhancement of SO_2-calcite reaction with high SO_2 concentration and relative humidity.

In the literature, research groups tried to determine the air pollution effects on the carbonate stones which were realized under artificial (in laboratory conditions) or

natural atmospheric conditions (Cheng et al. 1987; Johansson et al, 1988; Gauri et al, 1989; Ausset et al., 1996; Böke et al., 1999; Gauri and Bandyopadhyay, 1999; Ocak et al., 2009). These protection studies can be grouped into four.

The first group of the studies was focused on conversion of gypsum back to calcite ($CaCO_3$) by using the carbonate solution on the sample surfaces and they achieved to form calcite on the surface, but it was in the form of the powder (Skoulikidis and Belayannis, 1984). Therefore formed calcite crystals were poorly adhered to the original marble surface and material loss could not be eliminated. This technique is reported as ineffective for the protection of protection. The reaction can be expressed as follows;

$$CaSO_4.2H_2O + CO_3^{2-} \rightarrow CaCO_3 + SO_4^{2-} \qquad (2.22)$$

Second generation studies focused on using synthetic polymers as coating agents for the protection of natural stones against atmospheric SO_2 and water. Unfortunately, high SO_2 absorption and entrapment of water vapor of the synthetic polymer coatings accelerated sulphation reactions on the marble surfaces. Furthermore, at the end of the useful time of the old coating, reapplication of the new polymer coatings was not an easy task because of the difficulty of removing old coating from surface. The removal of old coating needed the use of mechanical device or chemical cleaning agents. These mechanical/chemical peeling agents triggered further degradation on marble surfaces (Gauri et al., 1973; Johanson et al., 1994; Elfving et al., 1994; Gauri and Bandyopadhyay, 1999; Thompson et al., 2003).

Some water soluble organic and inorganic compounds were used to reduce SO_2-calcite reaction on the marble sample surfaces in the third group of studies. Cationic surfactant (Abil Quat 3270), nonionic surfactant (Tween 20) (Böke et al., 2002) and anionic certain surfactants such as phosphate (PO_4^{3-}), oxalate ($C_2O_4^{2-}$), oleate ($C_{17}H_{33}COO^-$) (Böke and Gauri 2003; Thompson 2003) were used to decrease the calcium carbonate solubility to create insoluble layers on the marble surfaces for the protection. Böke et al. (2002) reduced the gypsum formation 10% relative to control sample by using the cationic and nonionic certain surfactants. Later they achieved to obtain calcium oxalate, calcium oleate or calcium phosphate layer on the marble surfaces and these compounds reduced the SO_2-calcite reaction approximately by 15 %.

Some biodegradable polymers such as polyhydroxybutyrate (PHB), high and low molecular weight poly-L-lactide (PLA) were used as coating agent on the marble surfaces to inhibit SO_2-calcite reaction. As it's well known, some of the biodegradable polymers have good moisture, gas barrier beside degradability which helps renewability of the new coating application on the marble surfaces. Researchers exposed coated and uncoated control marbles at nearly 8 ppm SO_2 concentration at 100 % relative humidity conditions in a reaction chamber for several months. They reported that the use of high molecular weight PLA polymers on marble surfaces have significant protection up to 60% at the end of 3 months. High molecular weight PLA polymer determined as a promising protective coating agent in reducing gypsum formation on marble surfaces in the polluted environments (Ocak et al., 2009).

The protection studies have been continued with the development of nanoparticle use in every area. Nanocomposites are becoming as promising new materials on the protection studies. So far the nanoparticles has been used in polymer matrices improved optic, electronic, magnetic, catalytic, mechanic, chemical and tribological properties of the surfaces (Mittal et al., 2010; Zhang et al., 2003). Optimum amount of nanoparticle addition is critical. Scarfato et al. (2012) pointed out that low loading of clay (<6 wt.%) more effective in the mechanical, barrier and thermal properties than high loadings (> 6 wt.%). In the protection areas, many different types of nanocomposites such as the silicone containing polymer matrices (Zielecka and Bujnowska, 2006), silica nanoparticles added siloxane protective composition matrices (Manoudis et al., 2009), silica added Poly(methyl methacrylate (PMMA) and perfluorinated polyether (PFPE) polymer matrices (Manoudis et al., 2007), nanosilica added flouroalkylsilane coatings (Su et al., 2006), organoclay added epoxy and silane coating agents (Christopher et al., 2008) and organomodified montmorillonite (Cloisite 30B) added Fluoline CP and Antipluviol S resins (Scarfato et al., 2012) were used to investigate the protection capabilities and additive effects of nanoparticles on mechanical, barrier, thermal and morphological properties of the coatings (Manoudis et al., 2009; Christopher et al., 2008; Manoudis et al., 2007; Zielecka and Bujnowska, 2006; Su et al., 2006). As mentioned before, water action on the surface of stone is the most effective parameter for decay of surface. The above mentioned synthetic polymer/nano composites were mainly tested based on water protection efficacy, color changes etc. They achieved creating super hydrophobic surfaces by the use of synthetic polymer/nano composites (Manoudis et al., 2009).

CHAPTER 3

KINETICS AND DECAY RATE MODELS OF CARBONATE STONES

There were many models which were used for the determination of the kinetics and modeling decay rates of carbonate stones in the polluted environments (Erk and Dudukovic, 1984; Tambe et al., 1991; Couborn et al., 1993; Yerrapragada et al., 1994; Gauri and Bandyopadhyay, 1999; Boke and Gauri, 2003). The shrinking unreacted core model, deposition velocity model, artificial neural network model and pore models such as distributed-pore model and random-pore models are the most commonly used models for carbonate rocks such as marble, dolomite and limestone in previous studies. While limestone/dolomite is a porous material, marble is a nonporous and compact material. Due to compositional and structural differences in the types of carbonate rocks, kinetic modeling has to be used carefully. The models, assumptions and defined parameters from various studies are summarized in Table 3.1

The shrinking unreacted core model (SUCM) is the mostly widely used model for the determination of the kinetics and modeling of decay rates of marbles in laboratory and outdoor conditions under SO_2 and NO_2 environment. The outcomes of the model are the determination of mass transfer coefficient (h_d), the kinetic rate constants (k_s) which are expressed in cm/h; and the internal diffusion (D_e) in cm^2/h which will be explained in the following mathematical derivations of the SUCM.

Table 3.1. Summary of assumptions and defined parameters of the previous studies.

Reaction & Models	**Assumptions**	**Determined Parameters**	**Referance**
Dolomite-SO_2 (in laboratory) & SUCM	• Pore diffusion resistance neglected • Small rate due to low temperature • Essentially constant rate • External mass transfer and chemical reaction resistances effected the reaction. • Linear regression	• h_d ranged 524-549 cm/h • 1^{st} order reaction k_s= 280cm/h • 1/2 order reaction, k_s= 0.19 $mmol^{0.5}$ $cm^{0.5}h^{-1}$	Tambe et al., 1991
Dolomite, Marble-SO_2 (in laboratory) & DVM	• V_d equal to inverse of overall resistance • α= 1 for marble and α= 2 for dolomite • Deposition velocity (V_d) depends on humidity, T, wind speed, surface wetness and crust thickness	• Deposition velocity or rate (V_d) for marble varied between 0.02-0.23 cm/s • V_d for dolomite varied between 0.02-0.10 cm/s	Couborn et al., 1993
Marble-SO_2 (in laboratory and outdoor) & SUCM	• Rate controlling parameters were h_d, k_s and D_e. • Reaction rates depend on mass transfer, reaction and diffusion controlling rates.	• k_s and D_e defined as 312 cm/h and 0.14cm^2/h in laboratory • k_s, D_e, order of reaction (α_1, α_2) defined as 375 cm/ h 0.11cm^2/h, 0.7and 0.3 for outdoor cond.	Yerrapragada et al., 1996
Limestone-SO_2 (in laboratory) & SUCM, DPM,ANN	• The controlling parameters were reaction kinetics and diffusion for SUCM. • Chemical conversion of the reactant changed in its porosity for DPM.	• Three model fitted well with observed data • ANN was the most accurate	Bandyopadhyay et al., 1996

* SUCM; Shrinking Unreacted Core Model, DVM; Deposition Velocity Model, ANN; Artificial Neural Network Model and, DPM; Distributed Pore Model

(Cont. on next page)

Table 3.1. (Cont.)

Reaction & Models	Assumptions	Determined Parameters	Referance
Limestone-SO_2 (in laboratory) & DPM	• The pore volume and surface area changed • Reaction rate accelerated in early phase (due to high surface area) then decreased due to reduction of surface.	• k_s = 4.90 x$10^{-6}$$cm^{2.98}$/ $mmol^{0.66}$h • "n" as 0.66. • Porosity increased. • Results well-fitted to experiment values	Tambe et al., 1994
Marble-SO_2 and NO_2 (at outdoor) & SUCM	• Ignored the rate of mass transfer of SO_2 and NO_2 • Turbulent cond. in outdoor • Reaction kinetically controlled in early stage • Rate was diffusion controlled due to long exposure	• k_s = 395 cm/h • D_e = 0.13 cm^2/h	Yerrapragada et al., 1994
Naked/coated limestone and sandstone-SO_2 & DVM	• Lausanne atmospheric simulation chamber used • Assumption: homogeneous dispersion of fly ash and soot particle on stones	• V_d decreased with time for two stone types • During the first 4 months, V_d higher for naked stones • v_d for soot particle coated < V_d for fly ash coated < naked stones	Ausset et al., 1996
Cement, asphalt and stucco-SO_2 & DVM	• Mass transport conditions; Turbulent flow, steady state and psuedo-1st order processes • V_d related to gas solid reactivity (ϕ)	• V_d of asphalt & cement 0.04cm/s and 2.5cm/s • SO_2 conc., R.H and pressure independent for V_d values	Judeikis and Steward, 1976

* SUCM; Shrinking Unreacted Core Model, DVM; Deposition Velocity Model, ANN; Artificial Neural Network Model and, DPM; Distributed Pore Model

3.1. Shrinking Unreacted Core Model (SUCM)

In this section, the sulfation reaction data from the reaction chamber and ambient air modeled by using shrinking unreacted core model (SUCM) to investigate the change in rate parameters such as the order of reaction, the rate constant, the rate of diffusion etc. SUCM has been frequently applied to gas solid reactions (Erk and Dudukovic., 1984; Tambe et al., 1991; Gauri and Bandyopadhyay, 1999; Fogler, 2005).

Tambe et al. (1991) schemed the model as the boundary layer (a) and its boundary concentrations such as C_{Ab} outside layer concentration (bulk concentration) and C_{As} inner concentration at the sample surface (surface concentration); gypsum crust layer (b); the outer of the original sample is the leached zone (c) and unreacted core under the leaching zone (d) (Figure 3.1). SUCM was applied for crust growth due to SO_2 reaction in laboratory conditions and crust growth due to SO_2 + NO_2 reaction in outdoor conditions in various studies (Tambe et al., 1991; Yerrapragada et al., 1994; Yerrapragada et al., 1996; Gauri and Bandyopadhyay, 1999).

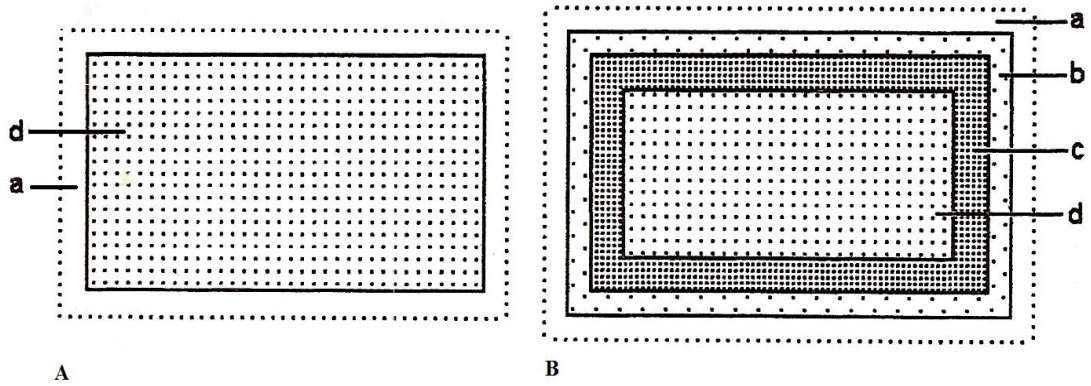

Figure 3.1. Schematic diagram of dry deposition reaction for unreacted (A) and reacted carbonate stone specimen (B), (Source: Gauri and Bandyopadhyay, 1999)

3.1.1. Rate Constants Regarding SO_2 Reaction

In this model, the rate controlling parameters are the mass transfer coefficient (h_d), the kinetic rate constants (k_s) and the internal diffusion (D_e). In the literature, researchers accepted the rate of reaction was equal to the inverse of the corresponding resistances such as aerodynamic resistance (R_1), surface uptake resistance (R_2) and product layer resistance (R_3) (Gauri and Bandyopadhyay, 1999).

$$r_A = \left(\frac{1}{R_1 + R_2 + R_3} \right) A_0 C_{AS} \tag{3.1}$$

$$r_A = \left(\frac{1}{h_d} + \frac{1}{k_s} + \frac{\delta}{D_e} \right)^{-1} A_0 C_{AS} \tag{3.2}$$

Where, r_A is the rate of reaction (mol/h), δ is the product (gypsum) layer thickness (μm), A_0 is the external surface area of the sample (cm^2) and C_{AS} is the concentration of the SO_2 (mol/cm^3) at the sample surface and calculated by using the concentration of the SO_2 at outside the boundary layer (mol/cm^3) (C_{Ab}). Furthermore, previous studies assumed as the overall reaction mechanism which was summarized in the following reaction. In this equation, a, b, c, and d refer to the stoichiometric coefficients, A and B are the reactants and P and Q are the products (Tambe et al., 1991; Yerrapragada et al., 1996; Gauri and Bandyopadhyay, 1999).

$$aA_{(g)} + bB_{(s)} \rightarrow cP_{(g)} + dQ_{(s)} \tag{3.3}$$

There is a relation between the gas consumption rate (r_A) and the solid reactant conversion (r_B) (Yerrapragada et al., 1996; Gauri and Bandyopadhyay, 1999; Fogler, 2005). Additionally previous studies defined the relation between the rates of reaction with respect to the conversion of solid B. In this equation, ρ_B is the density (g/cm^3), M_B is the molecular weight and dV_R/dt is the volume of the reacted carbonate stone in time (h) (Yerrapragada et al., 1996; Gauri and Bandyopadhyay, 1999).

$$\frac{r_A}{a} = \frac{r_B}{b} \tag{3.4}$$

$$r_B = \frac{\rho_B}{M_B} \frac{dV_R}{dt} \tag{3.5}$$

The overall reaction mechanism (eqn 3.3) was applied to SO_2-calcite reaction in the literature (eqn 3.6) (Yerrapragada et al., 1996; Gauri and Bandyopadhyay, 1999).

They defined the equations of the mass-transfer-controlling (r_m), reaction-controlling (r_k) and the diffusion-controlling rate (r_D) (Tambe et al., 1991; Yerrapragada et al., 1996; Gauri and Bandyopadhyay, 1999; Fogler, 2005).

$$CaCO_3 + SO_2 + 2H_2O + 1/2O_2 \rightarrow CaSO_4.2H_2O + CO_2 \tag{3.6}$$

$$r_m = A_0 h_d (C_{Ab} - C_{As}) \tag{3.7}$$

$$r_k = A_0 k_s C_{As}^n \tag{3.8}$$

$$r_D = \frac{A_0 D_e C_{As}^n}{\delta} \tag{3.9}$$

Where, n is the order of reaction. The order of reaction determined as a first order reaction in several studies (Tambe et al., 1991; Yerrapragada et al., 1996; Gauri and Bandyopadhyay, 1999). After the determination of all resistances, the net rate (r_A) of the gaseous reactant (SO_2) can be calculated by using eqn 3.2. When the eqns 3.4 and 3.5 are substituted in the eqn 3.2 the following expressions are obtained (Yerrapragada et al., 1996; Gauri and Bandyopadhyay, 1999).

$$\frac{\rho_B}{M_B}\frac{dV_R}{dt} = \frac{b}{a}\left(\frac{1}{h_d} + \frac{1}{k_s} + \frac{\delta}{D_e}\right)^{-1} A_0 C_{As} \tag{3.10}$$

Rearranging

$$\frac{d\delta}{dt} = \alpha \frac{M_B}{\rho_B}\left(\frac{1}{h_d} + \frac{1}{k_s} + \frac{\delta}{D_e}\right)^{-1} C_{As} \tag{3.11}$$

Finally, analytical solution becomes

$$\left(\frac{1}{2D_e}\right)\delta^2 + \left(\frac{1}{h_D} + \frac{1}{k_s}\right)\delta = \alpha \frac{M_B}{\rho_B} C_{As} t \tag{3.12}$$

The kinetic rate constants (k_s) and the internal diffusion (D_e) can be found as unique values by regression analysis of the experimental data by using eqns 3.10-12. D_e and k_s values of the marble, limestone and dolomite were obtained from several studies and represented in the Table 3.1. On the other hand, the calculation of the mass transfer coefficient, h_d, requires experimental determination due to laminar flow condition in the laboratory. The equation of the mass transfer coefficient can be represented by following equation (Gauri and Bandyopadhyay, 1999)

$$h_d = \frac{D_{AB} N_{Sh}}{d_p} \tag{3.13}$$

The mass transfer coefficient is related with the Sherwood number (N_{Sh}), the equivalent diameter of the experimental slab (d_p) and the binary diffusion coefficient of the air-SO_2 system (D_{AB}). In this equation, first D_{AB} values should be calculated from the Chapman-Enskog equation (Bird et al., 2007) where M_A and M_B are the molecular weights of air and SO_2, T is the temperature (^oK), P is the pressure (atm), σ_{AB}= ½(σ_A+σ_B) is the average collision diameter, Ω_{AB} is the temperature-dependent collision integral (Bird et al., 2007).

$$D_{AB} = 0.0018583 \frac{\sqrt{T^3 \left(1/M_A + 1/M_B\right)}}{p \sigma_{AB} \Omega_{AB}} \tag{3.14}$$

Equations for the calculation of Sherwood, Schmidt and Reynolds Numbers that are required for the calculation of the mass transfer coefficient are given below. In addition that following equations used for the assumption of the forced convection around a solid sphere and its mass transfer analogy (Tambe et al., 1991; Gauri and Bandyopadhyay, 1999; Incropera et al., 2002; Fogler, 2005)

$$N_{Sh} = 2.0 + 0.6 N_{\mathrm{Re}}^{0.5} N_{Sc}^{0.33} \tag{3.15}$$

$$N_{\mathrm{Re}} = \frac{d_p V \rho_g}{\mu} \tag{3.16}$$

$$N_{Sc} = \frac{\mu}{\rho_g D_{AB}} \tag{3.17}$$

Reynold and Schmidt numbers were used in the Rantz-Marshall correlation (for laminar flow which valid for N_{Re} range 0-200) (eqn 3.15). The mass transfer coefficient can be determined by using calculated Sherwood Numbers and the binary diffusion coefficient of the air-SO_2 system. Gauri and Bandyopadhyay (1999) presented the rate constants and effective diffusivities for marble, limestone and dolomite reactions in SO_2 atmosphere which were obtained from previous studies. Yerrapragada et al. (1996) determined the rate of growth of crust with time due to SO_2 reaction which was represented in Table 3.1. Unique values of k_s and De were obtained as (312 cm/h) and (0.14 cm^2/h), respectively. These unique values have a correlation coefficient of 0.98 with the best-fit equation. Tambe et al. (1991) also determined the mass transfer coefficient (h_d) by using eqns 3.13-17 and the values of h_d were ranged between 524 and 555 cm/h

Table 3.2. k_s and D_e for different type of stones in the presence of SO_2 (Source: Gauri and Bandyopadhyay, 1999).

Sample Type	**Name**	**Surface Rate Constants k_s (cm/h)**	**Effective Diffusivity D_e (cm^2/h)**
Marble	Carrara Marble	312	0.14
Limestone	Cordova Cream	510	0.55
	Cordova Shell	289	0.41
	Louder	224	0.45
	Bedford	134*	0.083*
Dolomite	Laurel Dolomite	183	0.37

* The order of reaction of all stones is 1 except for Bedford limestone (order is 0.96 in 10 and 20 ppm SO_2)

The shrinking-core model for particles with unchanging size in five steps (Levenspiel, 1999) was adapted to the SO_2-marble reaction in this study. The first step is assumed a thin air film formation on the marble surface, and gaseous SO_2, diffusion through the film surrounding the particle to the surface of the solid marble. Afterwards, the penetration and diffusion of SO_2 through the blanket of ash (here refers formed sulfation products or crusts) to the surface of the unreacted core step is the second step. The reaction between gaseous SO_2 and solid marbles including calcite crystals at the

surface defines the third step. Then, fourth step is the diffusion of gaseous products through the ash back to the exterior surface of the solid. Finally, diffusion of gaseous products back into the system through the thin air film is the last step. Levenspiel (1999) also defined that these five steps as the rate controlling steps of the reaction. For instance, if no gaseous products are formed, steps 4 and 5 can be ignored. Furthermore, first three steps defined the reaction as the rate controlling step. The Table 3.3 gave conversion-time expressions for various shapes of particles for the shrinking-core model.

Table 3.3. The conversion-time expressions for various shapes of particles for the shrinking-core model (Source: Levenspiel, 1999).

Shape of particle	**Film diffusion control**	**Ash diffusion control**	**Reaction control**
Flat plate			
$\alpha = 1 - \frac{1}{L}$ L=half thickness	$\frac{t}{\tau} = \alpha$ $\tau = \frac{\rho_p L}{bK_1 C_A}$	$\frac{t}{\tau} = \alpha^2$ $\tau = \frac{\rho_p L^2}{2bD_e C_A}$	$\frac{t}{\tau} = \alpha$ $\tau = \frac{\rho_p L}{bK^n C_A}$
Cylinder			
$\alpha = 1 - \left(\frac{r_c}{R}\right)^2$	$\frac{t}{\tau} = \alpha$ $\tau = \frac{\rho_p R}{2bK_1 C_A}$	$\frac{t}{\tau} = \alpha + (1-\alpha)\ln(1-\alpha)$ $\tau = \frac{\rho_p R^2}{4bD_e C_A}$	$\frac{t}{\tau} = \alpha + (1-\alpha)^{\frac{1}{2}}$ $\tau = \frac{\rho_p R}{bK^n C_A}$
Sphere			
$\alpha = 1 - \left(\frac{r_c}{R}\right)^3$	$\frac{t}{\tau} = \alpha$ $\tau = \frac{\rho_p R}{3bK_1 C_A}$	$\frac{t}{\tau} = 1 - 3\left(1-\alpha\right)^{\frac{2}{3}} + 2(1-\alpha)$ $\tau = \frac{\rho_p R^2}{6bD_e C_A}$	$\frac{t}{\tau} = 1 - (1-\alpha)^{\frac{1}{3}}$ $\tau = \frac{\rho_p R}{bK^n C_A}$

The reaction controlling step can be assumed independently such as surface chemical reaction and ash or product layer controlled. These values were also calculated by shrinking core model for constant particle size (Levenspiel, 1999). For the constant particle size shrinking core model, some assumptions were used to calculate conversion

of the $CaCO_3$ to gypsum (X_B). Firstly, rectangular slabs assumed as spherical samples with constant particle sizes. Tambe et al. (1994; 1996) used the same assumption (i.e. rectangular slab as spherical samples) for previous approach of the shrinking unreacted core model. For this reason, initial radiuses of the assumed spherical marbles need to be converted from rectangular marble slabs by using the following equation (Tambe et al., 1994):

$$\frac{S_p}{V_p} = \frac{3}{R_0} \tag{3.18}$$

Where, S_p is the surface area of particle, V_p is the bulk volume of the particle, R_0 is the initial particle radius. Then, conversions of the $CaCO_3$ for the coated and uncoated marbles were calculated by using following equations (Levenspiel, 1999).

$$1 - X_B = \left(\frac{volume.of\ .unreacted\ .core}{total.volume.of\ .particle} \right) \frac{\frac{4}{3}\pi r_c^3}{\frac{4}{3}\pi R^3} = \left(\frac{r_c}{R} \right)^3 \tag{3.19}$$

$$\frac{1}{\tau} = 1 - \left(\frac{r_c}{R} \right)^3 = X_B \tag{3.20}$$

The values of the kinetic rate constants and the internal diffusion were calculated by using the linear regression analysis from the Table 3.3.

3.1.2. Rate Constants Regarding SO_2 + NO_2 Reaction

Concentrations of SO_2 and NO_2 gases in outdoor conditions can unpredictably change. However, in laboratory studies, experiments were conducted under controlled atmosphere. For this reason, adequate data should be collected in a short period of time. Moreover, presence of the NO_2 gas in the atmosphere makes choosing the best mathematical model due to existence of SO_2-NO_2 and complex NO_2-water reaction (Gauri and Bandyopadhyay, 1999). In the literature, overall reaction of the SO_2-NO_2-

calcite is represented with the following equation (Yerrapragada et al., 1994; Yerrapragada et al., 1996; Gauri and Bandyopadhyay, 1999)

$$2CaCO_3+SO_2+2NO_2+6H_2O+O_2 \rightarrow CaSO_4.2H_2O+Ca(NO_3)_2.4H_2O+2CO \qquad (3.21)$$

Yerrapragada and coworkers (1996) defined the equation of the crust growth rate for the case that the surface reaction is only controlled by the rate. C_{SO2} and C_{NO2} are the concentration of the gases, α_1 and α_2 are the orders of reaction and k_{sn} is the SO_2 + NO_2 reaction rate constant.

$$\frac{d\delta}{dt} = 2\alpha_n k_{sn} \frac{M_B}{\rho_B} C_{SO_2}^{\alpha_1} C_{NO_2}^{\alpha_2} \qquad (3.22)$$

If diffusion and mass transfer coefficients are incorporated in to the above equation, overall crust thicknesses can be approximated by using the following equation. In this equation, D_{en} is the effective diffusivity which is related with the combined SO_2 and NO_2 deposition upon the diffusion of Ca^{2+} ions to surface and h_d is the SO_2 mass transfer coefficient. k_{sn}, D_{en}, α_1 and α_2 can be calculated by using the following equation from experimental data with regression analysis. Moreover, δ is the crust thickness, M_B is the gram molecular weight of calcite (100.9) and ρ_B is the density of marble (2.714 g/cm^3) (Yerrapragada et al., 1996)

$$\left(\frac{1}{2D_{en}C_{SO_2}}\right)\delta^2 + \left(\frac{1}{k_{sn}C_{SO_2}^{\alpha_1}C_{NO_2}^{\alpha_2}} + \frac{1}{h_d C_{SO_2}}\right)\delta = 2\alpha_n \frac{M_B}{\rho_B} t \qquad (3.23)$$

Gauri and Bandyopadhyay (1999) conducted experiments to determine α_1 and α_2 by exposing marble slabs to 10 ppm SO_2 and NO_2 for 200 hours. The sulfate and nitrate ion ratios (α_1 and α_2) were 0.7, 0.3 respectively and these values were used for modeling the SO_2 + NO_2 reaction systems.

Deterioration of the carbonate stones were studied under laboratory and outdoor conditions (Yerrapragada et al., 1994; Yerrapragada et al., 1996; Gauri and Bandyopadhyay, 1999). Yerrapragada et al. (1996) studied the sulfonation reaction on Carrara marble in 10 ppm of SO_2 concentration present in an environmental chamber at

laboratory and 10 ppb of SO_2 and 25 ppb NO_2 concentration in outdoor conditions. The k_{sn} and D_{en} values were calculated as 312 cm/h and 0.14 cm^2/h in laboratory and 375 cm/h and 0.11 cm^2/h in lab condition and outdoor respectively. Yerrapragada et al. (1994) exposed Carrara marbles to the ambient air that had 10 ppb SO_2 and 25 ppb NO_2 in six sites throughout Louisville, Kentucky up to 20 months. The calculated k_{sn} and D_{en} by using regression analysis were 395 cm/h and 0.13 cm^2/h respectively.

CHAPTER 4

POLYMER BIO-NANO COMPOSITES

4.1. Biodegradable Polymers

Polymer is known as a chemical compound or mixture of compounds composed of repeating structural units and forms after the polymerization process (Gooch et al., 2010). Polymers can be expressed as very high molecular weight covalently bonded long-chain molecules according to their chemistry (Sperling et al., 2006) and classified as synthetic (man-made) and natural polymers (bio-based) by source. There are many natural polymers in nature such as wood, leaves, fruits, seeds and animal furs and they have been used for food, clothing and furniture through the ages (Shen et al., 2009).

The first synthetic polymers such as phenol-formaldehyde resin and bakelite were discovered in the first decades of the 20^{th} century (Nair and Laurencin, 2006). Current consumptions of the synthetic polymers in the worldwide reached 200 million tones with 5% annual growth (Siracusa et al., 2008). Synthetic polymers are petroleum derived and non-degradable polymers. Ever since non-degradable synthetic polymers have been come into life, they have been used in very wide range of significant applications such as packaging, agriculture, food, consumer products, medical appliances, building materials, industry, and aerospace materials. However these polymers have negative effects on the environment due to their resistance against physical, chemical and biological degradation. Their degradation in the environment takes long time and their huge consumption caused the extensive solid waste accumulation in the last century. Additionally, non-degradable polymers are thought to be contributing global warming due to carbon dioxide release by their incineration. Therefore, the usage and acceptability of the synthetic non-degradable polymers have been begun to diminish in some areas such as agriculture, surgery, pharmacology, packaging and the environment (Dorgan et al., 2001; Luckachan and Pillai, 2011).

The biodegradable biopolymers have been attracted attention in academic researches and industrial applications due to their attractive properties such as biocompatibility, biodegradability and low-toxicity in degradation (Luckachan and

Pillai, 2011). Their water and gas barrier properties are also comparable with synthetic ones (Weber et al., 2000). Commonly, the biobased polymers were used for the food packaging materials relating to some criteria such as water vapor, gas, light, aroma barrier properties, optical properties like transparency, temperature and chemical resistance, antistatic, strength, welding and molding, marking and printing properties and migration/scalping requirements (Haugaard et al., 2001). Although an important fraction of biobased polymers obtained from the renewable materials. Biodegradable plastics can be produced by using petrochemical raw materials and bio-based feedstock. Shen and coworkers (2009) represented degrability of biodegradable polymers from various sources in the Figure 4.1.

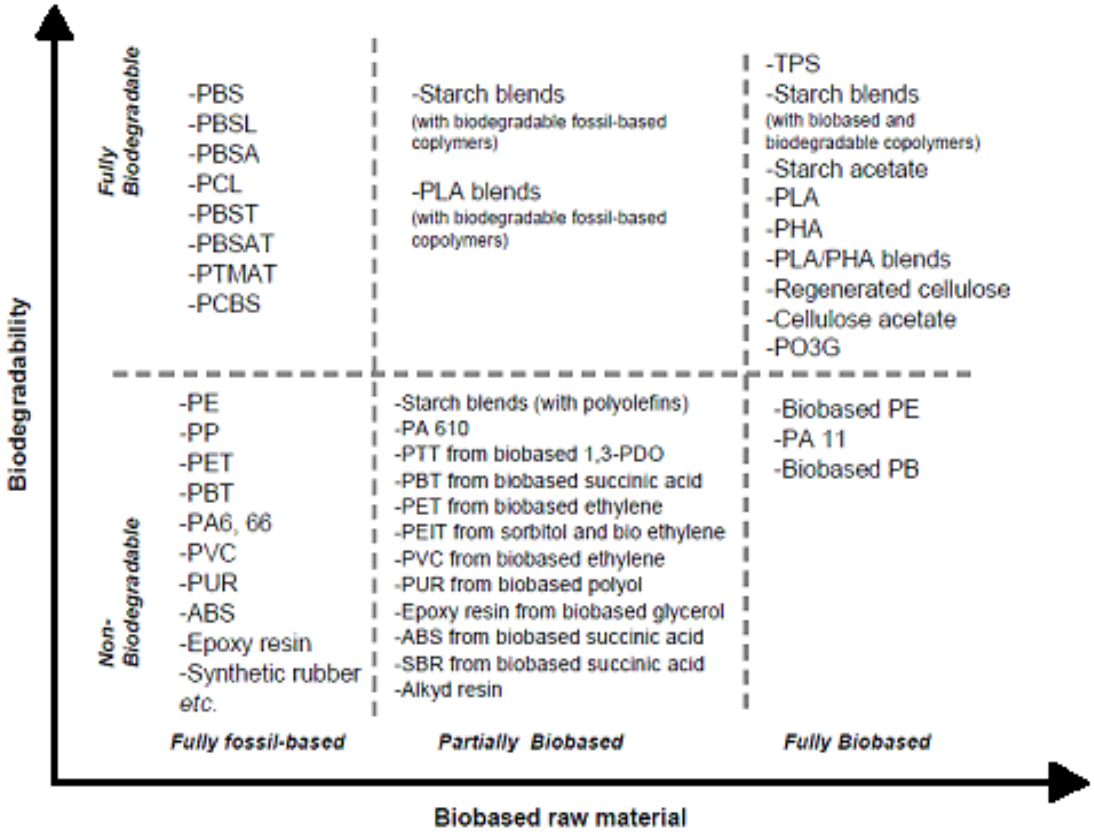

Figure 4.1. Biodegradability of biobased raw materials
(Source: Shen et al., 2009).

The derivatives of the polysaccharides, proteins and lipids belong to the directly extracted from biomass type polymers. Use of classical chemical synthesis comprises renewable biobased monomers such as polylactide. Polylactide (PLA) polymerized from lactic acid monomers. Polymers produced by microorganisms or genetically modified bacteria is the another group of biobased polymers. The

polyhydroxyalkonoates (PHA) can be expressed as a good example for this category. Biobased polymers origins and their production methods for three categories were represented in following Figure 4.2 (Weber et al., 2000 and 2002).

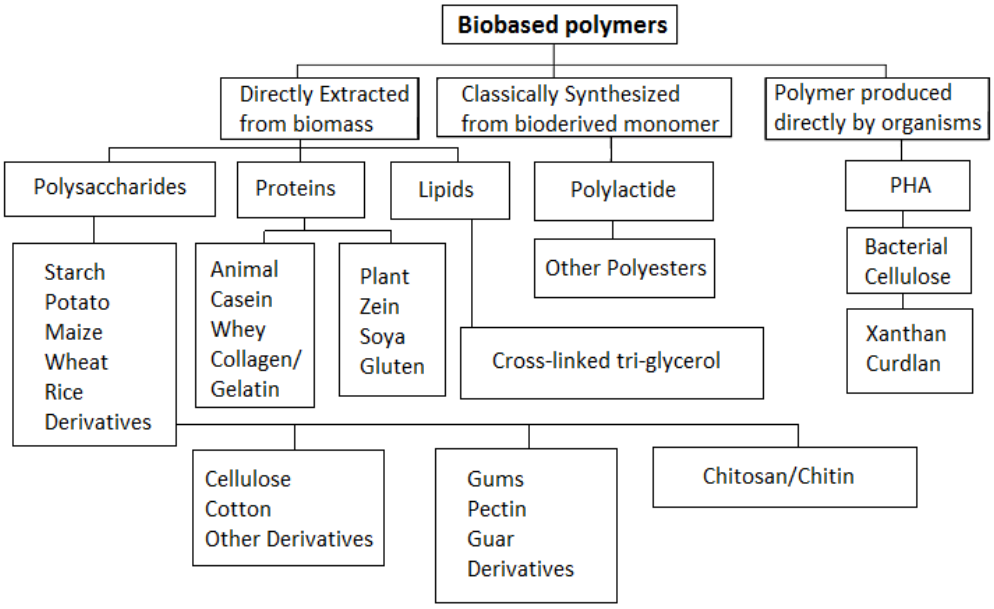

Figure 4.2. Biobased polymers based on their origin and method of production (Source: Weber et al. 2000).

Applications of the biodegradable polymers were subject of many researches. Nair and Laurencin (2006) showed the use of biodegradable polymers in medical applications; tissue engineering such as liver, bone, cartilage, skin and nerve regeneration, and controlled drug delivery. Similarly, Chandra and Rusthi (1998) expressed the medical applications of the biodegradable polymers in surgical sutures, bone fixation devices, vascular grafts, adhesion prevention, artificial skin and drug delivery systems, agricultural applications as agricultural mulches, controlled release of agricultural chemicals and agricultural planting containers and packaging application. Aliphatic polyesters (PLA/PLAGA) were used for bone regeneration due to their good osteocompatibility and adherent cells properties (Nair and Laurencin, 2006). Poly(3-hydroxybutyrate-co-3-hydroxyvalerate) P(3HB-3HV) was used to control insecticides in agricultural field. The insecticides were combined with the P(3HB-3HV) pellets and saved the farmer crops. Furthermore, polyhydroxyalkanoates (PHAs) in bacterial inoculants was used to increase the fixation of nitrogen in plants (Philip et al., 2007)

The commercial use of fully biodegradable cellulose acetates in osmotic drug delivery and taste-masking, coatings, pressure sensitive tapes, packaging and wood sealers are common. Water resistant biopolymers such as Poly (ε-caprolactone) (PCL), polyhydroxylalkanoates (PHAs) and poly(lactic acid) (PLA) especially used to obtain sheets, bottles, and diverse shaped products with melt-extrusion method instead of synthetic polymers due to water barrier properties (Guzman et al., 2011). The packaging materials should provide a constant gas concentration inside the package for food packaging applications. Therefore, a gas barrier property of the packaging material is critical (Weber et al., 2000, 2001; Haugaard et al., 2001; Guzman et al., 2011). Weber et al. (2000) gave the comparison of the oxygen permeability of biobased materials and conventional mineral-oil-based materials at 23 ºC and 50% RH which showed that biobased materials also have comparable gas barrier properties to that of synthetic polymers.

They also reported higher water vapor transmittance rates for biobased polymers are than some conventional mineral-oil-based plastics. Very few biobased materials showed high water vapor barrier such as PLA and PHB. They mentioned that the increase in humidity may decrease manifold the gas barrier properties of the hydrophilic biobased packaging materials. However, gas barrier properties of the PLA and PHA are not affected from the humidity (Weber et al. 2000). Due to their biodegradable and biobased structure and good gas and water barrier properties, PLA is thought as promising surface coating material to protect marble monuments.

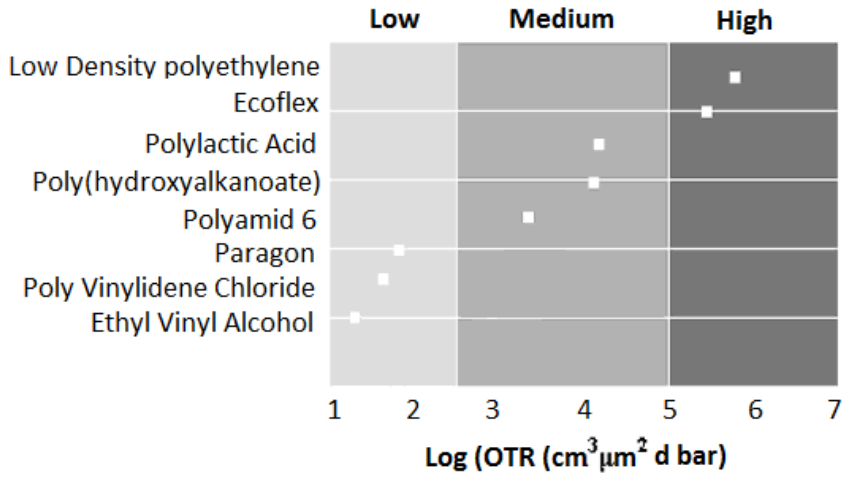

Figure 4.3. Oxygen permeability of bio and mineral-oil-based materials (@ 23 ºC, 50% RH) (Adapted from Weber et al. 2000).

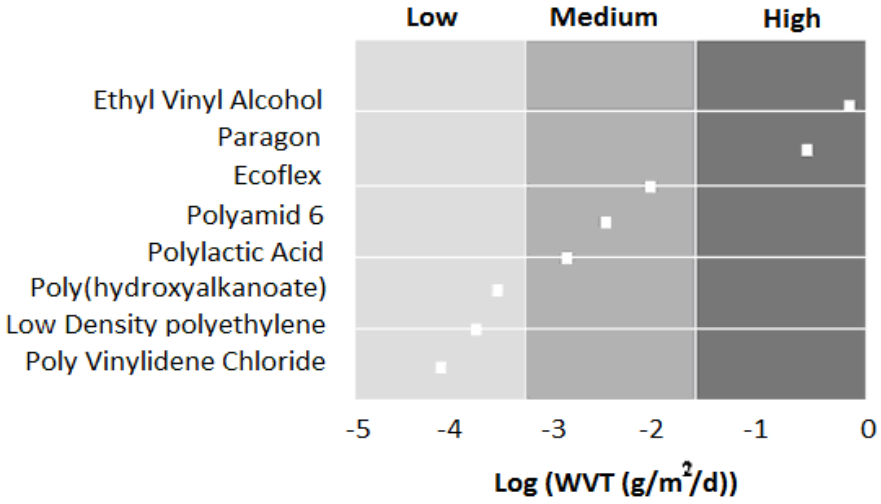

Figure 4.4. Water vapor transmittance of bio and mineral-oil-based materials (@ 23 ºC, 50% RH) (Adapted from Weber et al. 2000).

4.1.1. Polylactic Acid (PLA)

Poly(lactic acid) (PLA) has been attracting increasing interest in academic and industrial areas such as agricultural, cosmetics, biomedical, food, wastewater management and environmental fields in recent years (Luckachan and Pillai, 2011). PLA is the polyesters which is usually hard and brittle (Södengard and Stolt, 2002). Furthermore, biological and chemical routes can be used for the PLA production. The biological synthesis can be classified as an environmentally friendly technique because PLA is fermented from sugar beet, sugar cane, corn, potatoes, and other biomasses. PLAs are the fully biodegradable biobased polymers which totally biodegradable over 333 K. Their biodegradation process and lifecycle in the environment are represented in Figure 4.5. After the biodegradation of the PLA, the microorganisms play a significant role to metabolize CO_2, H_2O and biomass (Guzman et al., 2011).

PLA have numerous advantages such as ability to recycle back to lactic acid (non-toxic) and so reduction of landfill volumes (Södengard and Stolt, 2002). The lactic acid can be derived from intermediates with renewable origins such as acetaldehyde and ethanol, or from chemicals derived from coal like acetylene, or oil like ethylene. Lactic acid (2-hydroxypropanoic acid) is one of the smallest optically active molecules, which can be either of L (+) or D (-) stereoisomer (Södengard and Stolt, 2002). PLAs can be produced in four forms such as poly(D-lactic acid) (PDLA), poly(L-lactic acid) (PLLA),

poly(D,L-lactic acid) (PDLLA) and meso-poly(lactic acid). The three stereoforms of lactide are represented in following Figure 4.6. Mostly used PLAs in the biomedical researches are PLLA and PDLLA. Furthermore, PLLA is used for bone fixation and bone, cartilage, neural, tendon, and vascular regeneration (Nair and Laurencin, 2006; Ulery et al., 2011). Furthermore, Ulery et al. (2011) summarized the advantages of the polylactide as highly processible and many commercial vendors available for application on tissue engineering and drug delivery.

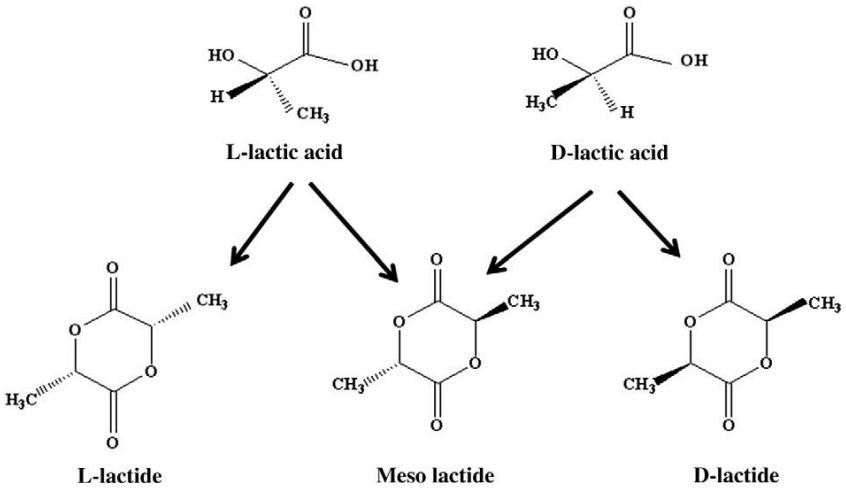

Figure 4.5. Stereoforms of lactide
(Source: Nampoothiri et al., 2010)

Solid state morphology and crystallinity affects the physical, mechanical and barrier properties of the PLA. The stereochemistry and thermal history of the PLA can cause either amorphous or semi-crystalline structure (Lim et al., 2008). Nampoothiri et al. (2010) reported that poly-DL-lactide (PDLLA) which is synthesized from the racemic mixture of L- and D-lactides has amorphous structure. D to L enantiomers usage ratio controlled the degree of crystallinity for heterotactic PLA. In addition to that, pure polylactides, poly (D-lactide) (PDLA) and poly (L-lactide) (PLLA) are semi-crystallines. Furthermore, the PLA materials have good water vapor barrier and have also relatively low gas transmittance (Weber et al., 2002). PLA is used as packaging materials for milk and cheese because of their high moisture barrier compared to the conventional HDPE bottles and PE-laminates (Weber et al., 2000). Due to its desirable properties, biodegradable biopolymers have been encouraged hope for protection studies as coating materials.

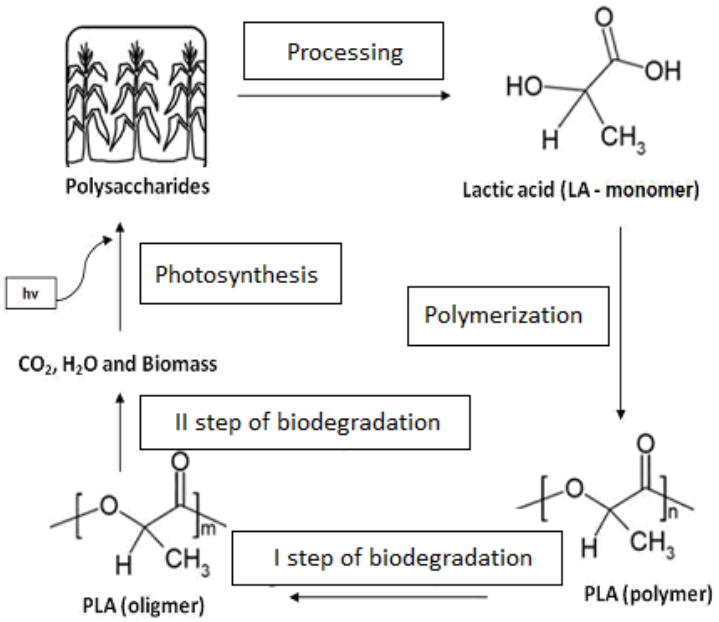

Figure 4.6. Life cycle of poly(lactic acid)
(Source: Guzman et al., 2011)

Recently, biodegradable polymers were used as a coating agent and showed good potential for stone protection (Ocak et al., 2009). Reversibility, degradability and allowance for a new treatment of the biodegradable polymers fulfill the principles generally accepted by the International Conservation Community (Chiellini and Solaro, 1996; Chiellini and Solaro, 2003). However, their mechanical properties are not strong enough compared to that of synthetic polymers. Layered silicate added bio-nanocomposites are used to overcome this problem and showed significant improvements in polymer properties such as mechanical and barrier properties.

4.2. Nanoparticles

A wide range of commercially available nanoparticles were added to polymer matrix to obtain polymer nanocomposites which had improved properties. Most widely used nanoparticles can be listed as;

- Nanoclays (MMT, bentonite)
- Nanosilica (N-silica)
- Nanoaluminum oxide (Al_2O_3)

- Polyhedral oligomeric silsesquioxane (POSS)
- Carbon Nanofibers (CNFs)
- Carbon nanotubes
- Nanotitanium oxide (TiO_2)

Layered silicate nanoclays are the most widely used nanoparticles due to their application versatility and improvement effectiveness.

4.2.1. Nanoclays

Layered silicate nanoclays like montmorillonite organoclays (MMT) are the most widely studied nanoparticles for the different types of the polymer matrices in the literature (Shen et al., 2002; Ha et al., 2007; Scarfato et al., 2012). The natural clay (bentonite) can be obtained by using two different routes such as in-situ alteration of volcanic ash (generally) and hydrothermal alteration of volcanic rocks (less common). Bentonite not only contains montmorillonite but also kaolinite, glass, illite, mixed layer clays, zeolite, and carbonates (Koo et al., 2006). The nanoclay addition in the polymer matrixes considerably improved the morphological, thermal, rheological, mechanical and barrier properties of the polymers (Alexander and Dubois, 2000; Rhim et al., 2009; Tabatabaei et al., 2011; Chafids et al., 2011). Layered silicates can be classified into three groups; 1:1, 2:1 and 2:2 unit crystal lamellae types. 1:1 types unit lamellar crystal is comprised of silica tetrahedron one crystal sheet combined with one-crystal lamellae of alumina octahedron. 2:1 type unit lamellar crystal is comprised of silica two crystal sheets tetrahedron combined with one crystal sheet of alumina octahedron between them. 2:2 type unit lamellar crystals is comprised of four crystal sheets, in which crystal sheets of silica tetrahedron and alumina or magnesium octahedron are alternately arranged (Ke and Stroeve, 2005). Ray and Okamato (2003) pointed out that most prevalently used layered silicates are the montmorillonite, hectorite, and saponite. Ray and Okamato (2003) reviewed the structure and chemistry for these layered silicates in detail (Table 4.1, Figure 4.7) (Ray and Okamato, 2003).

Montmorillonite particles are comprised of alumina-silicate layers or platelets (one layer physical dimensions may be 100 nm in diameters and 1nm thickness) with a regular gap between interlayer's and each layers included a central Al-octahedral sheet

which was joined together by fusing two tetrahedral silicon sheets. Moreover, an aluminum atom is surrounded by eight oxygen atoms for in the octahedral sheets and silicon is surrounded by four oxygen atoms in the tetrahedral sheets. Isomorphic substitutions of aluminum by magnesium in the octahedral sheet turn out negative charges and these negative charges are make amends for by alkaline-earth- or hydrated alkali-metal cations (Figure 4.7) (Alexander and Dubois, 2000; Ke and Stroeve, 2005; Mittal et al., 2009)

Table 4.1. Chemical formula and characteristic parameter of commonly used 2:1 phyllosilicates (Source: Ray and Okamato, 2003).

2.1 phyllosilicates	Chemical Formula	Particle length (nm)
Montmorillonite	$M_x(Al_{4-x}Mg_x)Si_8O_{20}(OH)_4$	100-150
Hectorite	$M_x(Mg_{6-x}Li_x)Si_8O_{20}(OH)_4$	200-300
Saponite	$M_xMg_6(Si_{8-x}Al_x)Si_8O_{20}(OH)_4$	50-60

M, monovalent cation; x, degree of isomorphous substitution (between 0.5 and 1.3)

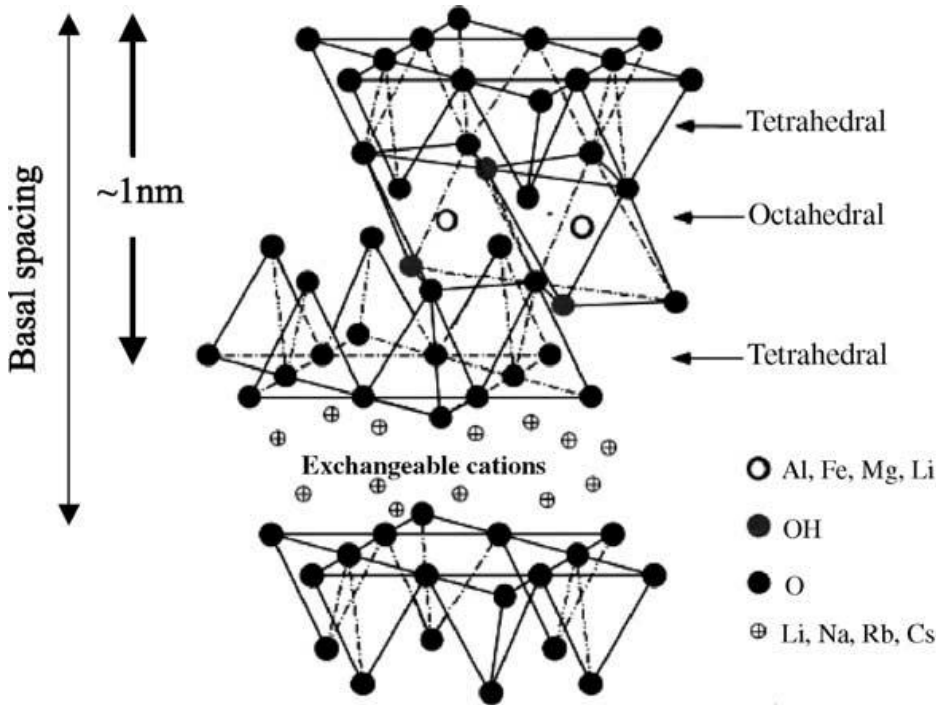

Figure 4.7. Structure of 2:1 phyllosilicates (Source: Ray and Okamato, 2003).

Possible structure of polymer layered silicate nanocomposites depending on the dispersion of nanoparticles in the polymer matrix can be classified as: unintercalated (phase separated), intercalated and exfoliated composites (Figure 4.8) (Mittal et al., 2009). If the individual layered silicates platelets are totally delaminated in the polymer matrix with nanometers of average distance, the composite microstructure is classified as exfoliated (fully delaminated) (Ray and Okamato 2003; Mittal et al., 2009). If single or sometimes more than one extended polymer chain is inserted into the structure of the layered silicate with a crystallographically regular fashion, the composite microstructure is classified as intercalated (partially delaminated) nanocomposites. Generally, higher nanoclay content results in intercalated structure rather than exfoliated. Intercalated structure points out that organic-inorganic hybrid is formed but electrostatic interaction forces between the nanoclay platelets could not be completely maximized (Ray and Okamato 2003; Mittal et al., 2009). Phase separated structures are acquired due to the poor molecular interaction between layered silicates and polymer matrix which may have similar properties of the conventional composites (Ray and Okamato 2003; Mittal et al., 2009).

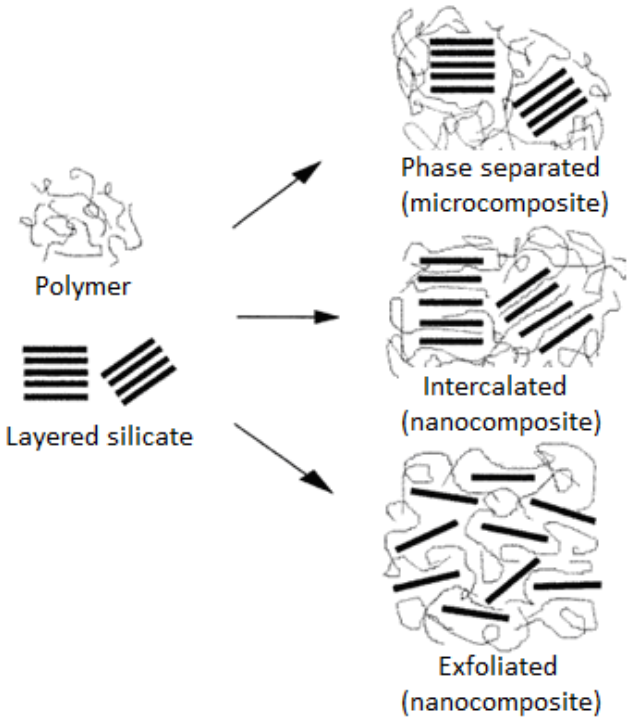

Figure 4.8. Schematic representation of the different types of composites (a) Phase separated microcomposite, (b) intercalated nanocomposite and (c) exfoliated nanocomposite (Adapted from Mittal et al., 2009).

The production methods of the polymer nanocomposites can be classified into three groups according to the processing technique and starting materials; template synthesis, intercalation of polymer or prepolymer from solution, *in-situ* intercalative polymerization and melt intercalation. Template synthesis is not commonly used polymer nanocomposite preparation method, since the method involves in-situ synthesis of the inorganic materials. On the other hand, in the other commonly used synthesis techniques polymer materials are synthesized in the presence of silicate nanoparticles (Mittal et al., 2009). In the intercalation polymerization technique, the organomodified silicate is dispersed in a solvent which can solve the polymer (Ray and Okamato 2003; Mittal et al., 2009). In the *in-situ* intercalative polymerization technique, the layered silicate is swollen in monomer or monomer solution and polymer formation can realize between the intercalated sheets (Ray and Okamato 2003; Mittal et al., 2009). On the other hand, in the melt intercalation method, above the softening point of the polymer at high temperature first the polymer is melted and the filler is blended with the polymer melt under shear (Ray and Okamato 2003; Mittal et al., 2009).

4.3. Polymer Nanocomposites

Nanocomposites can be basically described as particle filled polymers which included nanometer range dispersed particles. This nanometer sized particles are called nanoparticles. Ogata and coworkers (1997) pointed out that nanoparticle added polymers had significantly different chemical and physical properties both in micro and macro scale. Koo (2006) pointed out that the nanoparticles additions to the polymer matrix provide some advantages and disadvantages. The mechanical properties such as stiffness, toughness and tensile strength, gas and water barrier properties, thermal expansion and conductivity, synergistic flame retardant additive, dimensional stability, ablation and chemical resistance and reinforcement can be listed as advantageous improvements. On the other hand, increase of the viscosity which restricted the processability of the nanocomposite, dispersion difficulties, sedimentation, optical issues and black color which resulted generally for carbon containing nanocomposites can be listed as disadvantages of the nanoparticle addition (Koo et al., 2006). Several studies draw attention to some factors effecting the polymer nanocomposites properties; the nature of the polymer matrix (polymer chemistry, crystallinity, molecular weight

and whether thermoplastic or thermosetting properties of the polymer); types of the nanoparticles and their surface treatment; polymer nanocomposite morphology and synthesis methods (solvent blending, in-situ polymerization, melt compounding, and emulsion polymerization) (Koo et al., 2006; Mittal et al., 2009).

Nanoparticle addition to the polymer matrixes increased the stiffness, toughness, optical, electronic, magnetic, catalytic, chemical, tribological, morphological, thermal, rheological, mechanical, barrier properties**,** resistance to fire and ignition of the polymer and decreased brittleness or opacity (Alexander and Dubois, 2000; Zanetti et al., 2000; Zhang et al., 2003; Rhim et al., 2009; Sharma et al., 2009; Tabatabaei et al., 2011; Chafids et al., 2011). For these reasons, nanocomposites are basically used in various applications such as food, automotive, medical, agriculture and construction industries. Moreover, clay and silica minerals have been widely used in polymer matrix due to their low toxicity and availability (Alexandre and Dubois, 2000; Zanetti et al., 2000).

Many nanocomposites have been used for the protection studies in recent years. For instance, silicone containing polymer matrices (Zielecka and Bujnowska, 2006), silica nanoparticles added siloxane protective composition matrices (Manoudis et al., 2009), silica added Poly(methyl methacrylate (PMMA) and perfluorinated polyether (PFPE) polymer matrices (Manoudis et al., 2007), nanosilica added flouroalkylsilane coatings (Su et al., 2006), organoclay added epoxy and silane coating agents (Christopher et al., 2008) and organomodified montmorillonite (Cloisite 30B) added Fluoline CP and Antipluviol S resins (Scarfato et al., 2012) were applied to the stone surfaces and their protection capabilities were investigated against water effects on the stones (Zielecka and Bujnowska, 2006; Su et al., 2006; Manoudis et al., 2007; Christopher et al., 2008; Manoudis et al., 2009). Nanoparticle addition into polymer increased the surface hydrophobicity and decreased the water action effects on the coated marble samples (Manoudis et al., 2009 and 2007).

4.3.1. Polylactide Layered Silicate Bio-nano Composite (PLA/MMT)

Poly(lactic acid) (PLA) have been used in industrial areas such as agricultural, cosmetics, biomedical, food, wastewater management and environmental fields (Luckachan and Pillai, 2011). PLA synthesis is the environmentally friendly technique and PLA is the fully biodegradable (Guzman et al., 2011). Moreover, nanoclay addition

in the polymer matrixes improved the morphological, thermal, rheological, mechanical, barrier properties of the polymers (Alexander and Dubois, 2000; Rhim et al., 2009; Sharma et al., 2009; Tabatabaei et al., 2011; Chafids et al., 2011).

Jong-Whan et al. (2009) used different types of Cloisite Na^+, Cloisite 30B and Cloisite 20A nanoclays added PLA nanocomposites by using solvent casting method and determined water vapor permeability of the nanocomposites. The group reported Cloisite 20A nanocomposite as the most efficient and achieved to decrease water vapor permeabilities by 6-33%. Kumar and coworkers (2010) used Cloisite 20A and organically treated montmorillonite by using melt blending technique and they reported improved mechanical, thermal and morphological properties. Harintharavimal et al. (2010) studied organophilic modified montmorillonite added PLA bio-nano composites to investigate mechanical, thermal and morphological properties. They observed the same results which were obtained from the previous studies and they defined that nanoparticle addition enhanced the mechanical, thermal and morphological properties of PLA. Rhim et al. (1999) studied the tensile, water vapor barrier and antimicrobial properties of the Cloisite Na^+, Cloisite 30B and Cloisite 20A nanoclays added PLA bio-nano composites. They pointed out that bio-nano composite usage decreased the tensile strength, elongation at break and water vapor permeability as 10–20%, 11–17% and 6–33%. Koh et al. (2008) studied the Cloisite 15A, 20A and 30B added bio-nano composite membranes prepared by solution casting method and they achieved improved gas and water vapor barrier by increasing the nanoclay content.

Gas and water vapor barrier properties play significant role in the protection studies, since gas pollutants and water vapor enhance the deterioration of the carbonate stones. Layered silicates dispersed in polymer matrix force a tortuous pathway for the permeating gas molecule. Permeability of the nanocomposites are mainly affected by three significant factors such as layered silicate volume fraction, aspect ratio of width/thickness (in the order of 10-1000) and their orientation relative to the diffusion direction. The Fick's law is generally assumed for the transport mechanism within the polymer matrix which keeps up the same properties and characteristics like neat polymer. In the nanocomposites, polymer matrix volume is reduced and solubility is anticipated to decrease. Moreover, diffusion of the molecules is decreased due to more tortuous nanoparticle path in the polymer matrix. Moreover, shape and the degree of dispersion (degree of delamination) of the nanoplatelets mainly affect the tortuosity and diffusion of the molecules. The values of the tortuosity factor and the aspect ratio for

the exfoliated (fully delaminated) are higher than intercalated (partially delaminated). For this reason, exfoliated structures are more desired due to their effective barrier properties for gases (Choudalakis and Gotsis 2009). Zenkiewicz and coworkers (2008) studied to determine the permeability of polylactide nanocomposite films which were prepared by using two types of montmorillonite nanofillers (Cloisite 30B and Nanofil 2), two kinds of organic modifiers (poly(methyl methacrylate) and ethylene/vinyl alcohol copolymer) and two types of compatibilizers (polycaprolactone and poly(ethylene glycol)) as water vapor, oxygen and carbon dioxide barriers . They determined that Cloisite 30B was more effective and decreased the permeability compared to Nanofil 2 and the best barrier properties were obtained from the samples containing 75, 5, and 20 wt% of polylactide, Cloisite 30B, and poly(methyl methacrylate). The sample reduced the transmission rates of water vapor, oxygen, and carbon dioxide as 60, 55 and 90%, respectively (Zenkiewicz et al., 2008).

The nanoparticle improvements of the barrier, mechanical, thermal and morphological properties of biodegradable polymers are clear and bio-nano composite coating agents have not been tested yet for the protection of the carbonate stones in laboratory or outdoor conditions until now.

CHAPTER 5

EXPERIMENTAL METHOD

Experimental work in this study consists of two main parts: sulfation experiments in laboratory reaction chamber and field experiment in ambient air conditions. Before starting to exposure experiments, characterization of the bio-nano composites and surface properties of the coatings were also investigated. Prepared samples were coded as coated marble, C; uncoated marble, UC; 2 wt.% montmorillonite nanoclay added PLA, PLA/MMT2; 5 wt.% nanoclay added, PLA/MMT5; and 7wt.% nanoclay added composites PLA/MMT7. The numbers accounts for the weight percentage of the nanoclay content.

Table 5.1. Samples and conducted analysis before exposure.

Experiments	**Analysis**	**Method**	**Samples**	**n= Sample Numbers**
Film Properties	Structural characteristics of composite films	XRD	MMT and PLA/MMT2, 5 and 7 films	4F
	Dispersion of LS-polymer matrix	AFM	PLA/MMT2, 5 and 7 films	3F
	Dispersion of LS in PLA	STEM	PLA/MMT5 film	1F
Surface properties of coated marbles	Surface hydrophobicities	WCA	PLA, PLA/MMT2, 5 and 7 C and UC marbles	12 C and 3 UC
	Water absorption	WCAB	PLA, PLA/MMT2, 5 and 7 C and UC marbles	12 C and 3 UC
	Water Vapor Permeability	WVP	PLA, PLA/MMT2, 5 and 7 C and UC marbles	12 C and 3 UC
	Color Change	CA	PLA, PLA/MMT2, 5 and 7 C and UC marbles	12 C and 3 UC

XRD: X-ray Diffraction Analysis, AFM: Atomic Force Microscopy, STEM: Scanning transmission electron microscopy, WCA: Water Contact Angle, WCAB: Water Capillary Absorption, LS: Layered Silicates, CA: Color Alteration, C: coated, UC: uncoated, F: Film

Table 5.2. Samples and analysis in reaction chamber and outdoor conditions

Experiments	Analysis	Method	Exposure Time (days)	n= Sample Numbers
Laboratory conditions	Gypsum crust formation and kinetic parameters	IC SEM	15, 32, 60, 90, 120, 150 and 180	4C, 4SC, 1UC
	Coating thicknesses effect	IC SEM	30	12C
	Statically compare of results with triplicate samples	IC	30	12C, 3UC
Outdoor Conditions	Gypsum and nitro-calcite crust Time-course analysis	IC SEM	180, 270 and 600	12C, 12 SC, 3UC
	Coating thicknesses effect	IC SEM	180	12C
	Statically compare of results with triplicate samples	IC	180, 270 and 600	12C
	Surface hydrophobicities after exposure	WCA	600	4C, 1UC
	Coating transparency of coatings after exposure	CA	600	4C, 1UC
	Gypsum and nitro-calcite formation after exposure	FTIR	600	4C, 1UC

IC: ion chromatography, SEM: scanning electron microscopy, WCA: Water Contact Angle, FTIR: Fourier Transform Infrared, CA: Color Alteration, C: coated marble, UC: uncoated marble, SC: semi-coated marble

5.1. Marble Slabs and Bio-nano Composites Preparation and Coating of the Marbles

The rectangular slabs were cut from Marmara marble ((1cmx1.5cmx0.15cm) for laboratory and (7cmx5cmx0.2cm) for outdoor experiments) and polished with 400-grit silicon carbide powder. The polished slabs were cleaned by using ultrasonic bath in deionized water to remove fine particulates on the marble surfaces. The cleaned marble slabs were dried at 105 ºC, and cooled in a desiccator till to reach a constant weight. The weights of marble slabs were then recorded to check any possible water adsorption.

In this study, poly-L-Lactide (PLA) (PL65-1.24 g/cm^3, purchased from Purac) were prepared by using surface modified clay (Cloisite 10-A). The Cloisite 10-A (Southern Clay Products Inc.) is a natural montmorillonite (MMT) modified with a

quaternary ammonium salt (dimethyl, benzyl, hydrogenated tallow, quaternary ammonium) with an interlayer distance of 1.92 nm.

First of all, PLA biodegradable polymer (3% by w/v) was dissolved in chloroform. Then, solution was stirred approximately eight hours at room temperature. Simultaneously, different concentrations of MMT nanoparticles were also dispersed in chloroform in separate beakers. These solutions were stirred approximately fifteen hours at room temperature. After stirring, the nano particle dispersions were sonicated by using an ultrasonic probe sonicator (MISONIX 20±0.005 kHz.) for an hour at 15°C. Then, nanoparticle dispersion and polymer solution were stirred for an hour at room temperature prior to final one hour sonication at 15°C. Finally, 2 %, 5 % and 7 % by weight montmorillonite added nanocomposites were obtained. The prepared nanocomposite solutions were used for coating marble slabs by using dip-coating apparatus (Nima convert mechanism (dipper mechanism type D1L and micro-processor interface IU4)) at room temperature with 100 mm/min immersion rate and 150 mm/min retraction rate. Marble slabs were left for 30 second in the bio-nano composite solution between the immersion and retraction steps. Afterwards, solvent was removed from coatings by keeping in oven at 40 °C for several hours. The average thickness of coating was varied between 15-25 μm and the calculated amounts of the coating agent on the each marble surface were ranged between 4 and 5 g/m^2 for the all coated marbles.

5.2. Characterization and Surface Analysis of the Marble Surfaces

X-ray diffraction (XRD), Atomic Force Microscopy (AFM), Tunneling Electron Microscopy (TEM) and Scanning TEM coupled with energy dispersive X-ray (EDX) are the techniques most commonly used to characterize coated and uncoated surfaces. These analysis techniques also used to understand the polymer nanocomposite structures which were exfoliated or intercalated nanocomposites in the previous studies (Alexandre and Dubois, 2000). In this study, structural characteristics of the nanocomposites and quantitative information of the d-spacing and dispersion of layered silicates in the polymer matrix were investigated by using XRD and AFM analysis. Scanning transmission electron microscopy (STEM) analyses also used to investigate

qualitative information of the d-spacing and dispersion of nanoclays in the polymer matrix.

5.2.1. X-ray Diffraction Analysis (XRD)

The structural characteristics of coatings after evaporation of solvents were determined by XRD analysis which is the most generally used technique for obtaining first information from the nanocomposite structures (Bruno et al., 2008; Olad et al., 2011). The XRD spectra were obtained by using a Philips X'Pert Pro MRD operated at 40 kV and 40 mA, equipped with Cu Kα radiation at a wavelength of 1.54 nm. XRD analyses were conducted in the range of 2° and 8°. The basal spacing (d_{001}) of the layered silicate interlayers were calculated by using Braggs' equation.

$$\lambda = 2 \times d \times \sin\Theta \qquad (5.1)$$

Where λ is the wavelength of X-ray, θ is the diffraction angle and d is the interlayer distance (Rhim et al., 2009).

5.2.2. Atomic Force Microscopy (AFM)

The AFM analysis is an effective tool to investigate the nanocomposite coating surfaces even down to the nanometer scale (Camargo et al., 2009). AFM analysis can be used to understand the level of dispersion of the layered silicate nano particles in PLA polymer matrix. AFM analysis with tapping mode is generally used to obtain intrinsic contrast between soft polymer matrix and hard inorganic silicate nano particles (Liu et al, 2003). AFM was performed with a Nanoscope IV Multimode Scanning Probe Microscope (MMSPM) manufactured by Digital Instruments, Inc. with tapping mode. It was used to characterize the 2, 5 and PLA/MMT7 bio-nano composites.

5.2.3. Scanning Transmission Electron Microscopy (STEM)

STEM analysis plays a significant role on the characterization of nano-materials micro-structure from micron to atomic scale (Wang et al., 2007). Scanning electron

microscope (SEM) device which included STEM detector was used to prove nanoparticle structure in the bio-nano composite. PLA/MMT5 bio-nano composite was selected due to good barrier performances against water vapor and SO_2 gas and protection properties. Casted PLA/MMT5 was prepared for cutting to nano slices by using nanotome device and these slices were replaced carefully on the grids and STEM images of the layered silicates were obtained.

5.2.4. Determination of the Total Sulfate

SO_2 and NO_2 are known as important precursors of the formation of acidic deposition; therefore, they are responsible for deformation of the marble monuments. The reactions start with SO_2 and NO_2 results in gypsum ($CaSO_4.2H_2O$) and nitrocalcite ($Ca(NO_3)_2.4H_2O$) on the surface of stone. Gypsum is formed under two reaction steps (eqns 2.8-2.9). Calcium sulfite hemihydrate ($CaSO_3.1/2H_2O$) does not dissolved in water but it can be easily transformed to gypsum which dissolves in water. Total sulfate concentration was measured. Exposed slabs were immersed into 25 mL of ultra-pure water and 2% H_2O_2 for 72 hours in order to convert all the sulphation products to gypsum. Similarly, exposed and unexposed marble slabs were immersed into 100 mL of ultra-pure water and 2% H_2O_2 for 120 hours for the conversion of all sulphation products to gypsum and dissolved nitrocalcite for outdoor experiments. Later the dissolved sulfate and nitrate in water were analyzed with IC (Dionex with GP50 Gradient Pump and ED50 detector). IC calibration standards were prepared 2.3, 4.7, 7.4, 9.8, 12.5 and 15.4 ppm concentration from sulfate standard solutions.

5.2.5. Determination of Microstructures and Morphologies by Using Scanning Electron Microscopy (SEM)

Scanning electron microscope (Philips XL-30- SFEG equipped with an Energy Dispersive 34 X-ray (EDX) analyzer) analysis have been carried out to determine the microstructures and morphologies of coated and uncoated marble samples before and after exposure. Magnifications varying from 200 to 2000 were used in investigations.

5.2.6. Determination of Sulphation Products by Fourier Transform Infrared (FTIR)

FTIR analysis was done to monitor any change on the chemical structure of the nanocomposites and to determine the sulfation reaction products after 20 months of outdoor exposure by comparing the before exposure FTIR data. FTIR spectrum of pure calcium carbonate appeared as a strong band centered around 1453 cm^{-1}, characteristics of the C-O stretching mode of carbonate together with a narrow band around 873 cm^{-1} of the bending mode (Böke et al., 1999). The observed bands around 980 cm^{-1} and 652 cm^{-1} were characteristics of those reported in the literature for sulfite ion (Martin et al. 1987). The broad absorption at 980 cm^{-1} is to the symmetric and asymmetric bending mode (Figure 5.1a,b). The strong band centered around 1140 cm^{-1} which splits into two components at around 1146 cm^{-1} and 1116 cm^{-1} and the small peaks at 669 and 602 cm^{-1} is assigned to the stretching and bending modes of sulfate as seen in the pure gypsum spectrum (Figure 5.1c). Pérez-Alonso et al. (2004) mentioned that the strong nitrocalcite peak usually presents at 1051 cm^{-1}. Among described bands, the strong absorption band of carbonate at 1453 cm^{-1}, the sulfate band centered around 1146 cm^{-1}, and the characteristic band of sulfite at 980 cm^{-1} are used for the analysis of the related components.

The FTIR spectrum of the mixture of these components showed no significant interference to any of the analyzed peak of a component from the other two components present in the matrix, thus the chosen peaks could be safely used for the analysis of the individual components in their mixture (Böke et al. 1999).

In this thesis, the comparison of the peaks before and after exposure was based on the FTIR analysis of Böke et al. (1999) for the marble and reaction components, while Cervantes-Uc et al. (2007). Reported FTIR data used to predict the level of dispersion of nanoclays in the polymer matrix. Cervantes-Uc et al. (2007) investigated the thermal degradation of commercially available organoclays (Cloisite 10A, 15A, 20A, 25A, 93A and 30B) by FTIR (Figure 5.2) and all organoclays showed bands around at 3636 and 3395 cm^{-1} attributed to O–H stretching for the silicate and water, and at 1639 cm^{-1} related to O–H bending, while at 1040 cm^{-1} owing of Si–O–Si stretching vibration from silicate. Additionally, 917 cm^{-1} shows aluminates deformation from Al–OH–Al. They also observed some other bands at 2924, 2842 and 1475 cm^{-1}

except for the natural montmorillonite (Na^+) showing C– H methylene groups vibrations from the surfactant chemical structure (Cervantes-Uc et al., 2007).

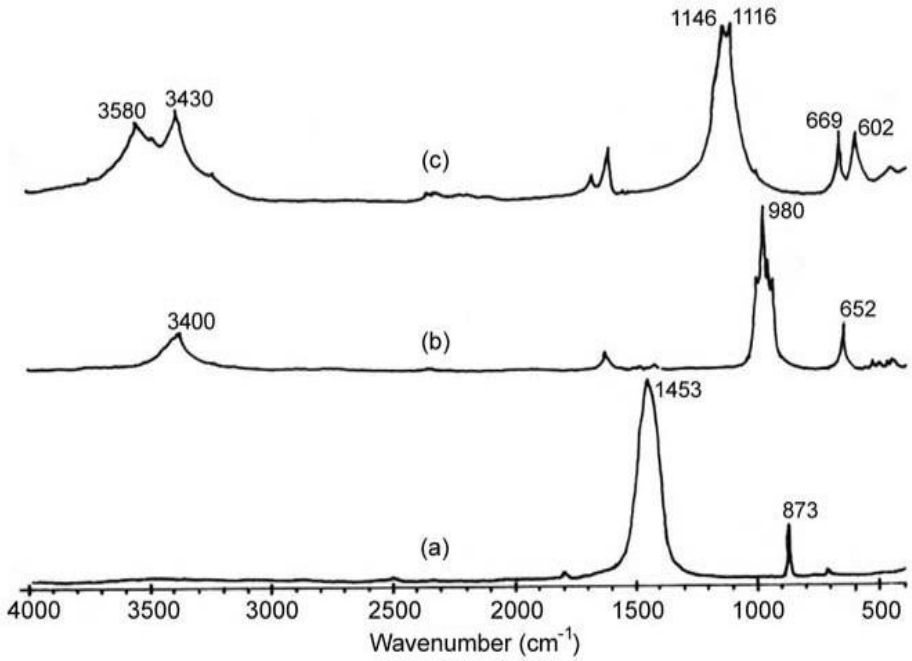

Figure 5.1. FTIR spectra of pure calcium carbonate (a), pure calcium sulfite hemihydrate (b) and pure gypsum (c) (Source: Böke et al. 1999).

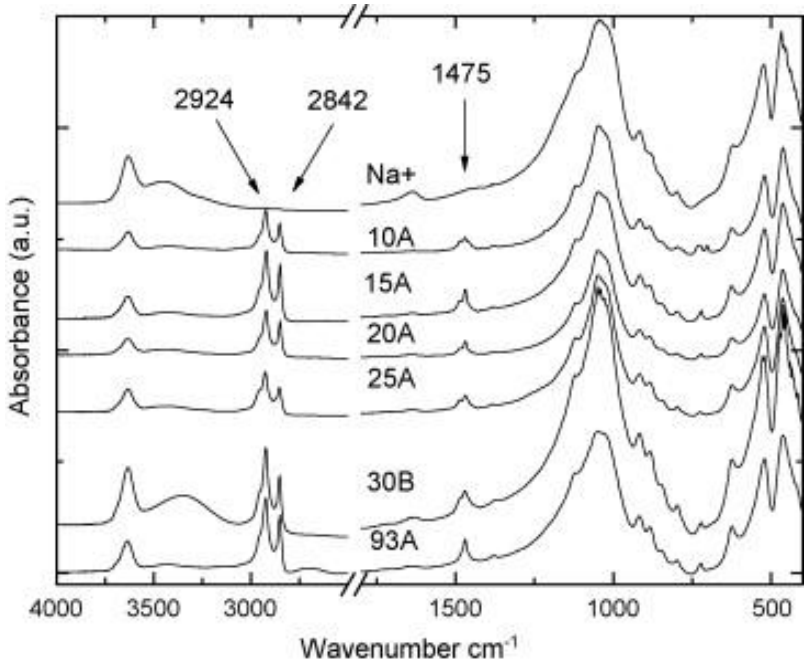

Figure 5.2. FTIR spectra of commercially available organoclays (Source: Cervantes-Uc et al., 2007).

The marble slabs surface were shaved with a lancet and taken 0.3-0.5 mg from shaved powder for the FTIR analysis before and after outdoor exposure. Then, this powder was mixed with 80 mg pure KBr and pressed with 10 tones/cm^2 to obtain pellets. Pressed pellets analyzed with Perkin Elmer Spectrum BX II model IR with a range of 400 – 4000 cm^{-1}.

5.3. Permeability Tests for Composite Coatings

In this part, experimental methods for the coating materials effects on surface hydrophobicities, water capillary absorptions and water vapor permeabilities were researched for bio-nano composite coating applications and evaluation. Additionally, color alteration test was realized to determine color variation or optical appearance of the coating materials due to esthetic perspective

5.3.1. Water Contact Angle Measurements

The degree of the hydrophobicity of surfaces was determined by measuring water contact angle values from the surfaces of the coated and uncoated marble slabs. Surface wettability is mainly referred to as hydrophobicity or hydrophilicity (Xua and Siedlecki, 2007). Water contact angle values were examined to determine the water hydrophobicity of the bio-nano composites by goniometer (Kruss G10) by using distilled water. A drop of distilled water was dropped with micro syringe on ten different points of the each coated marble slab surface. The reported contact angle values are the averages of these ten measurements.

5.3.2. Water Capillary Absorption Measurement

Porous structures generally include water due to the fact that thermodynamic equilibrium with the environmental humidity. On the other hand, rainwater and other pollutants penetrate into stone by the way of capillary absorption. A gravimetric sorption technique was used (Tsakalof et al., 2007; Manoudis et al., 2009) to determine the capillary water absorption. One face of the marble slab was coated and this treated

surface was placed on wet (distilled water) filter paper pads (Whatman Grade no: 4). Coated and uncoated marble slabs were weighed to determine the amount of water absorbed by capillary forces every ten minutes. The capillary water absorption value of uncoated marble was compared with the capillary water absorption value of the coated marble to calculate percent reduction of the water capillary absorption (RCA%) by using following equation (Toniolo et al., 2002; Tsakalof et al., 2007; D'Arienzo et al., 2008; Manoudis et al., 2009):

$$RCA\% = \frac{(m_b - m_c)}{m_b} \times 100 \tag{5.2}$$

Where, m_b is the mass of the water absorbed by the uncoated blank marble and m_c is the mass of the water absorbed by the coated marble.

Researchers carried out the water capillary absorption tests in previous studies and observed very rapid water absorption for marble nearly in the first 20 minutes (Peruzzi et al., 2003; Tsakalof et al., 2007; Manoudis et al., 2009; Ferri et al., 2011). The capillary water absorption experiment was carried out for 3 hours in this study.

5.3.3. Water Vapor Permeability Measurement

The cylindrical PVC containers were partially filled with water for vapor permeability test. The cylindrical PLA/MMT composite coated and uncoated marble slabs were fixed on the top of cylindrical container and sealed completely. These cylindrical containers were placed in the environmental chamber at 25% relative humidity and a constant temperature of 40 °C. The containers were weighed every 24 hours period until the weight change of the less than 5 % in two consecutive days then, the values used for the water vapor permeability (Tsakalof et al., 2007; Manoudis et al., 2009). The percent reduction of water vapor permeability (RWP%) was obtained from eqn 5.3 as follows (Toniolo et al., 2002; Tsakalof et al., 2007; D'Arienzo et al., 2008; Manoudis et al., 2009);

$$RWP\% = \frac{(m_b - m_c)}{m_b} \times 100 \tag{5.3}$$

Where, m_b is the mass of the vapor which penetrates the uncoated blank marble and m_c is the mass of the vapor which penetrates the coated marble.

5.3.4. Color Alteration Measurement

Color variations of the coated and uncoated marbles were measured by using colorimetric measurement instrument (Aventes) with AvaSoft 6.2 software. The measurements were realized on homogeneous spot areas of 4 mm in diameter, and the total color differences (ΔE), L^*, a^* and b^* coordinates were determined (Ocak et al., 2009). Triplicate coated and uncoated marble sets were used for color variations in this study and values were reported accordingly.

$$\Delta E^* = \sqrt{\Delta L^{*2} + \Delta a^{*2} + \Delta b^{*2}} \quad (5.4)$$

Where, L^* is the brightness (0 for black-100 for white), a^* is the red-green component (positive for red and negative for the green colors) and b^* is the yellow-blue component (positive for yellow and negative for the blue colors) (Ocak et al., 2009; Scarfato et al., 2012).

5.4. Weathering Experiments of the Marbles

Coated and uncoated (control) marbles were used for the sulfation reaction experiments in the laboratory scale reactor. Ambient air experiments were also conducted in a city atmosphere at sheltered outdoor conditions.

5.4.1. Sulfation Reaction Experiments

Coated and uncoated marbles (maximum 7 marble slabs) were exposed to nearly 8 ppm SO_2 and 100% relative humidity in a reactor which is showed in Figure 5.3 (Gauri and Bandyopadhyay, 1999; Böke et al., 2002; Böke and Gauri 2003). In the reactor, water was placed at the bottom of the reaction chamber. The dry air was passed over SO_2 permeation tubes (VICI Metronics Inc.), at the rate of 215 cc/min. The SO_2-air

stream is injected in the reactor beneath the water table to saturate the SO_2-air stream with water. The samples were placed in the desiccator only after the water had been equilibrated with the supplied concentration of gas. Afterwards, the coated and uncoated samples were tied to a glass stand by nylon threads so that they hang freely above the water table in the reactor (Figure 5.3). Not more than seven samples were exposed at one time to keep a constant concentration of SO_2 in the reactor. The concentration of SO_2 in the reactor was determined from the permeation rate which was obtained from the weights loss of the permeation tube over time.

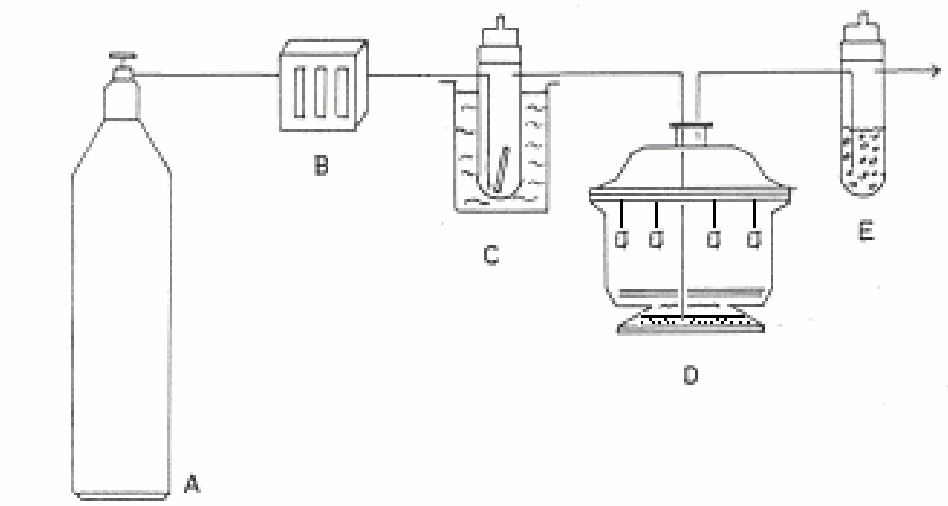

Figure 5.3. Schematic presentation of experimental sulphation reaction. Components of the experiment are; A: dry air cylinder, B: mass flow controller, C: permeation tube in 30°C, D: reaction chamber, E: washing bottles.

SO_2 concentration in the reaction chamber was obtained by using sulfur dioxide permeation tube (VICI Metronics Inc., Dynacal Standard-size of 10 cm). The dry air mixture passed over the permeation tube with an air flow rate at 215 ml/min by using mass flow controller. This air flow rate resulted in the permeation rate as 4580 ng/min/10 cm at 30 °C which was obtained by following weight loss in the permeation tube at certain time intervals. Then, this SO_2 weight loss was plotted versus time. The slope of the graph gives the permeation rate for the constant known SO_2 concentration (Figure 5.4). In this study, 8.1 ppm SO_2 concentration in air was calculated by using following equation (VICI, Technical note 1002)

$$C = \frac{PK_m}{F_T} \tag{5.5}$$

Where, C is the concentration of SO_2 in air gas mixture (ppm), P is the permeation rate ng/min/10 cm (from Figure 5.4), K_m is the molar constant for sulfure dioxide (0.382) and F_T is the total flow of air gas mixture (ml/min). Molar constant for SO_2 obtained from permeation tube catalog and calculated concentration is given as an example.

$$SO_2 \text{ (mg/h)} = \text{Slope}/24 = 6.629 / 24 = 2.75\text{x}10^{-1}$$

$$SO_2 \text{ (mg/min)} = 2.75\text{x}10^{-1} / 60 = 4.58\text{x}10^{-3}$$

$$SO_2 \text{ (ng/min)} = 4580$$

$$C(SO_2) = \frac{4580 \times 0.382}{215} = 8.1 ppm$$

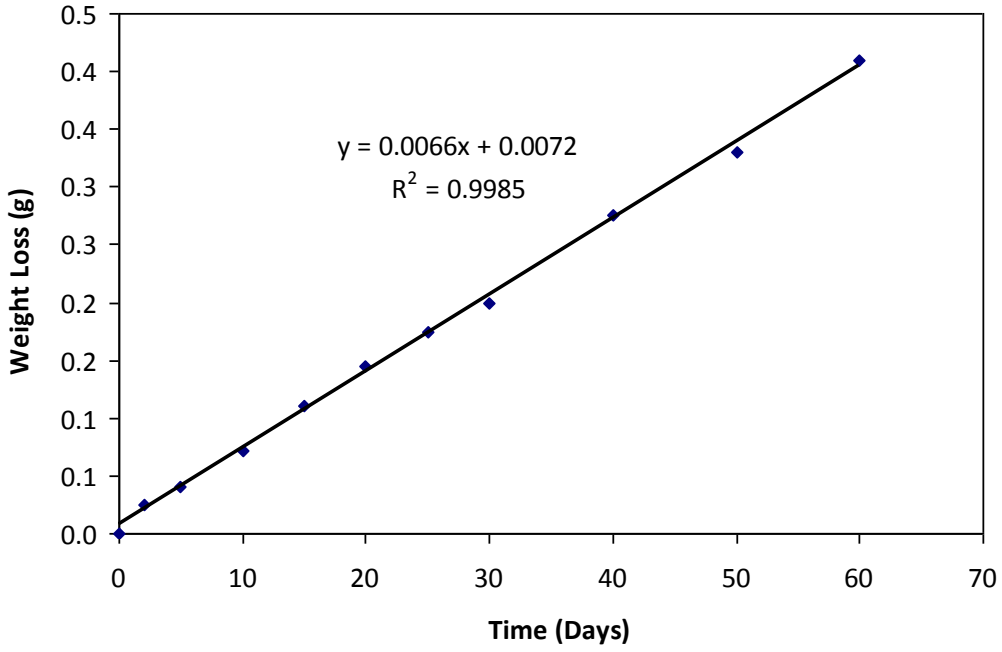

Figure 5.4. Weight loss of SO_2 permeation tube @ 30 □ C.

To determine the protection efficiency of the coating materials, the gypsum crust thicknesses formed on the coated and uncoated marble surfaces should be measured at the end of each exposure experiment. No direct way available to measure therefore the following equations used for the conversion of formed gypsum mass to the thickness of

gypsum crust on marble surface (Gauri and Bandyopadhyay, 1999; Böke and Gauri, 2003; Ocak et al., 2009)

$$Wp = \frac{M_p}{M_A} \cdot W_A \tag{5.6}$$

$$\delta_p = \frac{W_p}{A \cdot \rho_c} \cdot \frac{M_p \cdot \rho_c}{M_c \cdot \rho_p} \tag{5.7}$$

M_p = Molecular weight of gypsum ($CaSO_4.2H_2O$ = 172.17)

M_A = Molecular weight of sulfate ion ($SO_4^=$ = 96.056)

M_c = Molecular weight of calcite ($CaCO_3$ = 100.09)

W_A = Sulfate weight which formed on the marble surface (g).

δ_p = Crust thickness (cm),

ρ_c = Density of calcite (2.71 g/cm^3)

W_p = Weight of the product, gypsum (g)

ρ_p = Density of gypsum, (2.32 g/cm^3)

A = Surface area of the sample, (cm^2)

The weight of the gypsum, W_p, was determined the mass balance from the weight of SO_4^{2-} ions. Sulphation products formed on the marble samples dissolved in the known volume (L) of water. Dissolved SO_4^{2-} concentration is determined by IC (ion chromatography). The concentration of sulfate was used to calculate the weight of sulfate with following equation:

$$W_{A(sulphate)} = Volume.of.water(L) \times Sulphate.conc.(ppm) \tag{5.8}$$

The reactor included approximately 8 ppm constant SO_2 concentration and put the high numbers of the marble slabs in the reactor increased the surface area of the samples and changed the SO_2 constant concentration in the 10 liters environmental chamber. For this reason, only one bio-nano composites coated and uncoated control

marbles were run at the same time and duration due to the volume of reactor. However, the experimental results were statically evaluated by using repeat set for each coating materials. Therefore, once PLA/MMT2, PLA/MMT5 and PLA/MMT7 coated and uncoated marble samples were placed in the reaction chamber as triplicates to determine the variation in crust thickness during the same exposure experiment. At the end of the 30^{th} day, gypsum crust thicknesses of the triplicate samples were calculated. The calculated results were compared with each others by using relative standard deviation percentage (RSD %) which related with the standard deviations and mean values of the triplicate samples (eqn 5.9). The RSD% values mostly used in probability theory and statistics to express precision and repeatability of qualitative or quantitative chemical analysis;

$$RSD\% = \left(\frac{Std.deviation}{Mean} \right) \times 100 \tag{5.9}$$

The coating thicknesses effects on the protection abilities of the bio-nano composites also studied in this study. For the excellent protection abilities of the 5% PLA/MMT bio-nano composite, it was selected to research the coating thicknesses effects on the protection properties of the coatings. Marble plates were coated by using dip-coating device to obtain three layer of coating. After first layer of coating, the solvent was removed in an oven at 40 °C for several hours. Then second and third layer of the coating were followed similar procedure. The coating thicknesses of each coating were defined by using the 10 different measurements on the cross section of the PLA/MMT5 with SEM (Figure 5.5). These thicknesses were measured 17.39±1.41 μm for the first layer, 27.62±1.39 μm for second, 39.52±2.19 μm for the third layer.

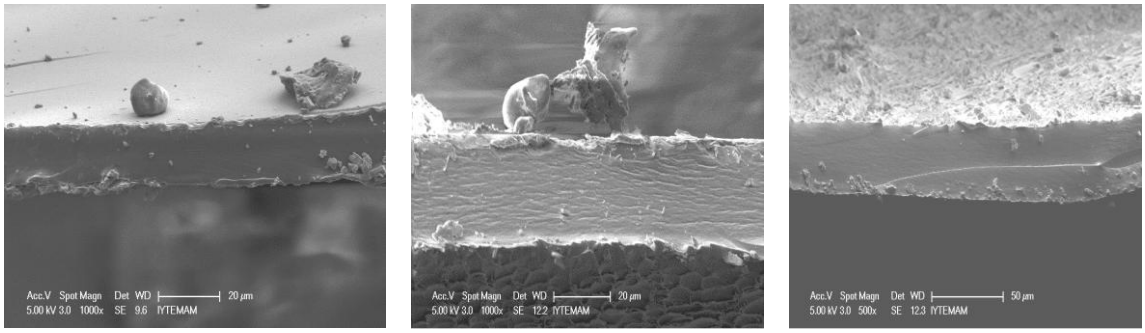

(a) **(b)** **(c)**

Figure 5.5. SEM images of the cross section of the PLA/MMT5 bio-nano composites thicknesses for one layer (a), two layer (b) and three layer (c) coating

5.4.2. Field Experiments

Izmir is greatly industrialized area and a large metropolis in the western extremity of Anatolia in the west coast of the Turkey. Moreover, Izmir is the third most populous city in Turkey and Izmir metropolitan area extends along the outlying the Izmir Gulf and inland to the Gediz River's delta. Izmir has a Mediterranean climate and it has long, hot and dry summers and mild to cool, rainy winters.

Air quality of Izmir is affected by combustion of fuels (mostly coal), increase of mobile sources like vehicles (mostly automobiles) and industrial process due to being the most significant industrial regions (especially, petroleum refineries, petrochemical industries and iron and steel factories in Aliağa and Kemalpaşa) presence in the area (Odabaşı et al., 2008).

Similar to the experiment in the laboratory, the marble slabs were coated with PLA/MMT2, PLA/MMT5 and PLA/MMT7 composites and pure PLA polymer and UC marbles were placed in Narlidere metropolitan district and exposed ambient atmosphere for 6, 9 and 20 months (Figure 5.6).

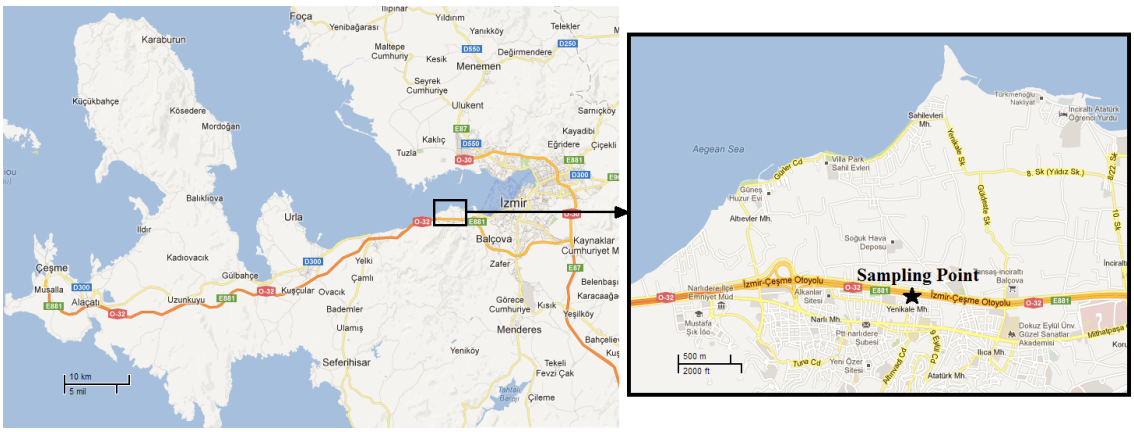

Figure 5.6. Location of outdoor sampling point in Narlıdere, Izmir

The individual quantities of the gypsum and nitrocalcite can be obtained from the quantity of the sulfate and nitrate ions by mass balance for the outdoor experiment. The mineral masses of the gypsum and nitrocalcite are divided to their densities of gypsum (2.32 g/cm^3) and nitrocalcite (1.89 g/cm^3) to calculate individual volumes. The total crust thicknesses were calculated by using the following equation for the outdoor conditions (Yerrapragada et al., 1996; Gauri and Bandyopadhyay, 1999).

$$\delta = \left(\frac{1.8 m_{SO_4}}{2.32} + \frac{3.8 m_{NO_3}}{1.89} \right) / A_0 \qquad (5.10)$$

Where, m_{SO4} and m_{NO3} are the masses of the sulfate and nitrate ions. A_0 is the surface area before the exposure.

Changes in the total crust thickness in the same environment were also investigated for marble slabs coated with neat PLA, PLA/MMT2, PLA/MMT5 and PLA/MMT7. Three replicas in each group of coating were exposed to ambient air and analyzed at the end of the 6, 9 and 20 months. The mean total crust thicknesses, standard deviation and percent relative standard deviation (RSD %) values were calculated by using eqn 5.7.

The coating film thicknesses on the protection abilities of the bio-nano composites also researched in this study. The PLA/MMT5 bio-nano composite coated surface was selected to investigate the coating thicknesses effect on the protection properties of the coatings due to the excellent protection abilities. The marbles were coated with PLA/MMT5 over and over to have coating three different coating thicknesses as 17.39±1.41 μm for the 1-layer, 27.62±1.39 μm for the 2-layer coated 39.52±2.19 μm respectively.

CHAPTER 6

RESULTS AND DISCUSSION

6.1. Structural Characterization of the PLA/MMT Bio-nano Composites

6.1.1. X-Ray Diffraction (XRD) Analysis

Investigation of the nanocomposite structure was achieved by XRD analysis (Bruno et al., 2008; Olad et al., 2011). The analysis of nanoclay and nanoclay polymer matrix were conducted in this study and XRD graph of the Cloisite 10A and nanocomposites prepared by various amounts of nanoclay were given in Figure 6.1. Basal spacing of Cloisite 10A nanoclay powder was calculated as 1.92 nm from Braggs' Law. If there is no change in basal reflections of the layered silicate polymer nanocomposites with respect to characteristic peak of nanoclay, it can be said that phase separated structure is obtained owing to incompatibility between the layered silicate and polymer matrix. Intercalated structures can be determined by monitoring peak shifts to lower angles and/or broader peaks as the spacing of the organoclays increases. Exfoliated structures do not give any diffraction peaks since distances between layered silicate platelets are higher than the detection limit of XRD (Bhattacharya et al., 2008; Pavlidou and Papaspyrides, 2008; Koo, 2006; Mittal 2010).

Complete disappearance of <001> reflection of Cloisite 10A nanoclay for 2 and 5 wt% Cloisite 10A loaded PLA coatings can be attributed to complete delamination of clay platelets (exfoliated structure). Since the distances between layered silicates increased to more than 46.22 Å from 19.02 Å, that of Cloisite 10A nanoclay, can be taken as an indication of possible exfoliation of nanoclay platelets in PLA matrix. Ozcalik and Tihminlioglu (2013) reported the distance between layered silicates (Cloisite 10A) to increase more than 51.9 Å from 19.02 Å in the corn zein matrix. They explained that the distance between layered silicates more than 51.9 Å could be taken as sign of possible exfoliation of the nanoclay in the polymer matrix. PLA/MMT7 sample

showed a peak broadening between 2θ values of 2.89 and 5.20 that can be attributed to intercalated and partially agglomerated structure (Figure 6.1). The results indicated that high interaction between the layered silicates and polymer matrix was achieved for only 2 and 5 wt% clay loaded samples.

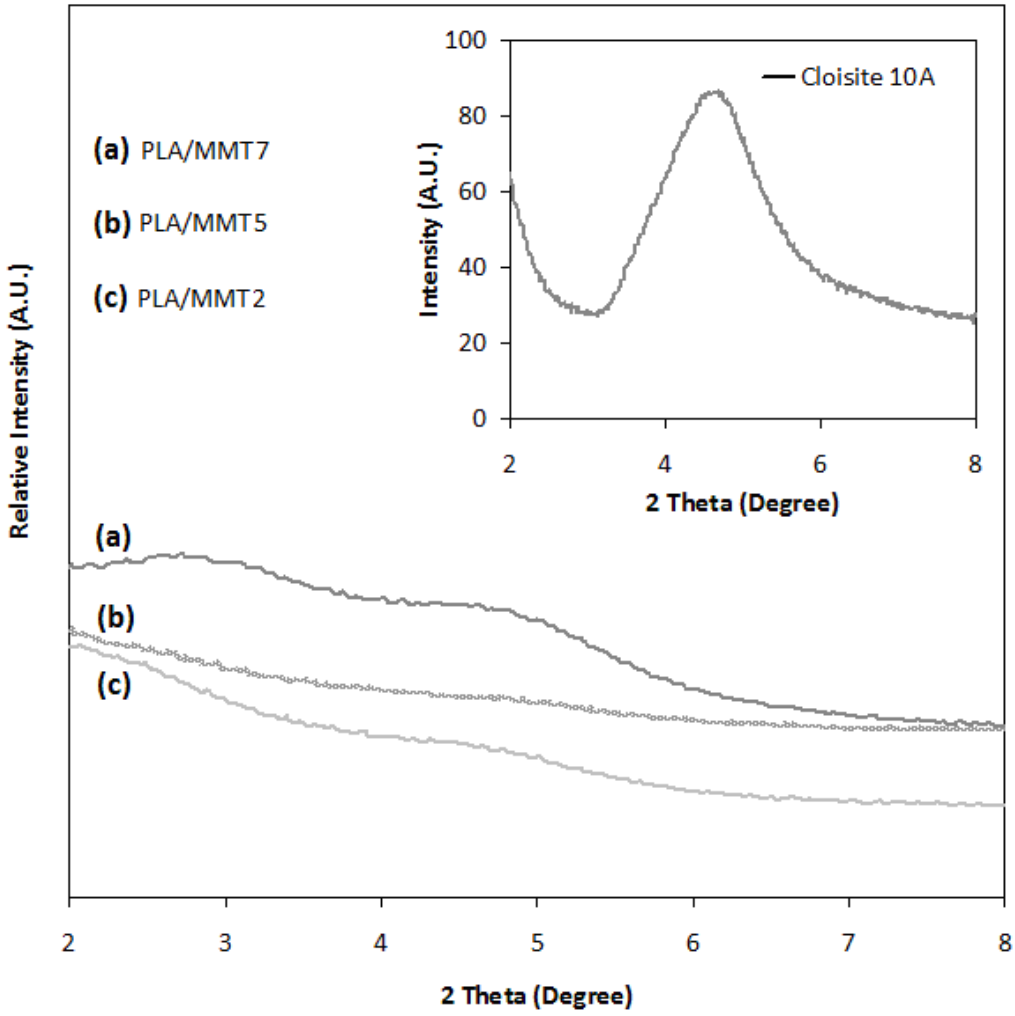

Figure 6.1. XRD graph of the pure montmorillonite (Cloisite 10A) and 7 (a), 5 (b) and 2% (c) montmorillonite (Cloisite 10A) added PLA

6.1.2. Atomic Force Microscopy (AFM) Analysis

AFM analysis is a powerful tool and is capable of giving valuable information about the dispersion of the layered silicate nano particles in PLA polymer matrix even down to nanometer scale. AFM analysis with tapping mode is generally used to obtain mechanic or intrinsic contrast between soft polymer matrix and hard layered inorganic silicate nano particles (Liu et al, 2003; Camargo et al., 2009). Malwela and Ray (2012)

pointed out that the tapping mode of the AFM analysis was used to understand molecular scale morphology, physical characteristics and topography of the polymeric materials. Several typical phase, height and 3D topography AFM images which were obtained from the PLA/MMT2, PLA/MMT5 and PLA/MMT7 bio-nano composites coated surfaces were shown in Figure 6.2, 6.3 and 6.4. Darker region in the AFM images attributed to the polymer and yellow features to the multilayered clay platelets. Park et al. (2004) pointed out that clay nanoparticles observed as a bright color due to the stiffer crystalline structure and polymer appeared as a dark color in the AFM tapping phase images. The AFM images showed complex shapes of the montmorillonite in the PLA matrix. Therefore, one-layer thicknesses estimation of the nanoparticles was very difficult for the PLA/MMT2, PLA/MMT5 and PLA/MMT7 bio-nano composites (Figure 6.2, 6.3 and 6.4). However, phase height and 3D topography AFM images pointed out that the stacked and partially intercalated silicate layers were formed in the bio-nano composite coatings. Moreover, AFM images which were obtained from the PLA/MMT5 bio-nano composite polymer surfaces pointed out that the stacked and intercalated silicate layers were dispersed homogenously in the PLA-matrix (Figure 6.3).

AFM images of PLA/MMT2, PLA/MMT5 and PLA/MMT7 coated marble surfaces in 2 and 5 μm scan sizes were given in Figure 6.5 and 6.6 also provide additional insight about the morphology of the nanocomposite. The Cloisite 10A nano particle lengths in the polymer matrix were ranged between 50-500 nm (Figure 6.5 and 6.6). It is reported that aspect ratio (L_{clay}/d_{clay}) of the layered silicates in the polymer matrix enhanced the mechanical and barrier properties of the nanocomposites (Ray et al., 2002; Ray and Okamato, 2003; Olad et al., 2011). Moreover, in the well dispersed states, Olad and coworkers (2011) pointed out that montmorillonite layered silicate aspect ratio can be up to the range of 1000 except for the broken layers. However, as a result of preparation process small plates would form and aspect ratio would decrease around 300-500 in the polymer matrix. The high aspect ratio is usually obtained from well dispersion of the individual clay layers in the polymer matrix, and nanocomposites with lower clay content are more likely to be in exfoliated structure (Olad et al., 2011). The length of the stacked layered silicate was 342±94.7 nm for PLA/MMT2, 345±89.7 nm for PLA/MMT5 and 280±92.8 nm for PLA/MMT7 bio-nano composites while the average width of the of the stacked layered silicate was measured as 120±59.8 nm for PLA/MMT2, 85±26.8 nm for PLA/MMT5 and 134±20.1 nm for PLA/MMT7 bio-nano

composites in this study. When the aspect ratios ($L_{stacked\ clay}/d_{stacked\ clay}$) of the stacked layered silicate were compared to each other, PLA/MMT2 was defined as 3.33±1.47, PLA/MMT5 was 4.42±1.45 and PLA/MMT7 was 2.13±0.76 and higher values were defined from the PLA/MMT5 bio-nano composite coating.

It is also observed that the stacked and intercalated silicate layers in the PLA-matrix for the PLA/MMT5 were dispersed more homogenously than PLA/MMT2 and PLA/MMT7 as can be followed from the AFM images (Figures 6.5 and 6.6). On the other hand, AFM images which obtained from the PLA/MMT7 surface pointed out that high loading of the nanoparticle caused agglomeration of the nanoparticles in the polymer matrix (Figure 6.4). These results showed similarity with previous studies on polymer/montmorillonite composites in the literature; (Becker et al., 2002; Ray et al., 2002; Ray and Okamato, 2003; Park et al., 2004; Špírková et al., 2011; Malwela and Ray 2012). For instance, Becker et al. (2002) studied the high-functionality epoxy resins such as bifunctional diglycidyl ether of bisphenol-A (DGEBA) through dispersion of octadecyl ammonium ion-modified layered silicates within the polymer matrix. The individual layers of the layered silicate were not seen from the AFM phase contrast images of the DGEBA nanocomposite containing 5 wt% layered silicate. They observed that some stacked layers and unhomogeneous distribution of the layered silicate in the polymer matrix (Becker et al., 2002; Ray and Okamato, 2003). Park et al. (2004) also studied the effect of compatibilizer on nanostructure of the biodegradable cellulose acetate/organoclay (Cloisite 30B) nanocomposites. They defined the one-layer thickness as 3.84 nm for the Cloisite 30B organoclay in the cellulose acetate polymer matrix.

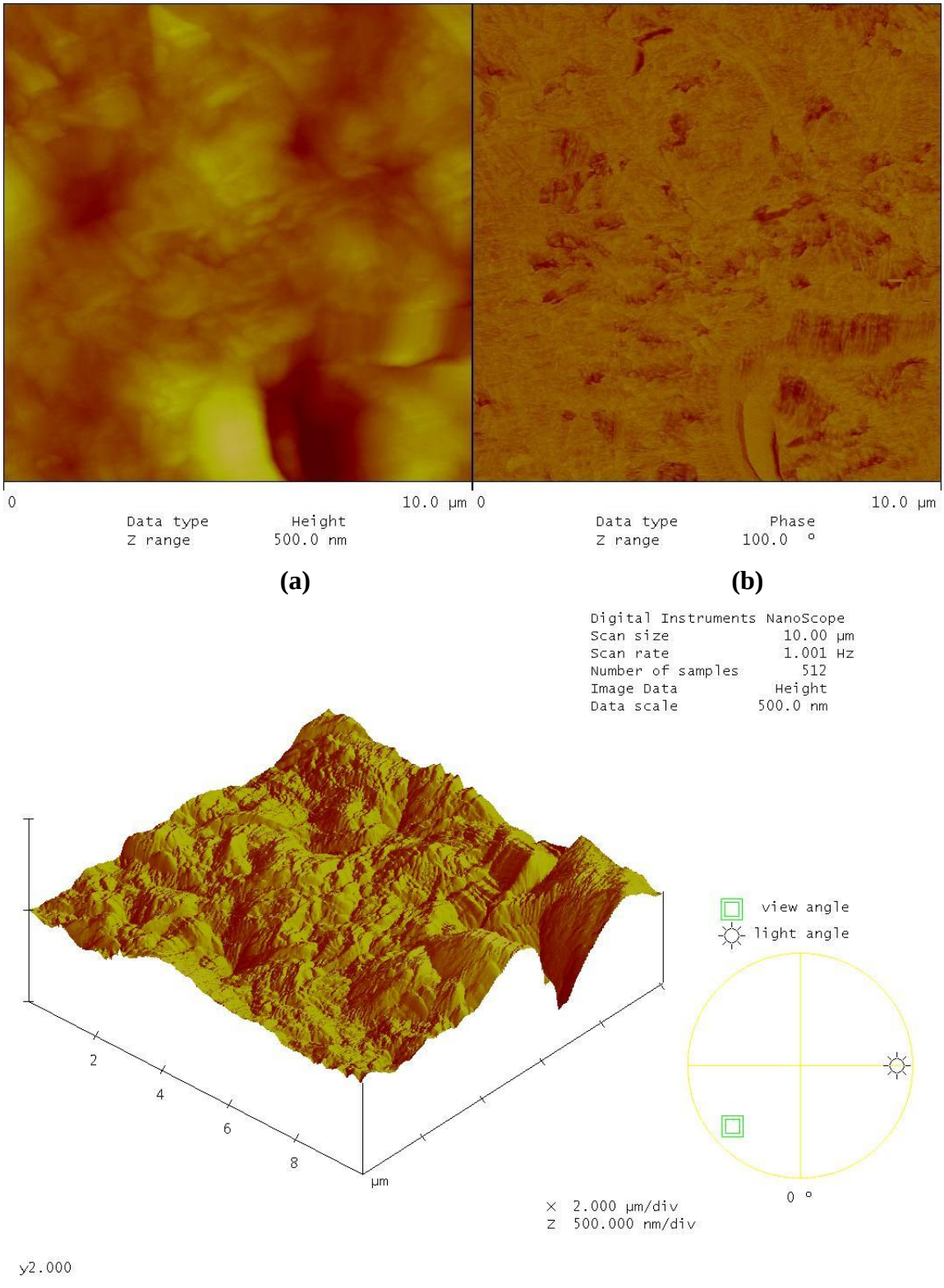

Figure 6.2. Height phase (a, b) and 3D topography (c) AFM images of the PLA/MMT2 bio-nano composites

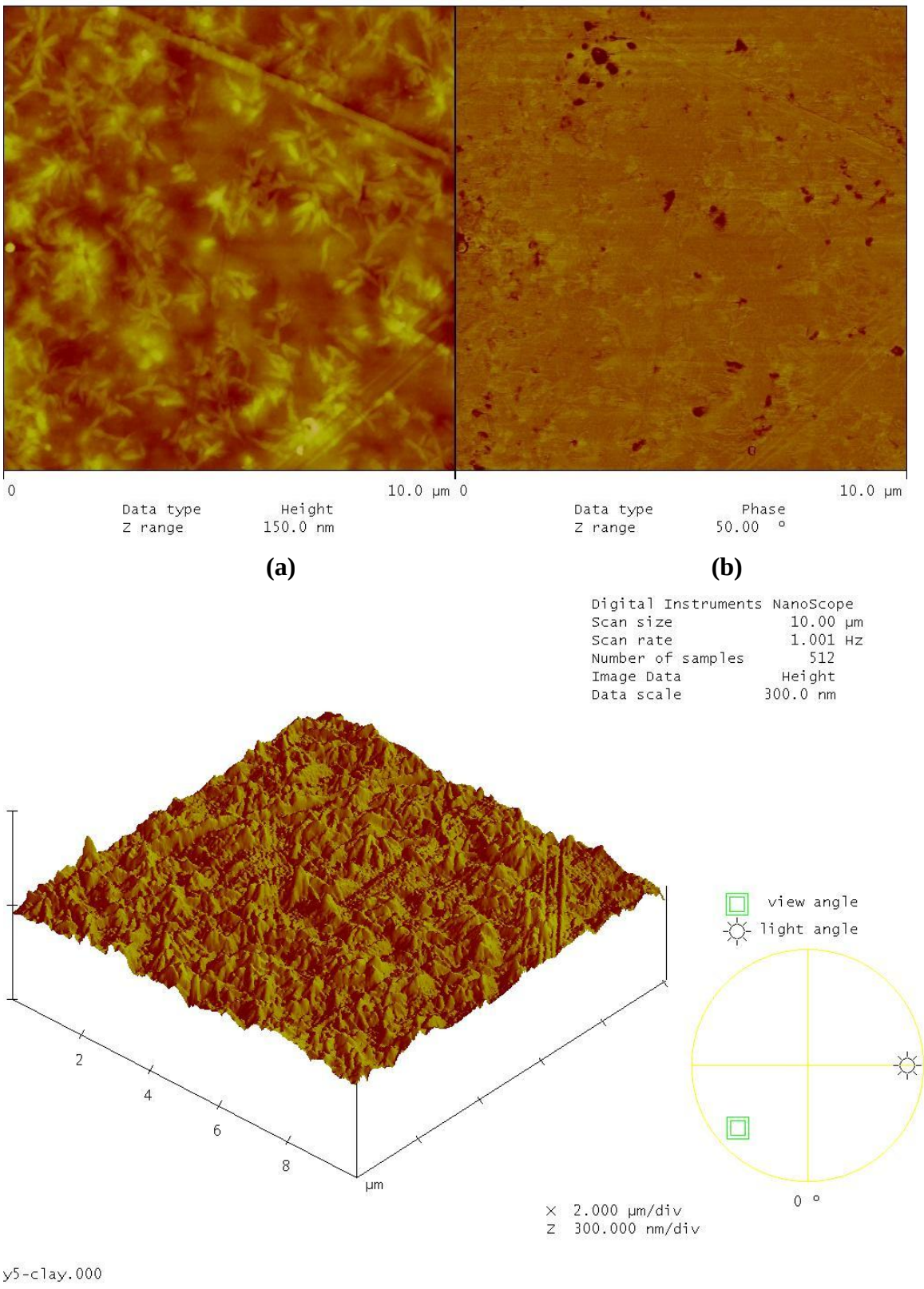

Figure 6.3. Height phase (a, b) and 3D topography (c) AFM images of the PLA/MMT5 bio-nano composites

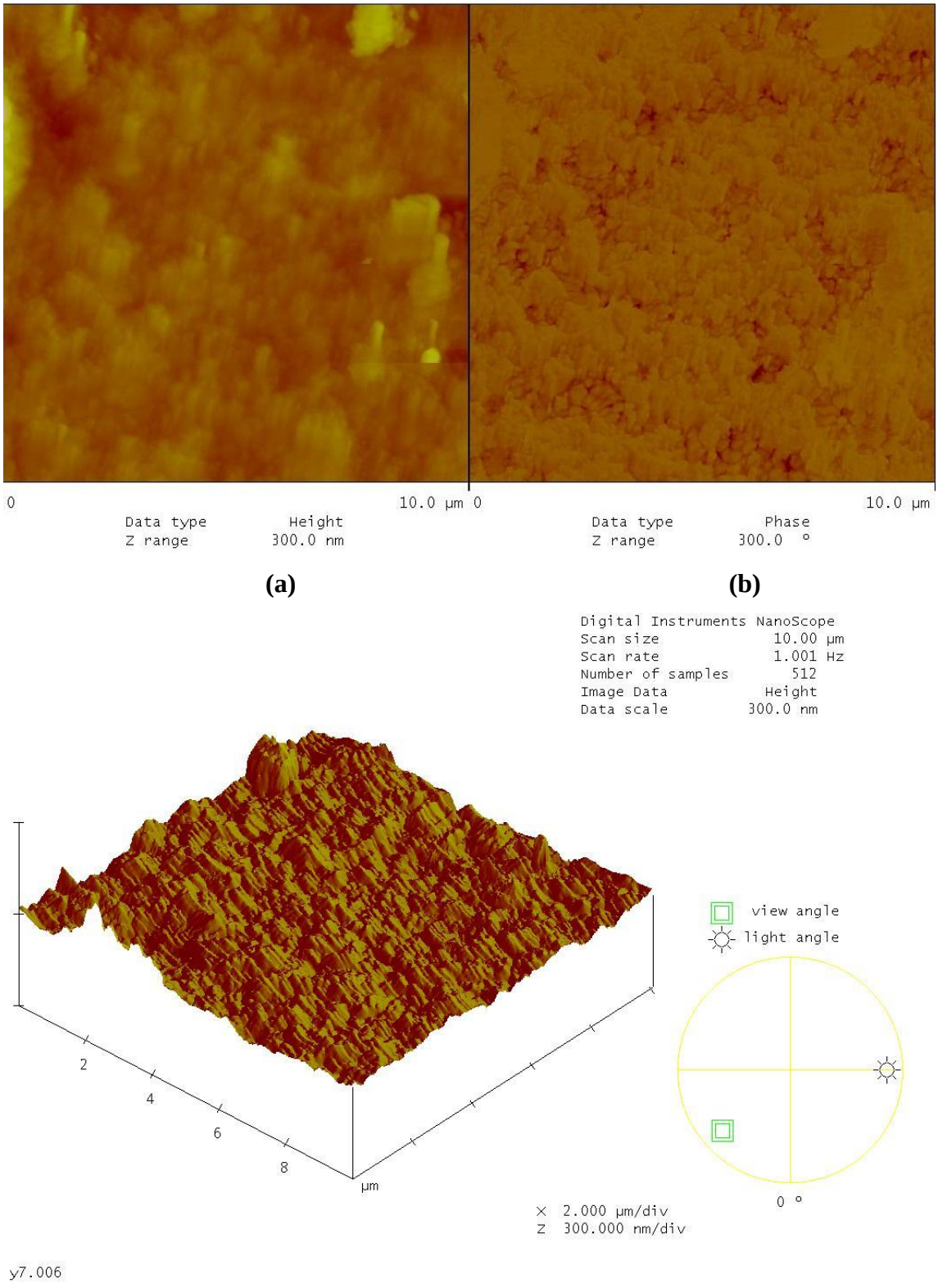

Figure 6.4. Height, phase (a, b) and 3D topography (c) AFM images of the PLA/MMT7 bio-nano composites

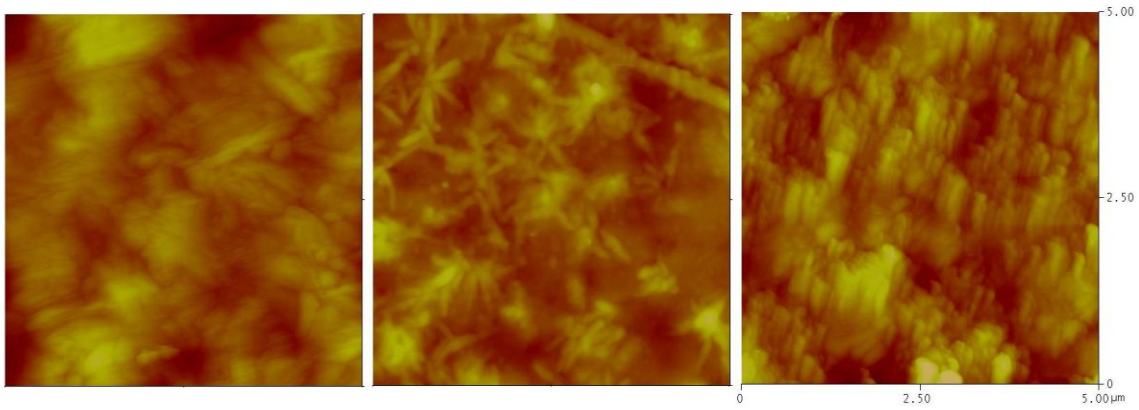

(a) **(b)** **(c)**

Figure 6.5. AFM images of PLA/MMT2 (a), PLA/MMT5 (b) and PLA/MMT7 (c) coated marble surfaces in a 5 µm scan size

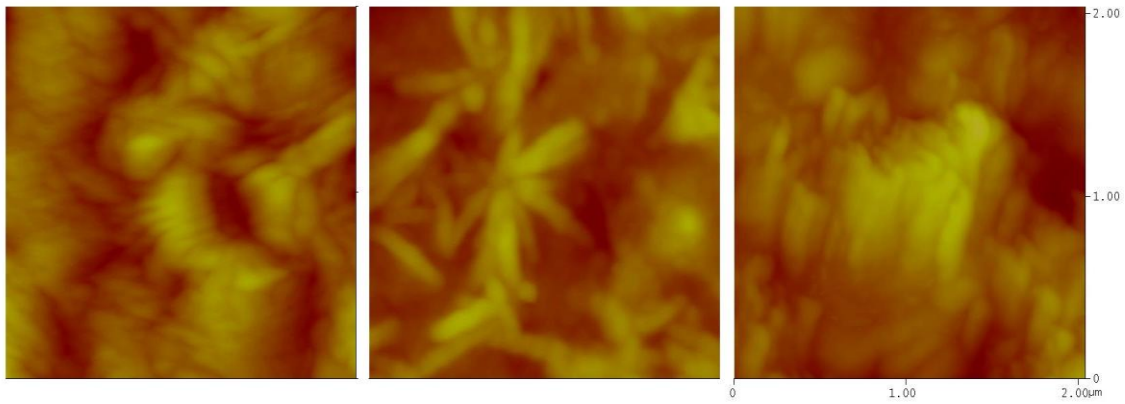

(a) **(b)** **(c)**

Figure 6.6. AFM images of PLA/MMT2 (a), PLA/MMT5 (b) and PLA/MMT7 (c) coated marble surfaces in a 2 µm scan size

6.1.3. Scanning Transmission Electron Microscopy (STEM) Analysis

STEM analysis is an important techniques and generally used for the characterization of the micro-structure of nano-materials from micron to atomic scale (Wang et al., 2007). In this study, STEM images provided information about layered silicate nano structure in the polymer matrix cross section. The layered silicate nano structures were easily observed from the STEM images (dark particles) similar to AFM images. Moreover, some exfoliated individual layered silicate two plates were also observed in the STEM images (Figure 6.7-b). This STEM image can be considered as a

sign for some level of exfoliation layered silicates in the polymer matrix. However, estimation of the one layer thickness of the layered silicate and the distance between the layered silicates platelets were very difficult from the STEM analysis.

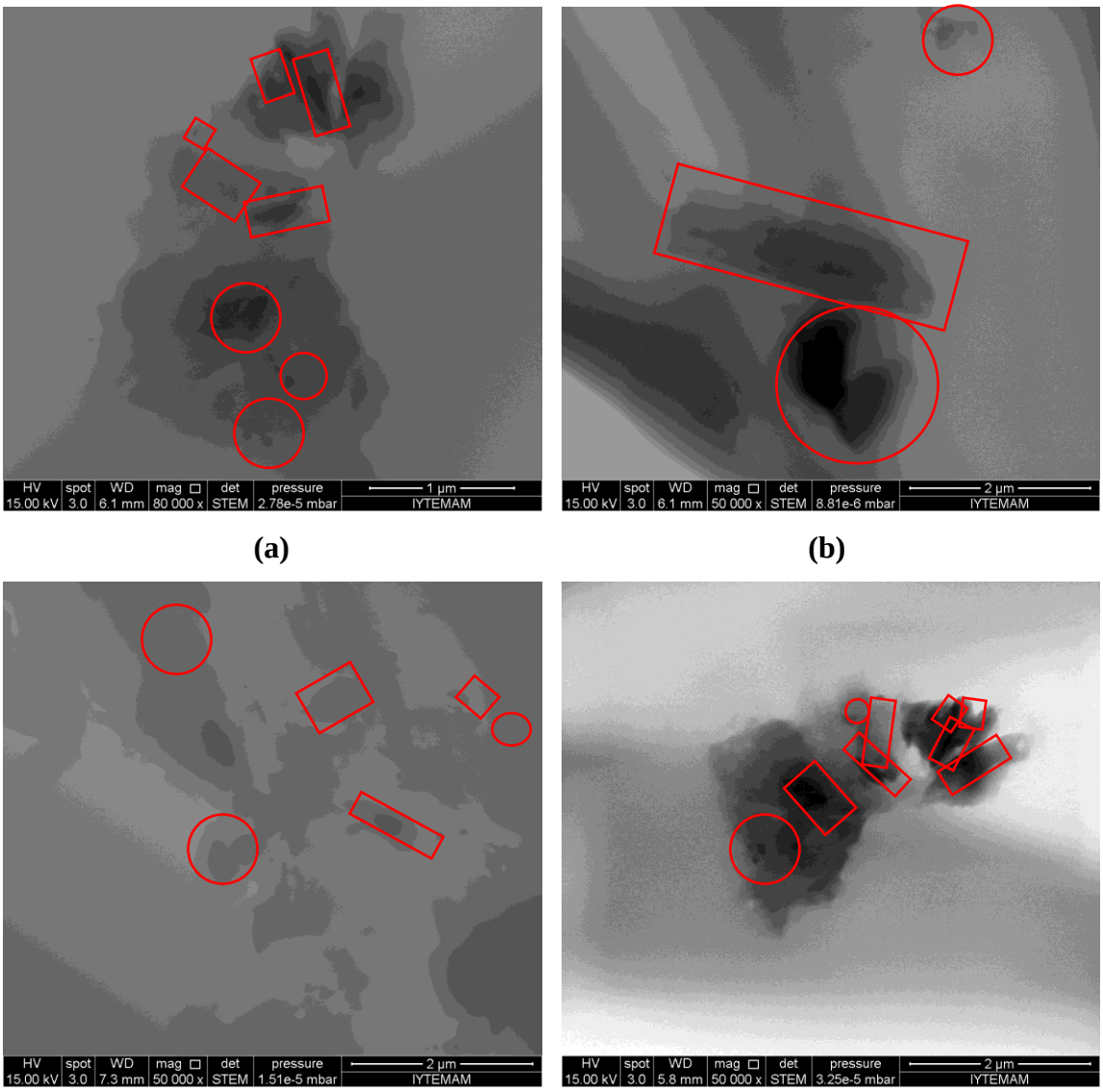

Figure 6.7. STEM images of the PLA/MMT5 bio-nano composite films

Finally, XRD analysis showed that the good delamination of the layered silicates for PLA/MMT2 and PLA/MMT5 coatings. AFM analysis showed that stacked and intercalated layered silicates for PLA/MMT5 were dispersed more homogenously than PLA/MMT2 and PLA/MMT7 composites. Moreover, some exfoliated individual layered silicates plates which observed from the STEM images proved that the exfoliation of the nano clays in the polymer matrix for PLA/MMT5.

6.2. Surface Properties

6.2.1. Water Contact Angle

Surface contact angle of the cleaned marble was measured to be 75±3.09° as hydrophilic (wettable) in our study (Figure 6.8). The static water contact angles of similar untreated marbles were reported as 40-50° (Manoudis et. al. 2009). Pure PLA coated marble surface contact angle value was 98±2.51° showing the considerable increase in wettability. The increase in nanofiller concentrations enhanced the hydrophobicity of the surfaces. PLA/MMT5 showed the highest static water contact angle value (108±2.49°). However, static contact angle value slightly decreased at %7 montmorillonite concentration (105°±2.61). Dominancy of exfoliated structures at low clay loading and dominancy of intercalated structures at higher loadings in polymer/clay matrices, were observed by Zhang et al, (2003), D'Arienzo et al., (2008) and Scarfato et al. (2012). For instance, Scarfato et al. (2012) studied the durability enhancement of concrete with the addition of layered silicate (Cloisite 30B) into different resin Fluoline CP-blend of an acrylic polymer and vinylidenefloired and Antipluviols-siloxane based) and similar decrease in contact angle were observed for both resins at 6 % addition of clay nanofiller.

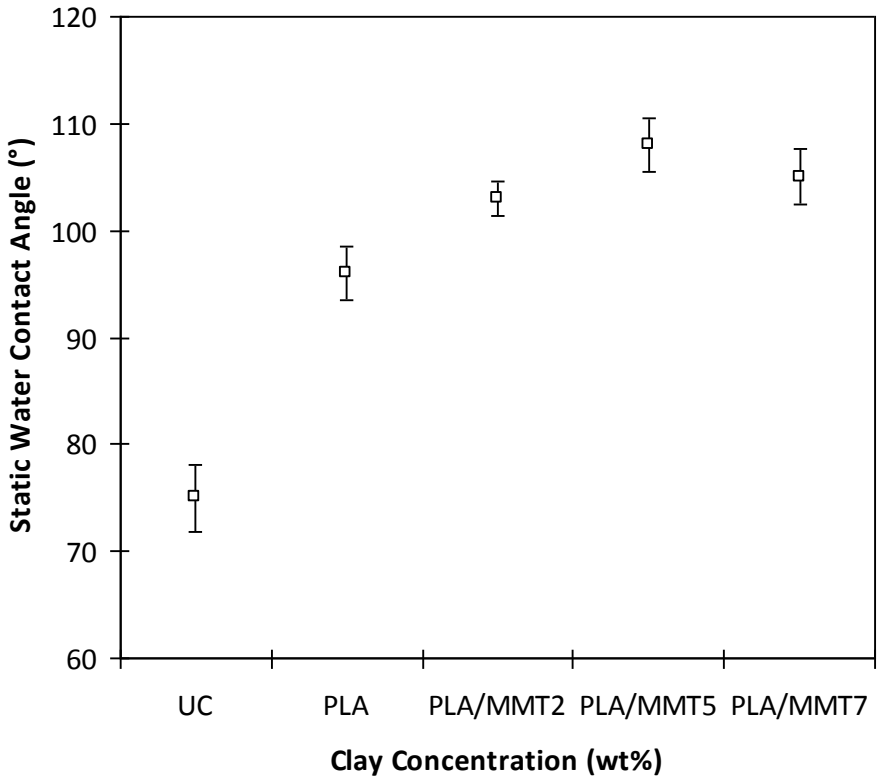

Figure 6.8. Static water contact angle measurements (θ_s) of the PLA, PLA/MMT2, PLA/MMT5 and PLA/MMT7 and UC marbles.

6.2.2. Water Capillary Absorption and Water Vapor Permeability

The porous stones absorb water by capillary forces when they are in contact with liquid water. The capillary absorption force depends on the pore size (range: 10 μm - 1 mm) and the geometry or shape of the pores (Siegesmund and Snethlage, 2011). The improvement in hydrophobicity of the surfaces could also be seen in the water absorption test from the differences between uncoated and coated marbles. Researchers carried out the water capillary absorption tests in previous studies observed that water absorption was very rapid for marble. In other words, water is completely absorbed by capillary nearly first 20 minutes similarly to this study (Tsakalof et al., 2007; D'Arienzo et al., 2008; Manoudis et al., 2009; Scarfato et al., 2012).

The average capillary water absorption for the uncoated Marmara marbles was determined as 4.17±0.19 mg/cm^{2}h. Manoudis et al. (2009) reported this value as 3-5 mg/cm^{2}h for white Greek marbles. The absorption of the water on the marble surfaces was decreased by using bio-nano composite coatings (Figure 6.9 and 6.10). The clay

nano particle addition up to the 5% decelerated the water absorption while it was higher for PLA/MMT7 coated marbles in accordance with the contact angle measurement. The reductions in capillary absorption were calculated as 46.01±1.80 for PLA, 65.81±3.60 for PLA/MMT2, 66.41±5.44 for PLA/MMT5 and 59.81±5.41 for PLA/MMT7 (Figure 6.10).

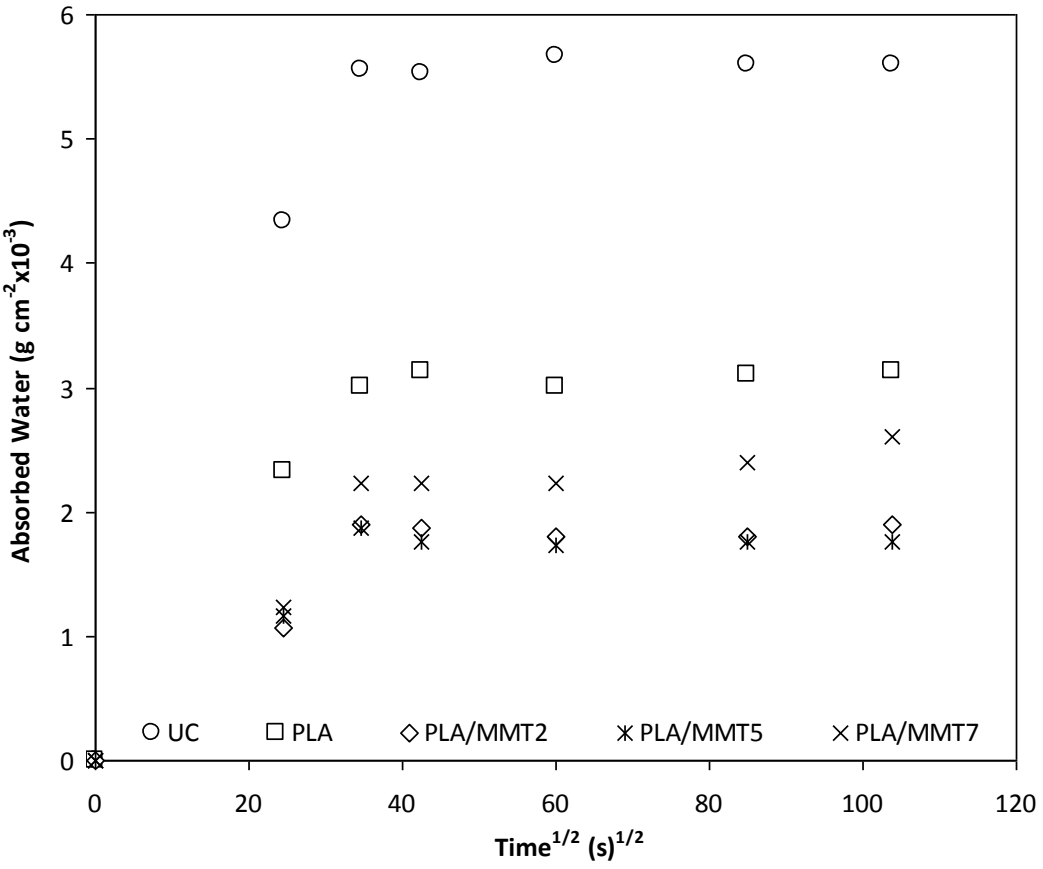

Figure 6.9. Average capillary water absorption values

Kumar and Krishnamoorti, (2009) reported that incorporation of anisotropic nanoparticles could significantly improve the barrier properties of polymers due to (a) the increased physical "tortuosity" of the diffusion path because of the well-dispersed nanoparticles; (b) changes in the local and segmental mobilities and the glass transition temperature of the polymer; and (c) alterations in the sorption resulting from competitive interactions between the penetrant molecules, nanoparticles, and the polymer matrix. Bharadwaj (2001) theoretically showed the effect of orientation of nanoparticles on permeability. The orientation of the anisotropic nanoconstituents increases tortuosity. Kumar and Krishnamoorti (2010) also mentioned that nanocomposites of exfoliated clays in poly(ethylene terephthalate) showed a 10- to 15-

fold reduction in oxygen permeability with 1 to 5 wt% clay addition due to the increased tortuosity.

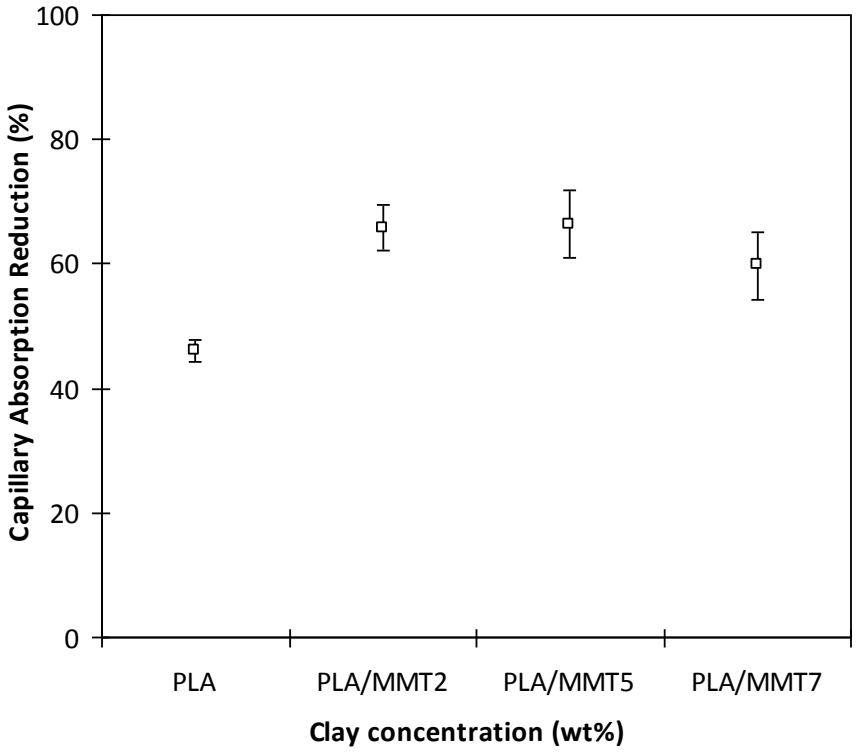

Figure 6.10. Reduction percentage in capillary water absorption. Error bars shows one standard deviation.

The application of coating on marble significantly reduced the water vapor permeability of the surface. The protection percentage against the water vapor permeability values were determined as 31.34±6.56 for PLA, 56.12±4.84 for PLA/MMT2, 59.33±4.24 for PLA/MMT5 and 54.48±2.82 PLA/MMT7 (Figure 6.11). The clay nanofiller addition increased the protection properties of the marbles against the water vapor permeability. The untreated Marmara marble water vapor permeability average value was found to be 0.00197±0.003 g/cm^{2}d. Manoudis et al. (2009) reported water vapor permeability value as 0.11-0.14 g/cm^{2}d for white Greek marbles. This result pointed out that Marmara marble water vapor permeability was considerably lower than the white Greek marbles. In the study of Shogren (1997), the water vapor transmission rates (WVTR) were measured at 25°C and ranged from 13 to 2900 g/m^2/day and increased in the order of PHBV < PLA (cryst.) < PLA (amorph.) < PCL < Bionolle < BAK 1095 < CAP< CAT. The group also reported that WVTR were

positively correlated with higher polymer solubility parameters, lower crystallinity, and higher free volumes.

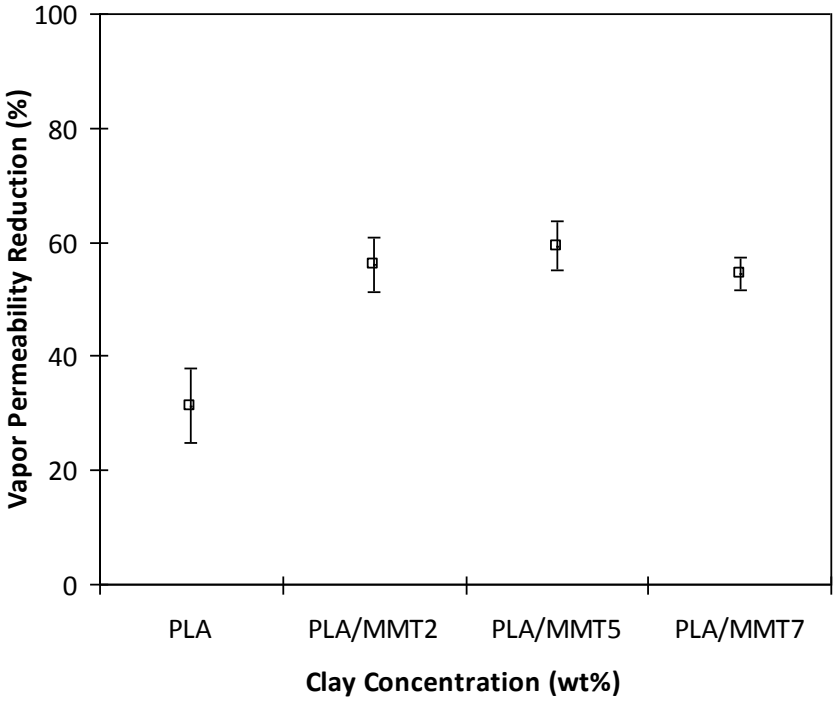

Figure 6.11. Percent reduction of the water vapor permeability. Error bars shows one standard deviation.

6.2.3. Color Alteration Tests

Transparency is one of the vital properties of the surface coating agent, since it should not change the optical appearance of the stone. Color variation or optical appearance of the coated and uncoated marbles just only related with the esthetic perspective and it is not related to protection properties of the coating materials. ΔE values for PLA, PLA/MMT2 and PLA/MMT5 coated marbles were 1.43±0.60, 1.87±0.85, 2.99±0.41 (Figure 6.12). However, ΔE value for PLA/MMT7 coated marble was found to be 4.93±0.96 based on their uncoated marble (Figure 6.12). Vichi et al. (2004) used three different intervals to classify color variations. ΔE values are classified <1 were accepted as not distinguished by the human eye; if the values 1<ΔE<3.3 are regarded as clinically acceptable and the values of ΔE>3.3 are referred as clinically not acceptable. Therefore PLA/MMT7 was not in the range of accepted value. In the literature, Tsakalof et al. (2007) studied color alterations on the Bayer LF, Rhodorsil 224, Wacker 290 Akeogard P and Ftorsam-39 coated surface of petrologically different

stone substrates, such as marble, travertine, sandstone and a newly baked brick. Only for the Bayer LF applied on marble ‘‘Ajax’’ and sandstone of Turkey, the ΔE values were classified <1. However, ΔE values were reported in the range 1<ΔE<10 for the all coating materials except for Ftorsam-39 (ΔE>10) on marble of Kilkis.

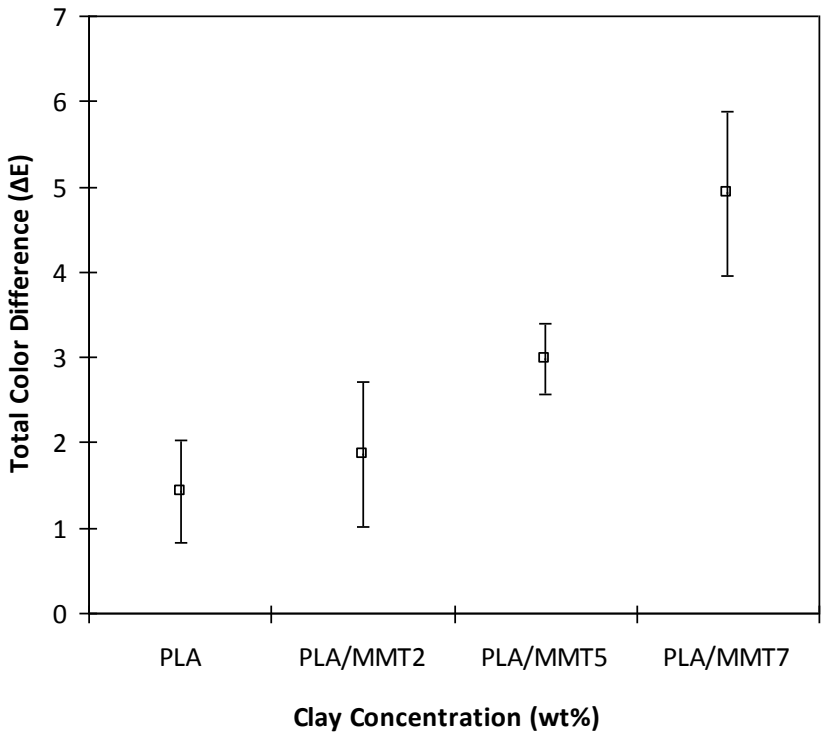

Figure 6.12. Total color variation (ΔE) of the PLA, PLA/MMT2, PLA/MMT5 and PLA/MMT7 coated marbles. Error bars represent one standard deviation.

6.3. SO_2-Calcite Reaction

The previous experimental section which included surface properties pointed out that nano particle addition into the polymer matrix enhanced the barrier and protection properties of the coating materials against water effects. After SO_2-calcite reaction, the calculated gypsum crust thicknesses was ranged from 13 (PLA/MMT5) to 58 micron (Uncoated) on the marble surfaces (Figure 6.13). When the gypsum crust thicknesses of uncoated (control) marbles were compared with the neat PLA and PLA/MMT bio-nano composites coated marbles, excellent inhibition of coating were obviously observed (Figure 6.13). Ocak et al. (2009) reported improvement for the protection effects of the PLA biopolymer coating application under similar extreme acidic conditions in the environmental chamber. The gypsum formation on the neat PLA biopolymer coating

decreased approximately 2-3 times compared to the uncoated control marbles. Meantime PLA/MMT coated surfaces showed significant reduction (~5 times) in the crust formation, underlining addition of nano clay effect on protection efficiency. When composite coated marbles compared to each other, the lowest gypsum formation was observed on PLA/MMT5 coated surfaces in agreement with capillary water absorption, vapor permeability and surface contact angle results. XRD, AFM and STEM results also indicated that 5% Cloisite 10A dispersed homogenously in the polymer matrix.

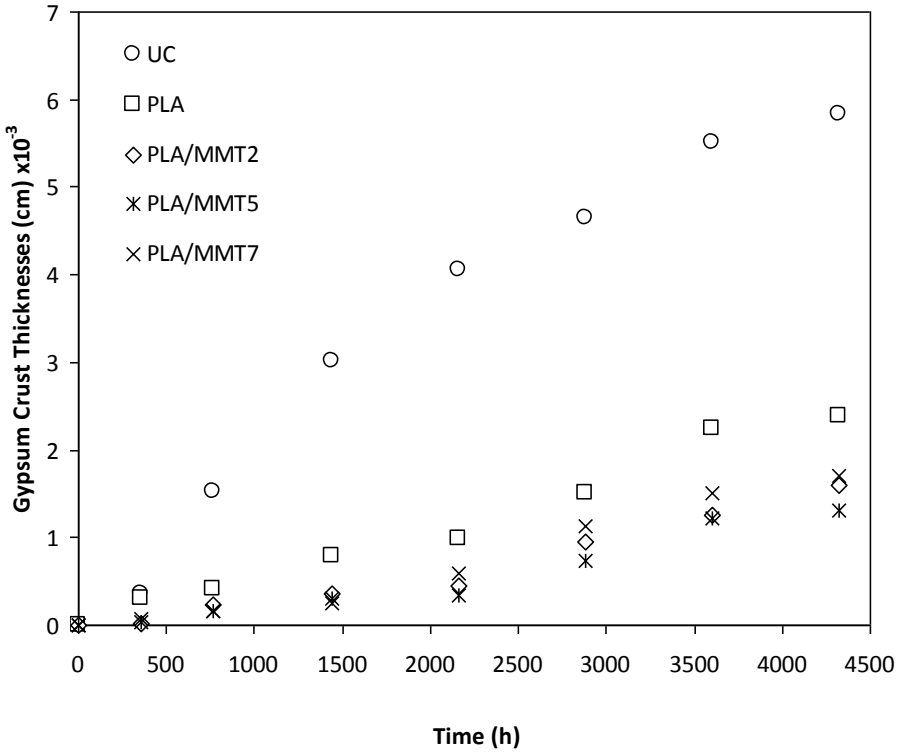

Figure 6.13. Gypsum crust thicknesses of coated and uncoated marbles

Generally acid attack experiments are not conducted in the reactor. Accelerated acid attack experiment for both the plain and nanocomposite treatments for 4 wt% of clay on concrete were investigated by Scarfato et al. (2012). The results were expressed in terms of relative mass losses percentage (i.e. mass loss of treated specimen/mass loss of untreated specimen x 100) at the end of eight cycles of immersion to a saturated solution of sodium sulfate followed by oven drying to constant weight. The group reported a good protective action of the treatments against the sulfate attack, in agreement with the capillary absorption and contact angle values. Due to immersion of treated concrete into sulfate ion solution, the pathway of acid attack occurred through

by capillary suction. The protective effectiveness was higher for the AS-based systems that exhibit higher contact angle values and the group proposed that nanoclay was adding extra benefit on the sulfate attack resistance due to an increase of nanocomposite barrier properties and a decrease for the substrate porosity (Scarfato et al., 2012).

SEM images of the uncoated marbles before and after 180 days SO_2-calicite reaction were represented in the Figure 6.14. Before the SO_2-calcite reaction, calcite crystals were easily observed on polished uncoated marble surface (Figure 6.14, a). After 180 days exposure durations, prismatic sulphation products were homogenously formed on the marble surface, and uncoated marble surfaces were entirely covered with the gypsum (Figure 6.14, b-d). Similar prismatic crystal structures were typical as a result of this reaction and reported in previous studies as well (Gauri et al., 1999; Boke et al., 2002; Ocak et al., 2009).

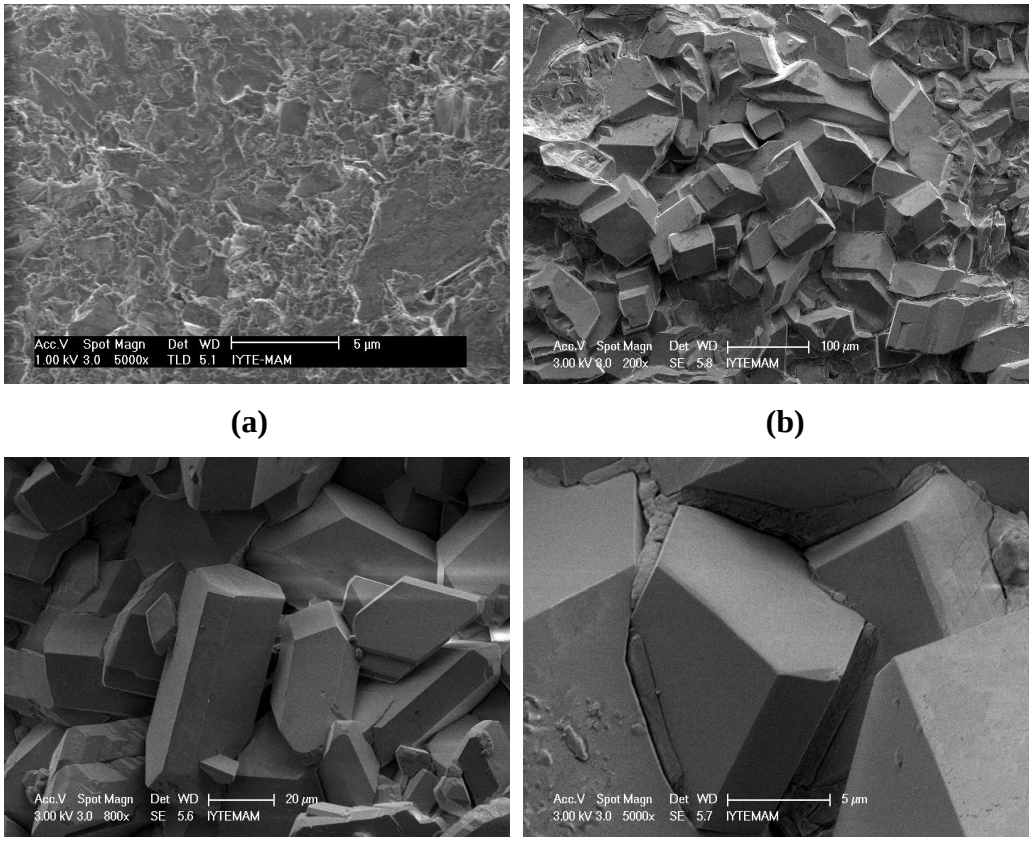

(a) **(b)**

(c) **(d)**

Figure 6.14. SEM images of the UC marbles before (a) and after 180 days (b-d) SO_2-calcite reaction

SEM images for coated marbles before putting into reaction chamber were represented in the Figure 6.15. The marble slabs were coated homogenously with bio-

nano composite coatings. Despite the fact that homogeneous coverage achieved, some bubbles were observed on the neat PLA coated surfaces which could be a result of fast solvent evaporation. However, these bubbles did not reach deep to the marble surfaces and film coverage around on the marble surface was sufficient (Figure 6.15, a).

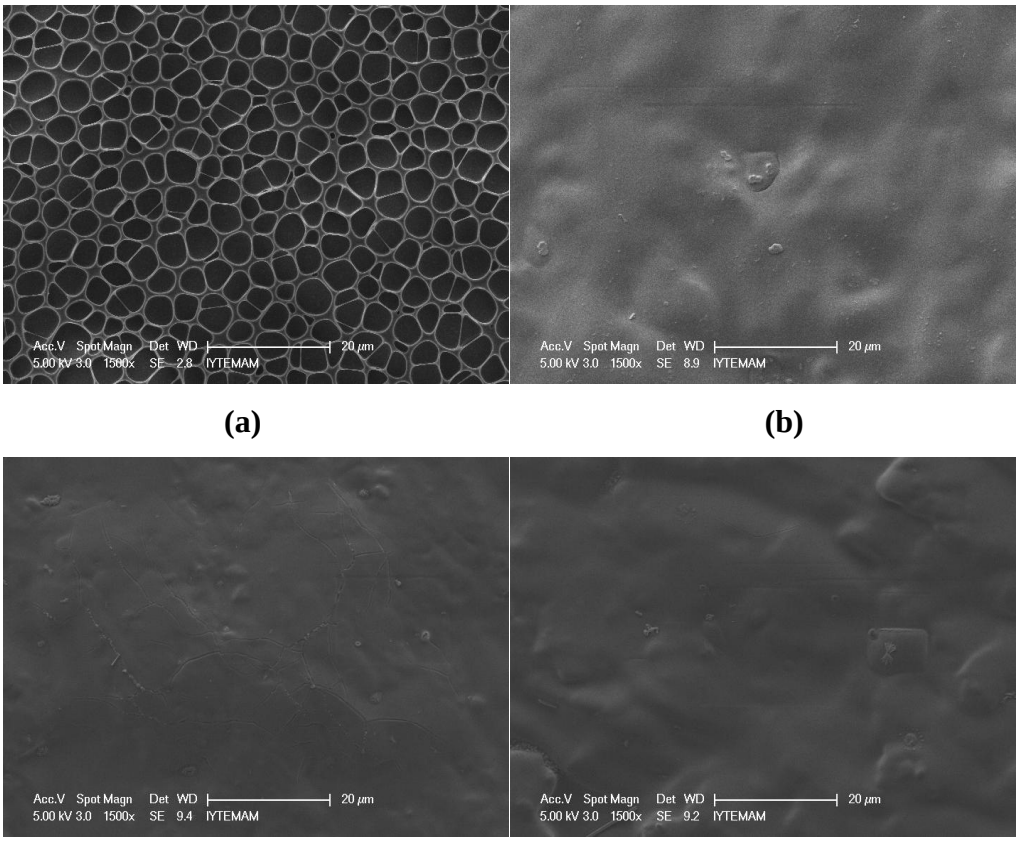

Figure 6.15. SEM images of the neat PLA (a), PLA/MMT2 (b), PLA/MMT5 (c) and PLA/MMT7 (d) coated marbles before SO_2-calcite reaction

Uncoated and coated marbles were analyzed to monitor sulphation reaction and degradation at after exposure of marble to SO_2 at certain time intervals. Any sulphation products were not observed for neat and composite coated marble surfaces up until 90^{th} day exposure of SO_2 to calcite (Figures 6.16-6.19). However, detection of low total sulfate on the coated marbles could be attributed to reaction initiation under coating layer. Similar protection results were observed on the high molecular weight PLA biodegradable polymers coated marble surfaces (Ocak et al., 2009). The amount of total sulfate on the composite coated marbles was lower than neat PLA coated marble surfaces (Figure 6.13).

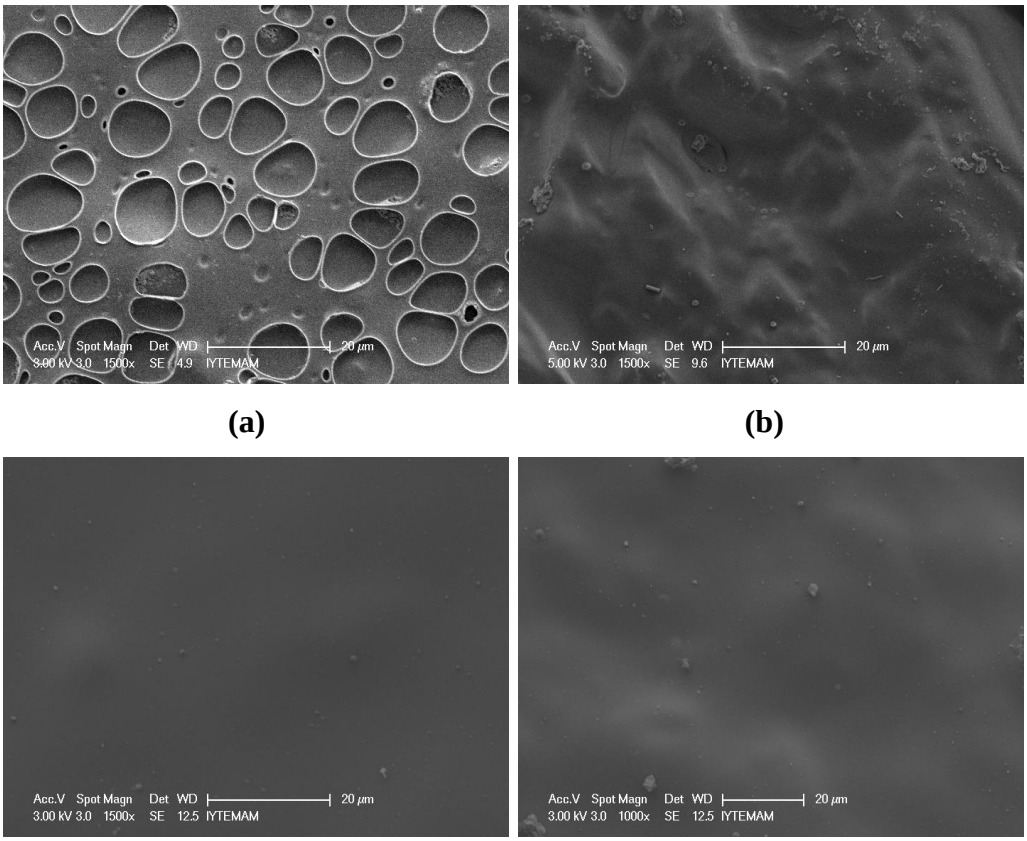

(a) **(b)**

(c) **(d)**

Figure 6.16. SEM images of the PLA (a), PLA/MMT2 (b), PLA/MMT5 (c) and PLA/MMT7 (d) coated marbles after 15 days SO_2-calcite reaction

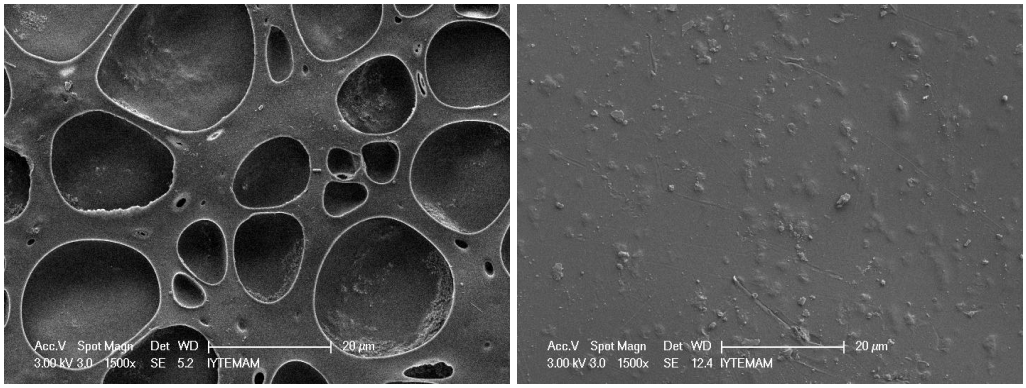

(a) **(b)**

Figure 6.17. SEM images of the PLA (a), PLA/MMT2 (b), PLA/MMT5 (c) and PLA/MMT7 (d) coated marbles after 32 days SO_2-calcite reaction

(Cont. on next page)

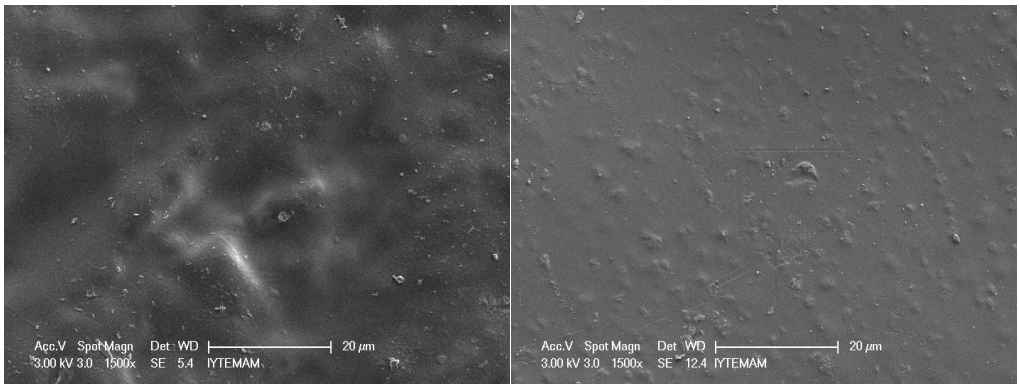

(c) **(d)**

Figure 6.17. (Cont.)

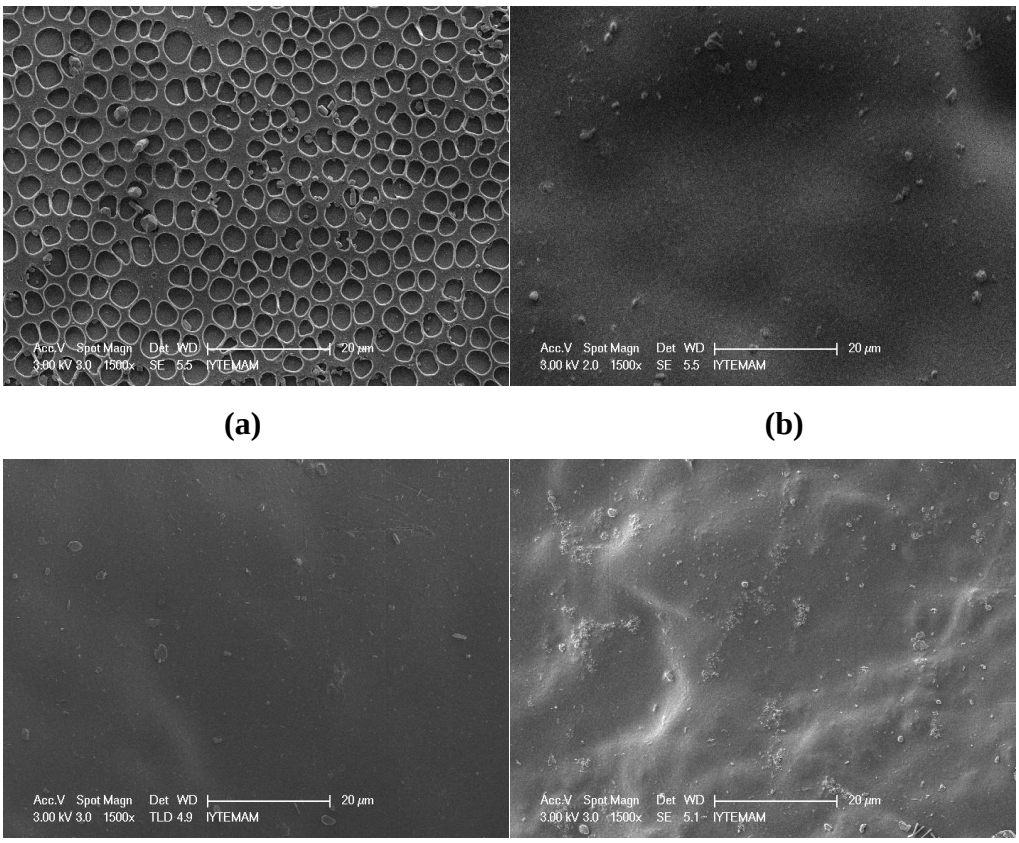

(a) **(b)**

(c) **(d)**

Figure 6.18. SEM images of the PLA (a), PLA/MMT2 (b), PLA/MMT5 (c) and PLA/MMT7 (d) coated marbles after 60 days SO_2-calcite reaction

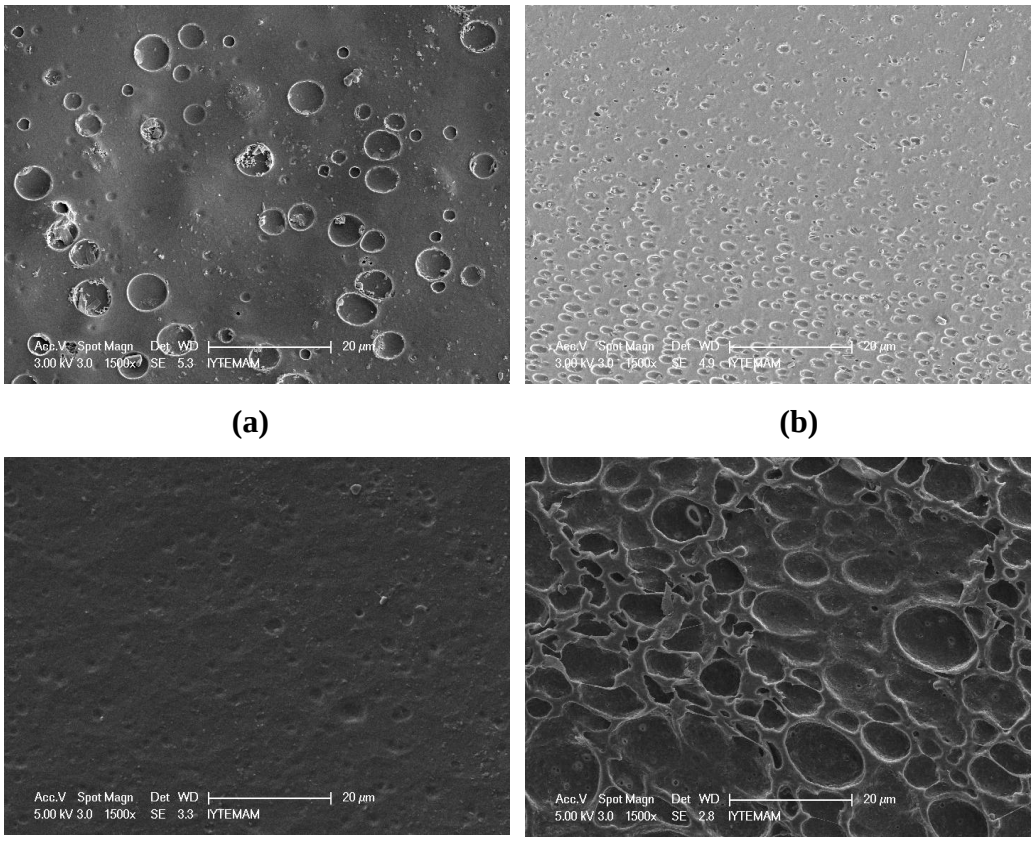

(a) **(b)**

(c) **(d)**

Figure 6.19. SEM images of the PLA (a), PLA/MMT2 (b), PLA/MMT5 (c) and PLA/MMT7 (d) coated marbles after 90 days SO_2-calcite reaction

After 120 days SO_2-calcite reaction, some holes, sulphation products crystals and evidence of the degradation were noticeable on the PLA coated marble surface (Figure 6.20, a). Despite, detection of total sulfate from the ion chromatography analysis, SEM images did not show any sulfation products structure on the surface of PLA/MMT2, PLA/MMT5 and PLA/MMT7 bio-nano composites coated marble (Figure 6.20, b-d). $CaSO_4.2H_2O$ and $CaSO_3.½H_2O$ formation under the coatings were similar to other times implying that protection of surface coating were still effective. Extension of experiment to 150 days, the sulfation products were easily begun to be observed on the all over the PLA coated marble surfaces (Figure 6.21, a). Similarly, some degradation started to be evidenced on the bio-nano composites coated marble surfaces (Figure 6.21, b-d).

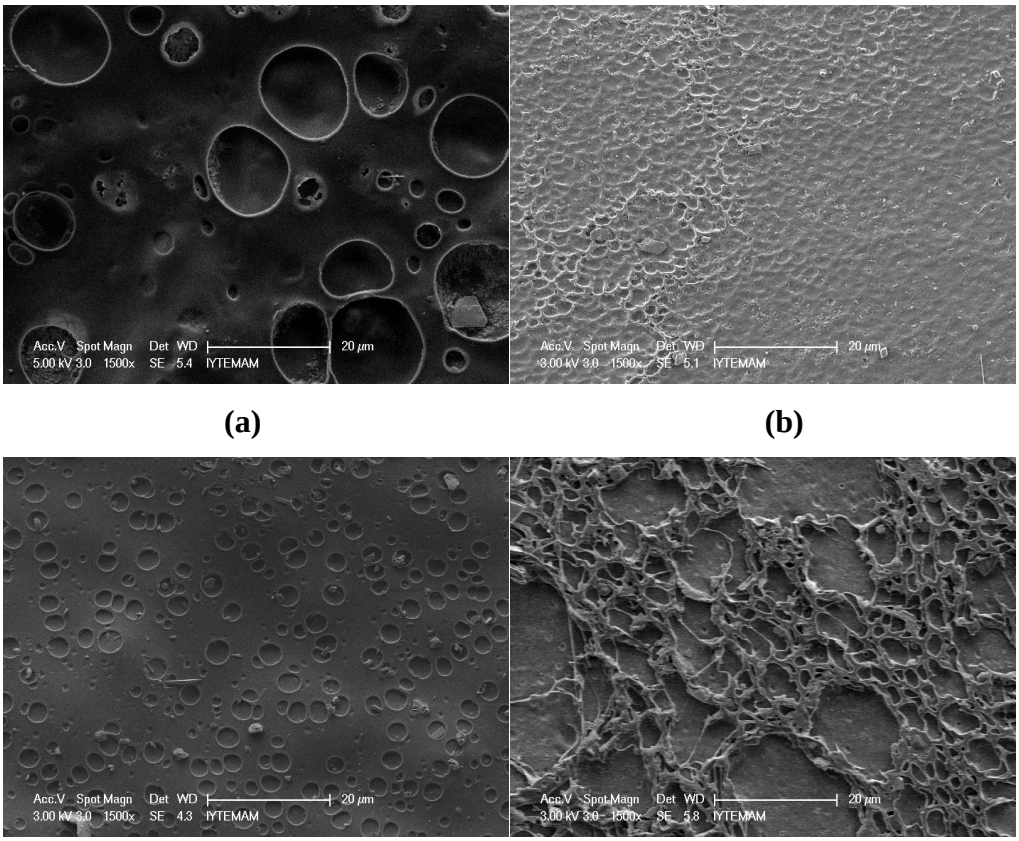

Figure 6.20. SEM images of the PLA (a), PLA/MMT2 (b), PLA/MMT5 (c) and PLA/MMT7 (d) coated marbles after 120 days SO_2-calcite reaction

SEM images of neat PLA coated marbles surfaces after 180 days of reaction showed that deformation signs such as holes and tears and formation of sulphation products such as crystals were observed perpetually on the PLA biodegradable polymer coated marble surfaces (Figure 6.22, a, b). The deformation of the PLA coating was observed on a large scale and while homogeneous calcium sulfite hemihydrate and gypsum formation were determined on the PLA film surfaces. In addition $CaSO_4.2H_2O$ and $CaSO_3.2H_2O$ crystals started to tear the PLA coating. This proved that sulphation products were formed under the film in the first stage and sulphation products grew and be seen on the film layer in second stage.

SEM images of PLA/MMT2, PLA/MMT5 and PLA/MMT7 coated marble surfaces at the end of the 180 days SO_2-calcite exposure pointed out that some deformation evidences were observed on the coating surfaces. The sulfation products were not observed around the bio-nano composites coating surfaces. However, some products (gypsum and calcium hemihydrate) crystals were started to be seen some location of PLA/MMT coated surfaces (Figure 6.23-25, b).

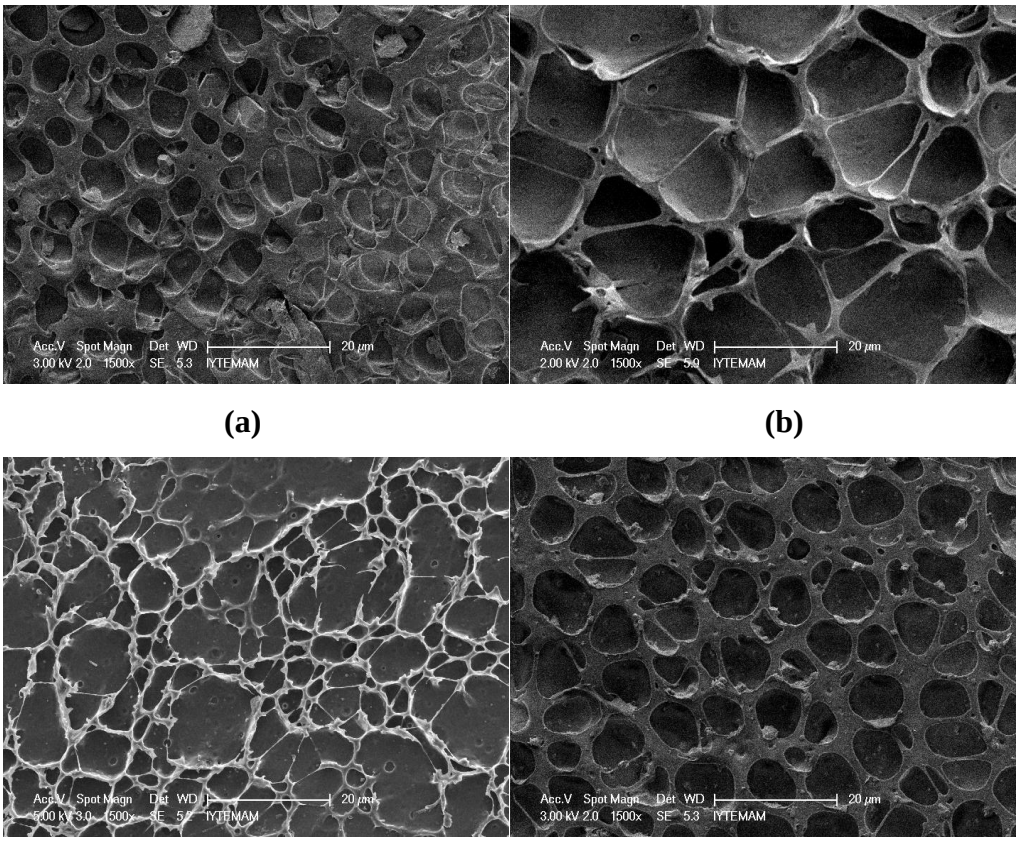

(a) **(b)**

(c) **(d)**

Figure 6.21. SEM images of the PLA (a), PLA/MMT2 (b), PLA/MMT5 (c) and PLA/MMT7 (d) coated marbles after 150 days SO_2-calcite reaction

The difference of the sulfation product crystals between the coated and uncoated sides were observed more remarkable after 180 days SO_2-calcite exposure (Figures 6.26) in the SEM pictures of semi coated marble surfaces. The huge sulfation product crystals were formed almost on the entire surface for uncoated samples (Figures 6.26).

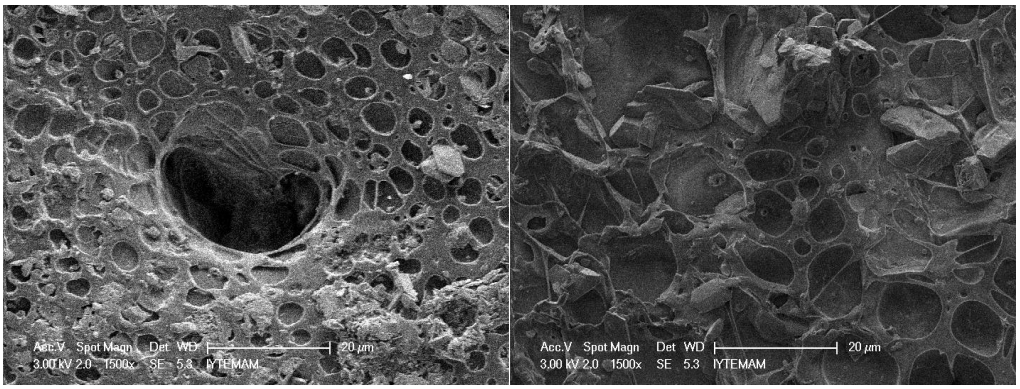

(a) **(b)**

Figure 6.22. SEM images of the neat PLA coated marbles after 180 days SO_2-calcite reaction.

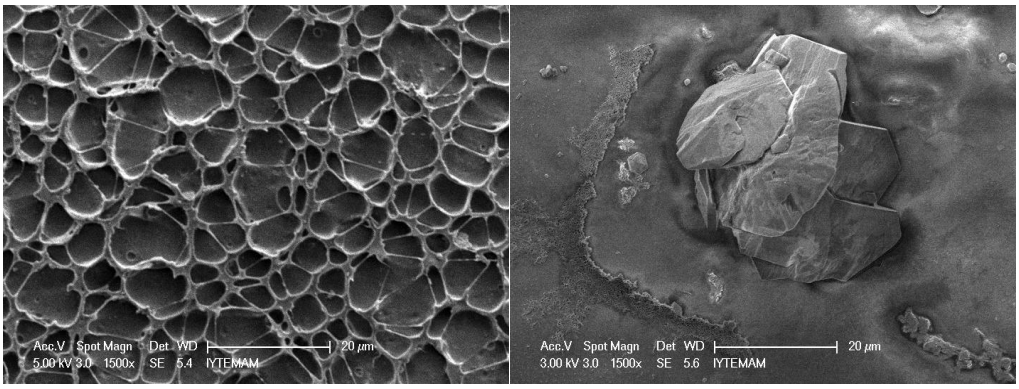

(a) **(b)**

Figure 6.23. SEM images of the PLA/MMT2 coated marbles after 180 days SO_2-calcite reaction.

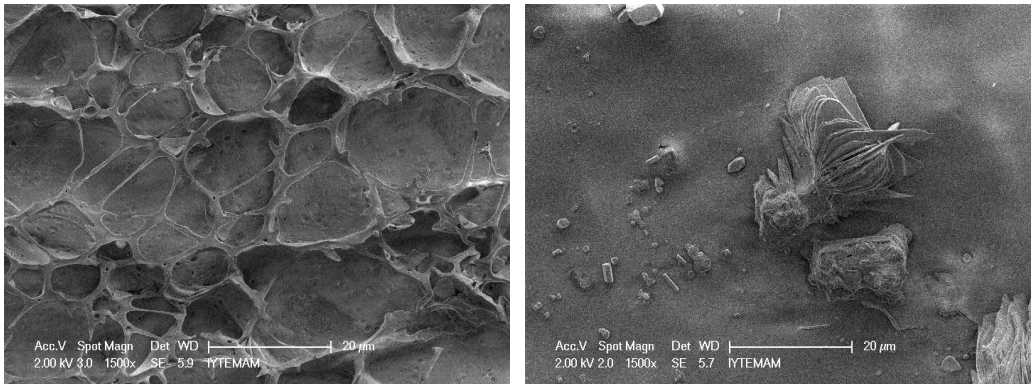

(a) **(b)**

Figure 6.24. SEM images of the PLA/MMT5 coated marbles after 180 days SO_2-calcite reaction.

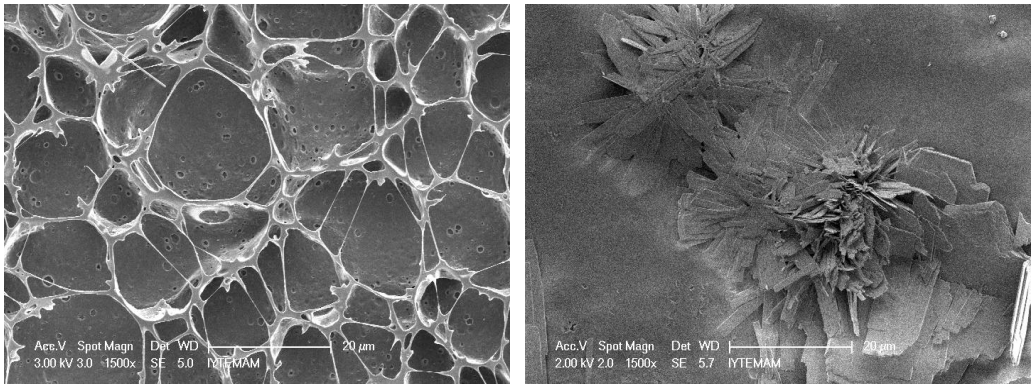

(a) **(b)**

Figure 6.25. SEM images of the PLA/MMT7 coated marbles after 180 days SO_2-calcite reaction.

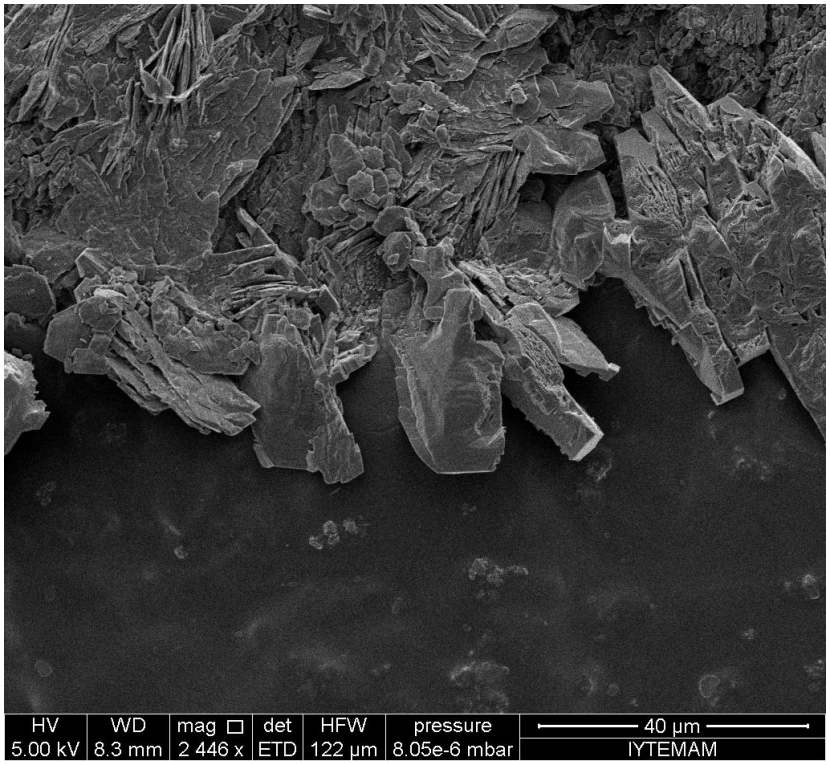

(a)

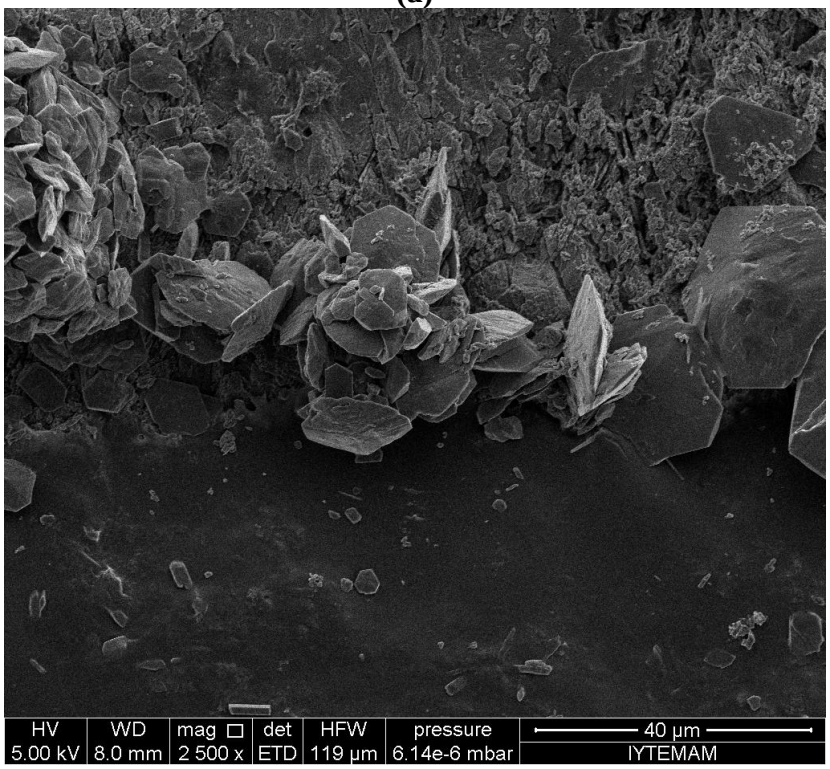

(b)

Figure 6.26. SEM images of the sulphation products on PLA (a), PLA/MMT2 (b), PLA/MMT5 (c) and PLA/MMT7 (d) semi-coated surfaces after 180 days

(Cont. on next page)

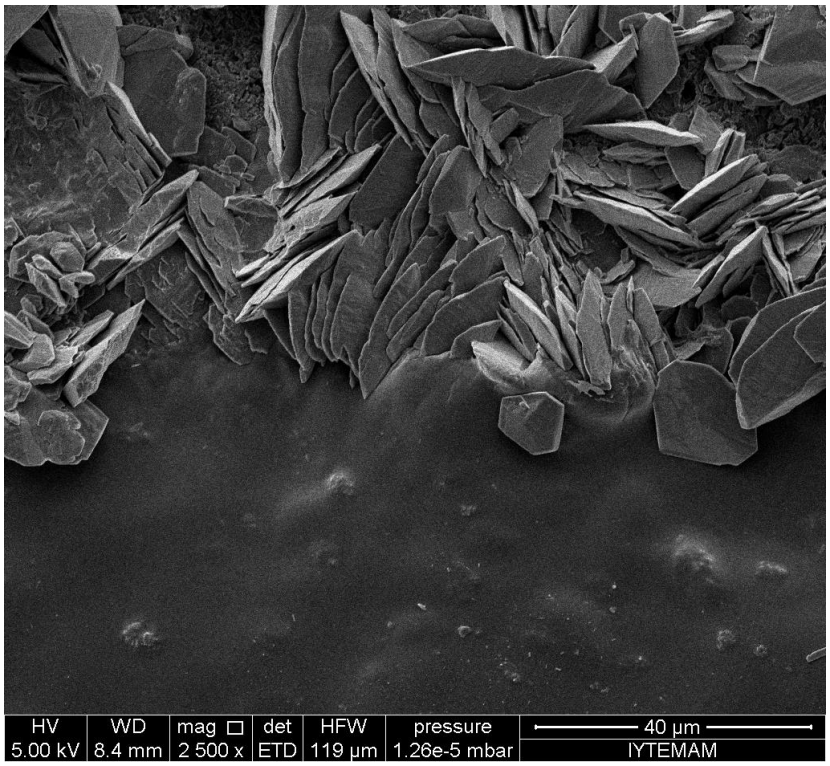

(c)

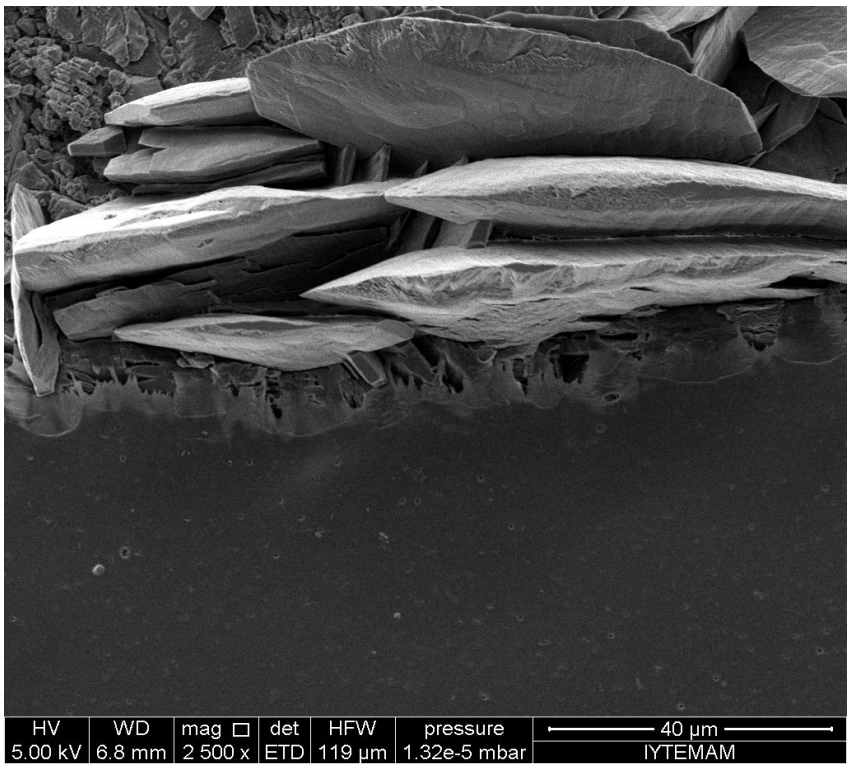

(d)

Figure 6.26. (Cont.)

To evaluate the deposition of SO_2 on the marble surfaces through the reaction one set of each neat PLA, PLA/MMT2, PLA/MMT5 and PLA/MMT7 coated and UC marble samples were placed in the reaction chamber with three replicas for control. Gypsum crust thicknesses were calculated at the end of the 30 days for SO_2-calcite reactions and gypsum crust thicknesses mean, standard deviation and percent relative standard deviation (RSD%) results were given in Table 6.1. The repeated samples crust thicknesses were statistically defined close each other and RSD% values were defined as lower than 20.

Table 6.1. The crust thickness based on coating thicknesses after 30 days SO_2-calcite exposure (n=3)

Samples	**UC**	**PLA**	**PLA/MMT2**	**PLA/MMT5**	**PLA/MMT7**
Mean	11.77	3.13	0.37	0.57	0.76
St. Dev.	0.3415	0.0664	0.0608	0.0850	0.0412
RSD%	2.9	2.1	16.5	14.9	5.3

6.3.1. The Effect of Coating Thickness

The coating thicknesses effect on the protection efficiency of composites was also studied in this study. PLA/MMT5 bio-nano composite coated marbles were prepared for investigation of this effect. The gypsum crust thicknesses were calculated as 1.79±0.150 μm, 1.61±0.166 μm, and 1.49±0.198 μm, for first, second, and third layer PLA/MMT5 coated surfaces respectively, It could be said that the increase of the coating film thickness reduced the gypsum crust formation on the marbles surfaces after 30 days exposure of marble to SO_2 and water vapor (Figure 6.27). Three layered coatings showed the lowest gypsum formation. The reason should be due to the large aspect ratio (length to thickness ratio) of the clay platelets which should increase the tortuosity (length) of the path of the gas as it diffuses into the nanocomposite and slows down the reaction.

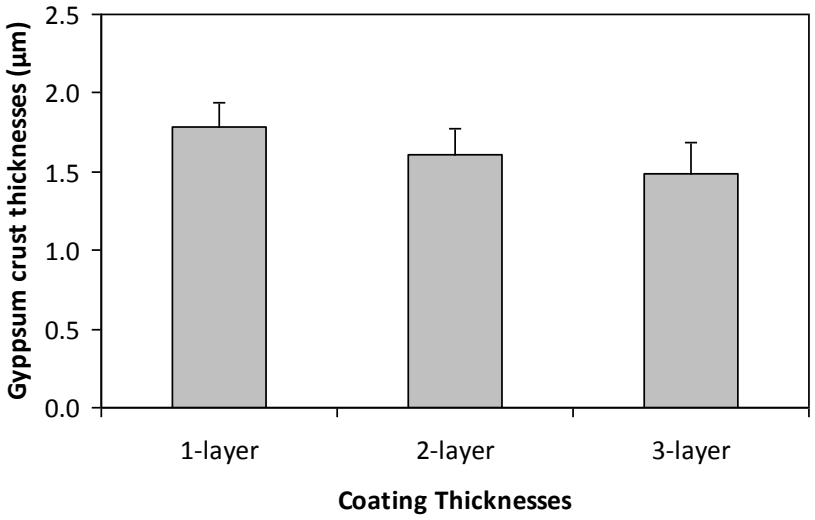

Figure 6.27. Coating thicknesses effect of the PLA/MMT5 bio-nano composites coatings on the formation of the sulphation products after 30 days SO_2-calcite reaction.

6.3.2. Kinetic Parameters of SO_2-Marble Reactions

For the determination of the reaction rate in the laboratory setup, the kinetic rate constants (k_s) mass transfer coefficient (h_d) and the internal diffusion (D_e) were determined by using shrinking unreacted core model. The previous studies showed that SO_2 calcite reaction is very fast and the reaction was kinetically controlled in the early stages. After product formation on the surface, reaction slowed down and diffusion through the product layer became to control reaction rate (Kulshreshtha et al., 1989; Yerrapragada et al., 1994; Gauri and Bandyopadyay, 1999). Moreover, Gauri and Banyopadyay (1999) and Yerrapragada et al. (1996) explained that three rate controlling steps which were film diffusion, ash or product diffusion and surface reaction controlling steps were each effective in the different phases of the crust growth. The k_s and D_e values can be obtained as unique values by non-linear regression analysis of the experimental data by using eqns 3.10-12 which related with the kinetic rate constants (k_s) mass transfer coefficient (h_d) and the internal diffusion (D_e). On the other hand, the calculation of the mass transfer coefficient, h_d, is needed to have first priority in the laboratory conditions due to laminar flow rate.

The mass transfer coefficient is related with the Sherwood number (N_{Sh}), the equivalent diameter of the experimental slab (d_p) and the binary diffusion coefficient of

the air-SO_2 system (D_{AB}) (eqn 3.13). The binary diffusion coefficient of the air-SO_2 system was found as 0.125 cm^2/s. The Sherwood number was related with Schmidt and Reynolds Numbers (eqns 3.15-17) and Sherwood, Schmidt and Reynolds Numbers were obtained as 2.481, 1.212 and 0.566 in this study. The equivalent diameter of the experimental slab (d_p) was defined as 0.36 for our slabs dimensions (1x1.5x0.15 cm). After determining the all unknown parameters, the mass transfer coefficient was calculated as 3044.36 cm/h. Tambe et al. (1991) determined the mass transfer coefficient (h_d) for uncoated marbles by using eqns 3.13-17 and the values of h_d were calculated in range of 524-555 cm/h for 2.07 cm equivalent diameter.

The unique values of the k_s and D_e were obtained by using shrinking unreacted core model with experimental data which were represented in the Table 6.2 for uncoated and coated marble slabs by using eqn 3.12. The equations from 3.1 to 3.12 by using formed crust thicknesses on the marble. The k_s value of the uncoated Marmara marble was defined as 323.76 (cm/h) and D_e was 0.49 cm^2/h. Similar values were obtained in the previous studies for the marbles as 312 cm/h for k_s and 0.14 cm^2/h for D_e in Table 3.1 (Yerrapragada et al., 1996; Gauri and Bandyopadyay, 1999). The experimental surface reaction or kinetic rate constant for Marmara marble (under 8 ppm SO_2) was found to be close to the literature value of Carrara marble (under 10 ppm SO_2). However, internal diffusion was determined to be higher than the literature value for uncoated marbles. This result also showed that Marmara marbles more endurable against extreme acidic weathering conditions when they compared with the Carrara marbles. Moreover, the k_s values were defined as 39.58, 19.67, 13.08 and 19.67 cm/h for the PLA, PLA/MMT2, PLA/MMT5 and PLA/MMT7 bio-nano composites coated marbles. The surface reaction constants were decreased for the coating marbles and lowest value was obtained for the sample of PLA/MMT5 coatings. Effective diffusivity values of the coated marbles were not calculated due to change of the rate controlling step. In model application, the rate controlling steps assumptions was also valid for the uncoated marble.

The reaction controlled steps for the coated marbles were investigated by using the shrinking core model for constant particle size (Levenspiel, 1999). The rectangular marble slabs were assumed as constant particle sized spherical samples and the initial radius of the samples was calculated as 1800 micron by using equation 3.18 (Tambe et al., 1994). The conversions of the $CaCO_3$ to gypsum (X_B) for the coated marbles were calculated by using eqns 3.19 and 3.20 (Levenspiel, 1999). The fitting of the

experimental data to the integral rate equations (from the Table 3.3) were done by using the linear regression analysis. The regression coefficients were calculated to define rate controlling steps which were kinetically or diffusional controlled for spherical constant size particle. The rate controlling steps for spherical shape and their regression coefficients for linearity were tabulated in Table 6.3.

Table 6.2. The calculated rate constants and effective diffusivities for marble-SO_2 reaction in the reaction chamber.

	Experimental*		**Literature****	
Samples	**D_e (cm^2/h)**	**k_s (cm/h)**	**D_e (cm^2/h)**	**k_s (cm/h)**
Uncoated	0.49	330.13	0.14	312
PLA	--	--	--	--
2% PLA/MMT	--	--	--	--
5% PLA/MMT	--	--	--	--
7% PLA/MMT	--	--	--	--

*Shrinking Unreacted Core Model (Eqn 3.10-12), **(SUCM)-Yerrapragada et al., 1996 (10 ppm SO_2 atmosphere)

Table 6.3. The rate controlling steps and their regression coefficients for linearity

	Regression Coefficients	
Samples	**Ash layer diffusion control (spherical)**	**Reaction control (spherical)**
Uncoated	0.9887	0.9546
Neat PLA	0.8814	0.9789
PLA/MMT2	0.8362	0.9653
PLA/MMT5	0.8147	0.9402
PLA/MMT7	0.8451	0.9528

The best fit or highest regression coefficient was determined from rate expressions controlled by diffusion through an ash or product layer for the experimental results which obtained from the uncoated marbles. This result proved that the reaction has slowed down and diffusion through the product layer began to control reaction rate

as mentioned in SUCM in the previous studies (Kulshreshtha et al., 1989; Yerrapragada et al., 1994; Gauri and Bandyopadyay, 1999). However, highest regression coefficients or best fits were obtained from reaction control (spherical) for the experimental results for all the coated marbles. These results pointed out that reaction controlling step was the kinetically controlled in the early stages. The surface reaction values were calculated from the reaction control equations from the Table 3.3 for spherical constant size particles. The new values of the surface reaction constants were found as 40.81 for PLA, 27.21 for PLA/MMT2, 27.21 for PLA/MMT5 and 40.81 cm/h for PLA/MMT7 coated marbles. The uncoated marble surface reaction constant calculated as 330.13 and coatings application on the marbles decreased the surface reaction constant values.

6.4. The Outdoor Experiment

The acid deposition occurs through two pathways: dry deposition or precipitation. Under the sheltered and dry environment condition were investigated in here. The natural stones like the carbonate rocks react with SO_2, NO_2 and acid aerosols produce a crust which mostly formed from largely made of gypsum ($CaSO_4.2H_2O$) and a small amount of nitrocalcite ($Ca(NO_3)_2.4H_2O$). The amount of the NO_2 concentration exceeded the SO_2 concentration in the modern atmosphere. However, several studies reported that formation of nitrocalcite was not exceeded the gypsum formation (Yerrapragada et al., 1994; Yerrapragada et al., 1996; Gauri and Bandyopadyay, 1999). Since, some NO_2 is used to oxidize SO_2 to sulfur trioxide (SO_3), in other words, presence of NO_2 enhanced the sulfating reaction as mentioned in previously (Eqns 1.3 to 1.5) (Johnson et al., 1988; Elfving et al., 1994; Henriksen et al., 1994; Gauri and Bandyopadhyay, 1999).

The outdoor experiments always include some difficulties when it compared with the laboratory experiments. Since, laboratory experiments are realized under the controlled atmospheres such as constant SO_2 and NO_2 concentrations, temperature, relative humidity and laminar flow conditions, adequate data can be collected in a shorter period of time in the artificial atmospheric chamber. However, outdoor conditions such as SO_2 and NO_2 concentrations, temperature, relative humidity and the presence of other pollutants can unpredictably change. After the exposure of coated marbles to sheltered outdoor environment, gypsum and nitrocalcite could form as a

form of crust on the marble (Yerrapragada et al., 1994; Yerrapragada et al., 1996; Gauri and Bandyopadyay, 1999).

In this part of study, the uncoated, PLA polymer, PLA/MMT2, PLA/MMT5 and PLA/MMT7 bio-nano composites coated marble slabs were exposed to city atmosphere to estimate protection abilities of the composites coating materials under sheltered area in Izmir. At the end of the 6, 9 and 20 months (4320, 6480 and 14400 hours) of exposure, total crust thicknesses formed on the surfaces of marbles were calculated and images of surfaces were observed by SEM. The decrease on the crust thicknesses on these surfaces were approximately 2-3 times lower for the PLA biodegradable polymer coated while it was 9-10 times lower for bio-nano composites coated surfaces at the end of 20 months of exposure (Figure 6.28). The comparison of nano clay added coatings, the lowest gypsum formation was obtained from the PLA/MMT5 coated marble surfaces similar to laboratory experiments. Scarfato et al. (2012) pointed out that the low clay loading (<6 wt%) enhance the mechanical and barrier properties of the polymers.

The SEM images of the uncoated marbles before and after 6, 9 and 20 months to outdoor atmosphere were presented in the Figure 6.29. In the first exposure duration at the 6 months, the calcite crystals were started to degrade obviously and crust products begun to observe on the uncoated marble surfaces (Figure 6.29, b). The degradation product crystals were observed on the many parts of the uncoated marble surfaces after 9 months exposure durations (Figure 6.29, c). The degradation product crystals were homogenously formed on the uncoated marble surfaces after 20 months SO_2-NO_2-calicite exposure duration (Figure 6.29, d-f). These SEM images brought into sharp relief on the detrimental effects of the atmospheric pollutions on the marble calcite crystals. Moreover, the structure of the formed crystals were resembled the gypsum crystals which observed in the SEM images of the laboratory experiments. Previous studies reported that mostly gypsum was formed on the carbonate stones after SO_2-NO_2-calicite reaction (Yerrapragada et al., 1994; Yerrapragada et al., 1996; Gauri and Bandyopadhyay, 1999).

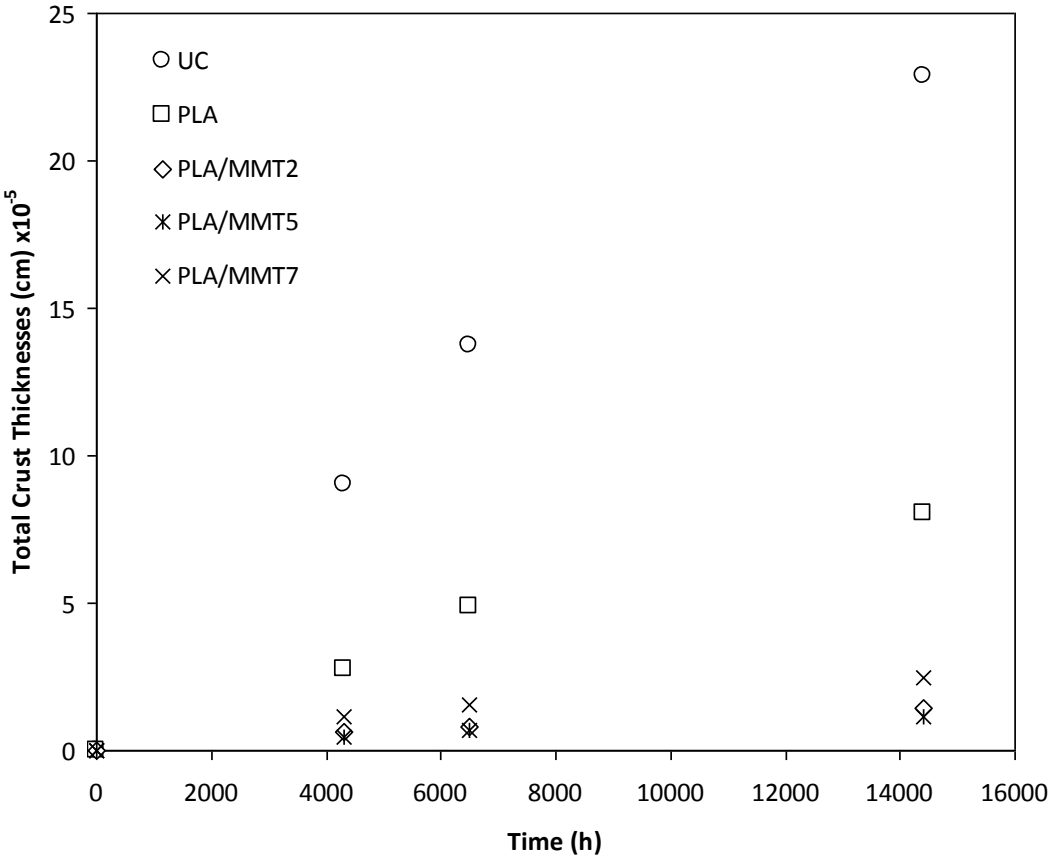

Figure 6.28. Total crust thicknesses of the PLA, PLA/MMT2, PLA/MMT5 and PLA/MMT7 bio-nano composite coated and uncoated marble slabs.

The SEM images of the PLA, PLA/MMT2, PLA/MMT5 and PLA/MMT7 bio-nano composite coated surfaces after 6 months SO_2-NO_2-calicite reaction were given in the Figure 6.30. Any significant degradation evidences or formed crust crystals were not observed on the PLA, PLA/MMT2, PLA/MMT5 and PLA/MMT7 bio-nano composite coated marble surfaces (Figure 6.30).

The SEM images of the PLA, PLA/MMT2, PLA/MMT5 and PLA/MMT7 bio-nano composites coated surfaces after 9 months SO_2-NO_2-calcite reaction were given in the Figure 6.31. As same as the 6 months exposure duration, there were not any significant degradation evidences or formed crust crystals on the PLA/MMT2, PLA/MMT5 and PLA/MMT7 bio-nano composites coated marble surfaces (Figure 6.31). However, degradation products crystals were begun to appear on the some parts of the neat PLA biodegradable polymer coated surfaces, some holes were appeared on the coating surface and these crystals begun to tear the polymer coating (Figure 6.31, a).

Crystals formed on the coatings proved the formation of the sulphation products on marble under the coating films.

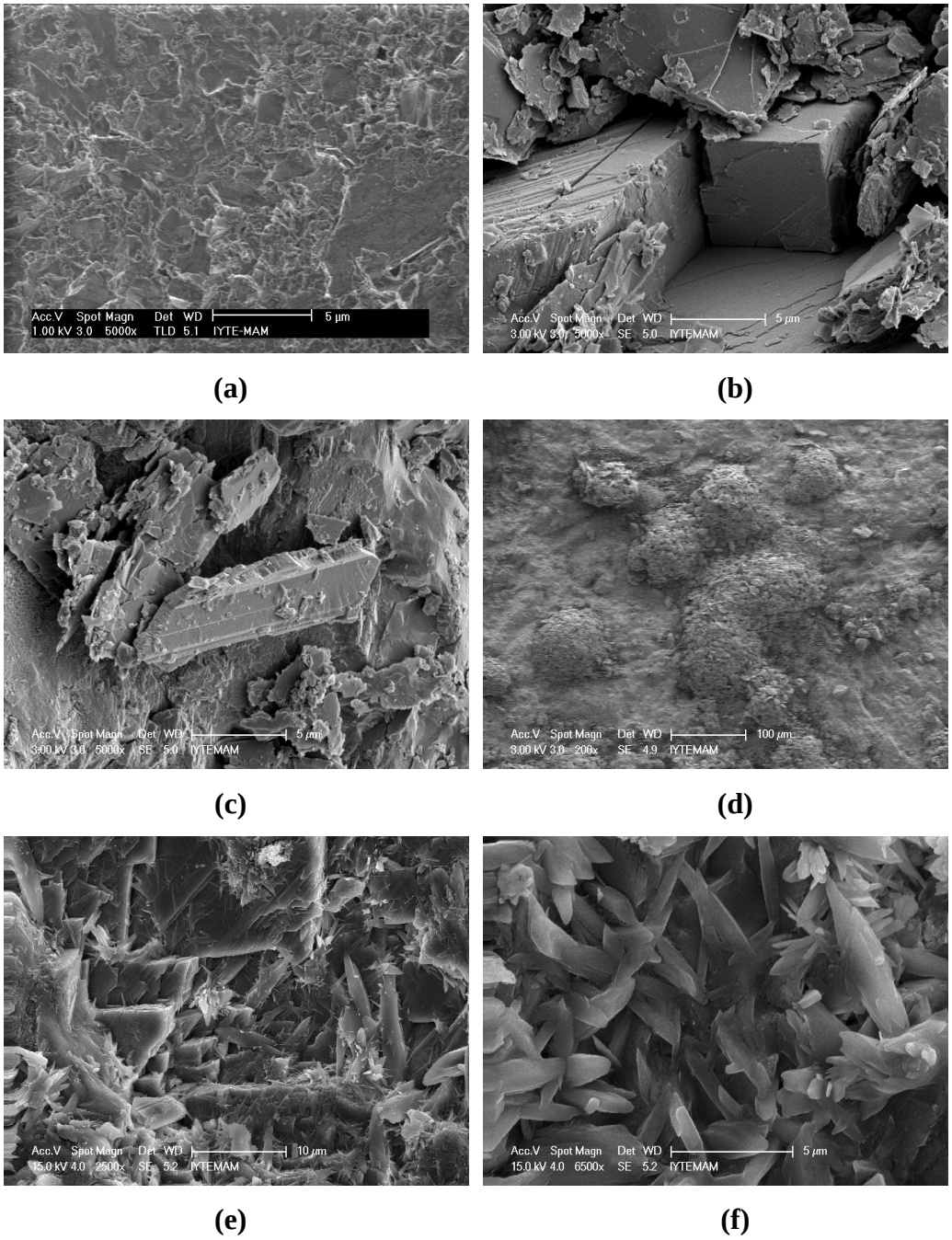

(a) **(b)**

(c) **(d)**

(e) **(f)**

Figure 6.29. SEM images of the uncoated marbles before (a) and after 6 (b), 9 (c) and 20 months (d-f) SO_2-NO_2-calicite reaction

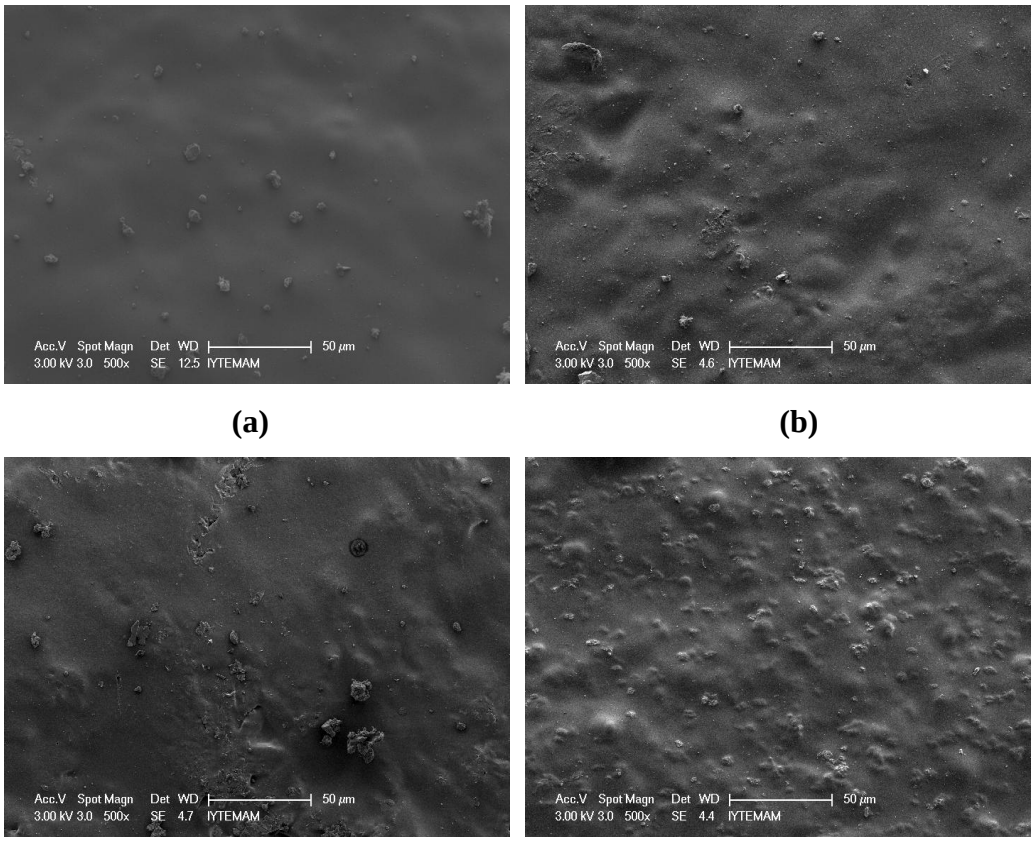

Figure 6.30. SEM images of the PLA (a), PLA/MMT2 (b), PLA/MMT5 (c) and PLA/MMT7 (d) bio-nano composites coated surfaces after 6 months of exposure to city atmosphere

After 20 months long-term exposure, degradation evidences were obviously started to be observed on the PLA biodegradable polymer and PLA/MMT bio-nano composite coated surfaces (Figure 6.32). For the PLA biodegradable polymer coated marble surfaces, not only deformation evidences such as holes and tears on the coated surfaces but also crust formation as crystals were homogenously observed in the SEM images (Figure 6.32, a). Gypsum or other crystal formed under the PLA film began to tear the coating materials. The small amount of the crystal structures were observed on the coating surfaces of PLA/MMT2 and PLA/MMT7 coated marble surfaces (Figure 6.32, b, d). Moreover, deformation evidences such as holes and tears were observed obviously on the PLA/MMT2 and PLA/MMT7 coating materials similarly as PLA coated surfaces (Figure. 6.32, b, and d).

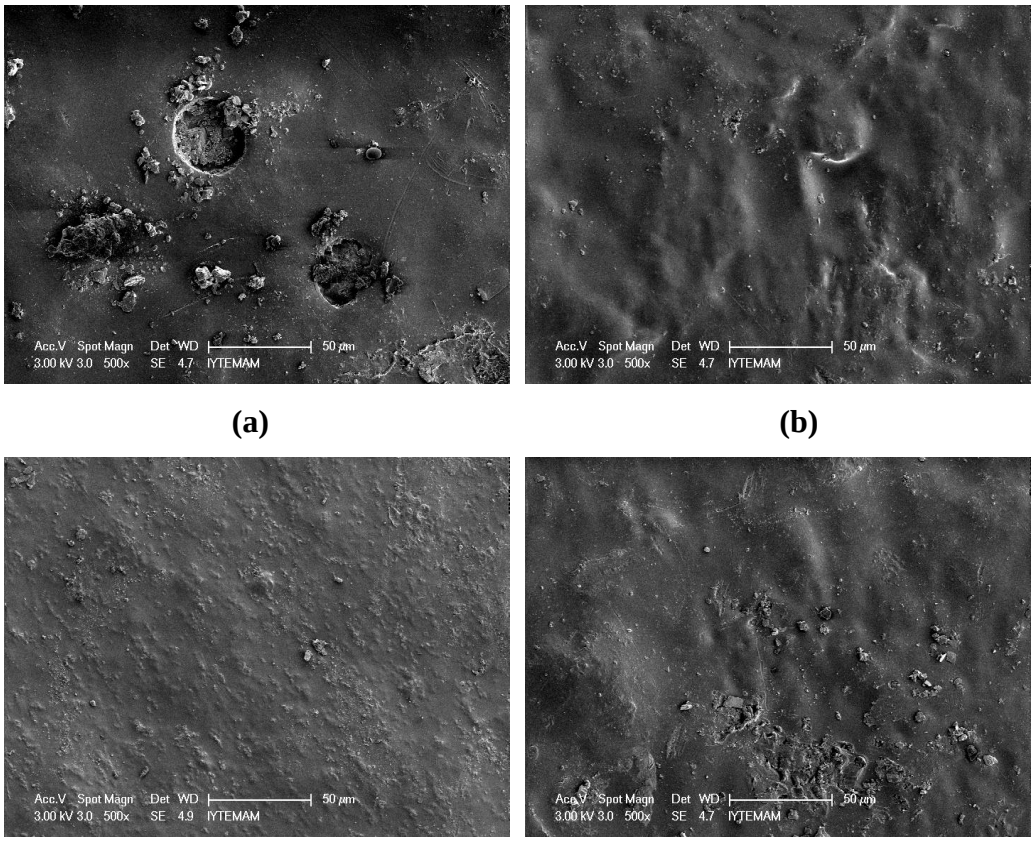

Figure 6.31. SEM images of the PLA (a), PLA/MMT2 (b), PLA/MMT5 (c) and PLA/MMT7 (d) bio-nano composites coated surfaces after 9 months of exposure to city atmosphere

Relatively less degradation evidences and crust formation were observed for PLA/MMT5 coated marble surfaces (Figure 6.32, c). Even though some holes were present on the surface of PLA/MMT5 coated surfaces, no tearing of crystal was observed (Figure 6.32, c). PLA/MMT5 coatings showed relatively better appearance when they compared with the other coatings after 20 months exposure to city atmosphere.

To demonstrate the experimental variation in the same batch 3 coated marble replicates were used at the end of the 6, 9 and 20 months exposure to city atmosphere. The crust thicknesses were calculated and RSD% values were ≤ 20% (Table 6.4).

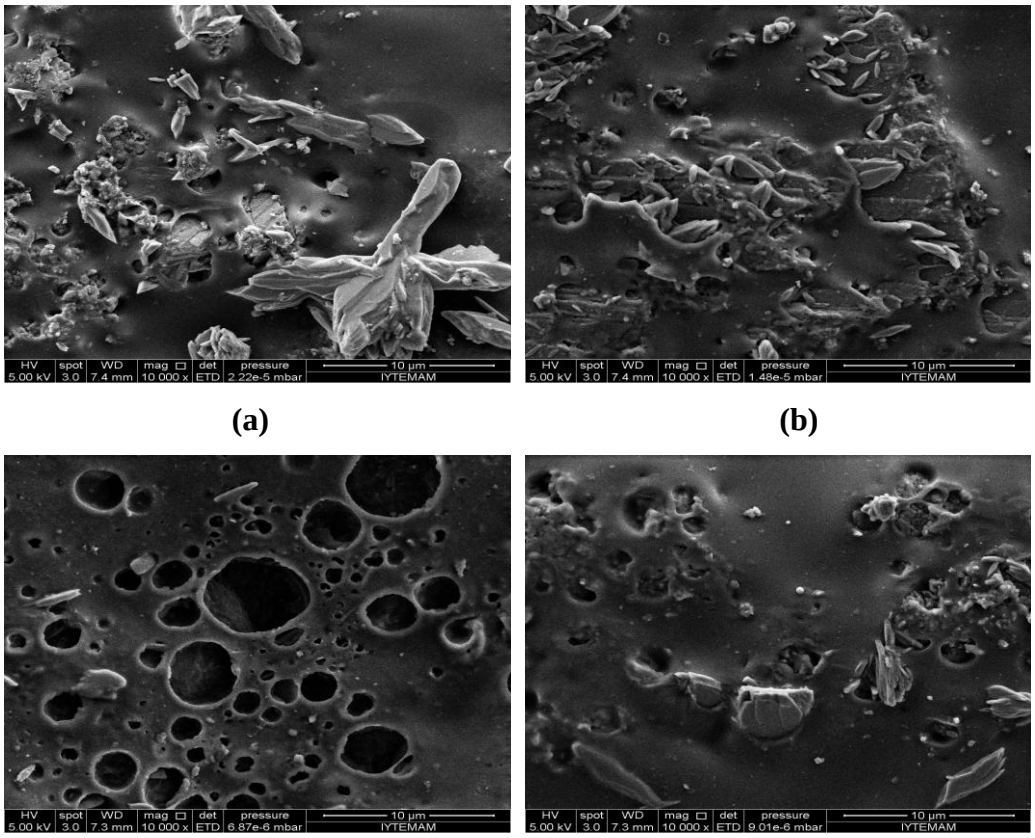

Figure 6.32. SEM images of the PLA (a), PLA/MMT2 (b), PLA/MMT5 (c) and PLA/MMT7 composite coated surfaces after 20 months of exposure to city atmosphere

Table 6.4. The crust thickness variation for the samples (n=3) at exposed to ambient air.

Time (months)	Sample	UC	PLA	PLA/MMT2	PLA/MMT5	PLA/MMT7
6	Mean	0.905	0.279	0.064	0.048	0.113
	St.Dev.	0.115	0.055	0.002	0.003	0.005
	RSD%	12.7	19.9	3.2	6.8	4.1
9	Mean	1.372	0.489	0.081	0.067	0.153
	St.Dev.	0.214	0.137	0.012	0.008	0.028
	RSD%	15.6	28	14.8	11.1	18.4
20	Mean	2.290	0.803	0.143	0.116	0.245
	St.Dev.	0.447	0.165	0.023	0.020	0.049
	RSD%	19.5	20.5	15.8	17.4	19.8

The measured ionic mass of the SO_4^{2-} was higher than the ionic mass of the NO_3^- at the end of the 6, 9, and 20 months of exposure to ambient air (Table 6.5). The gypsum formations were found to be higher than the nitro-calcite formation on the uncoated marbles for the outdoor conditions in the literature (Gauri and Bandyopadyay, 1999; Yerrapragada et al., 1996). The gypsum + nitro-calcite to gypsum ionic masses ratios were defined as 1.13:1 for 6 months, 1.16:1 for 9 months and 1.20:1 for 20 months exposure for the uncoated marbles while ionic masses ratios defined as 1.20:1, 1.16:1, 1.17:1 and 1.20:1 for PLA, PLA/MMT2, PLA/MMT5 and PLA/MMT7 respectively. Yerrapragada et al. (1996) found this ratio as 1.25:1 in the early exposure period for uncoated marble. The difference in the ratios could be resulted from difference in the concentration in the ambient air where the uncoated marbles exposed to. The ratio values which obtained from the coated marbles showed that coatings decreased the gypsum + nitro-calcite to gypsum ionic masses ratios on the marble surfaces. In other words, gypsum formation on the marble surface decreased when compared with the nitro-calcite formation.

Table 6.5. The average values of the ionic mass of SO_4^{2-} (*$m(SO_4^{2-})$, g*) and NO_3^- *($m(NO_3^-)$, g*) after 6, 9 and 20 months of exposure to ambient air.

Time (months)	Sample	UC	PLA	PLA/MMT2	PLA/MMT5	PLA/MMT7
6	$m(SO_4^{2-})$	0.905	0.279	0.064	0.048	0.113
	$m(NO_3^-)$	0.115	0.055	0.002	0.003	0.005
9	$m(SO_4^{2-})$	1.372	0.489	0.081	0.067	0.153
	$m(NO_3^-)$	0.214	0.137	0.012	0.008	0.028
20	$m(SO_4^{2-})$	2.290	0.803	0.143	0.116	0.245
	$m(NO_3^-)$	0.447	0.165	0.023	0.020	0.049

The atmospheric SO_2, NO, NO_2 and NO_x values were measured from the monitoring stations in some urban sites such as Karşıyaka, Güzelyalı, Bornova, Alsancak, Şirinyer, Çiğli and Bayraklı in Izmir by the Environmental Protection and Control Department (EPCD) of the Izmir Metropolitan Municipality. The daily, monthly and annual SO_2 values in the all monitoring stations and NO, NO_2 and NO_x values only in the Alsancak station were measured continuously from 2010 to 2012. The measured annual SO_2 concentrations were 15±3 μg/m^3 for 2010, 19±8.27 μg/m^3 for

2011 and 8±1.26 μg/m^3 for 2012. When the monthly mean values compared with each others, highest values measured as 21±10.86 and 17±12.01 μg/m^3 in March and December in 2010, 36±7.02 and 32±21.50 μg/m^3 in June and January in 2011 and 11±8.52 and 9±6.43 μg/m^3 in February and March in 2012 (EPCD, 2013). The results pointed out that SO_2 concentration was increased in the winter season. The annual NO, NO_2 and NO_x were defined as 61±46.75, 79±74.41 and 137±60.84 μg/m^3 for the year of 2012. When the monthly mean values of the NO, NO_2 and NO_x were compared with each other, highest concentrations were measured as 217±43.47 and 246±69.94 μg/m^3 in October and November for NOx, 201±38.59 and 243±69.60 μg/m^3 in October and November for NO_2 and 111±16.72 and 126±15.92 μg/m^3 in August and September for NO in 2012 (EPCD, 2013). For the measurements of the European cities and regions, NO_2 concentrations were measured as higher than the SO_2 concentrations similarly as in the Izmir metropolitan area.

The changes of the atmospheric gases pollutants in the ambient city atmosphere and their effects on the weathering of the marbles also investigated in this study. The PLA/MMT2, PLA/MMT5 and PLA/MMT7 composites and PLA coated and uncoated marbles were exposed ambient atmosphere for 6 months (from May 2010 to November 2010), 9 months (from May 2010 to February 2011) and 20 months (from May 2010 to February 2012). The first 6 months average SO_2, NO, NO_2 and NO_x concentrations were 14±3, 95±36, 70±65 and 162±33 μg/m^3, the first 9 months average SO_2, NO, NO_2 and NO_x concentrations were 17±7, 67±52, 93±82 and 157±57 μg/m^3 and the first 20 months average SO_2, NO, NO_2 and NO_x concentrations were 16±7, 65±48, 88±77 and 151±55 μg/m^3 were measured by the EPC Department of the Izmir Metropolitan Municipality. When the average the ionic mass of nitrate and sulfate values (Table 6.6) of the 9 months was compared with 6 months, the nitrate (approximately 2 times) and sulfate ionic masses were increased. The increase of the SO_2 (from 14±3 to 17±7 μg/m^3) and NO_2 (from 70±65 to 93±82 μg/m^3) concentrations enhanced the masses of the sulfate and nitrate on the uncoated marbles. Similar increases (mostly nitrate ionic masses) were observed for the all coatings after 9 months exposure durations. In the last 20 months exposure durations, the measured average SO_2 and NO_2 concentrations were decreased from 17±7 to 16±7 μg/m^3 and 93±82 to 88±77 μg/m^3. The formation amounts of the sulfate and nitrate ionic mass values were decreased after 20 months exposure durations when they compared with the values at the end of the 9 months exposure durations.

6.4.1. The Effect of Coating Thickness

The effects of the coating film thicknesses on the protection efficiencies of the bio-nano composites were investigated as similar to laboratory experiment. The PLA/MMT5 bio-nano composite was selected to investigate the coating thickness effects on the protection properties of the coatings due to the excellent protection abilities. The marbles were 1, 2 and 3 times coated with PLA/MMT5 bio-nano composites on top of each other as similar to laboratory conditions and we obtained 1, 2 and 3-layer coated marble slabs which had three different coating thicknesses. The coating thicknesses were defined as 17.39±1.41 μm for the 1-layer, 27.62±1.39 μm for the 2-layer coated 39.52±2.19 μm which measured from the 10 different points of the cross section of the bio-nano composite. The coating thickness effect of PLA/MMT5 coated on the formation of the sulfation products after 6 months outdoor conditions exposures were represented in the Figure 6.33. The gypsum crust thickness of the one-layer PLA/MMT5 coated marbles was found to be 0.98±0.13 μm, two-layer as 0.71±0.11 μm and three-layer as 0.63±0.11 μm. The increase in the coating film thickness reduced the gypsum and nitro-calcite crust formation on the marble surfaces after 6 months SO_2-NO_2-calcite reaction due to extra film resistance was created for the diffusion of pollutants

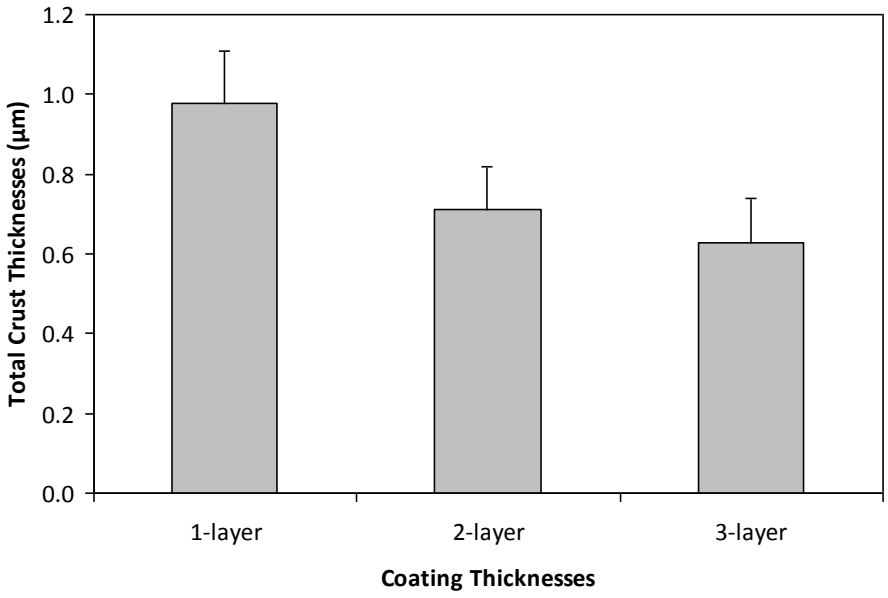

Figure 6.33. Coating thicknesses effect on the formation of gypsum after 6 months outdoor exposure.

6.4.2. The Evaluation of Kinetic Parameters under Outdoor Conditions

The kinetic and modeling decay rates of the marble were investigated to estimate the extent of reaction occurred on the coated and uncoated marble surfaces in ambient air. Similar to laboratory setup, rate controlling parameters which are the mass transfer coefficient (h_d) and the kinetic rate constants (k_s) and the internal diffusion (D_e) were assumed to be valid for the ambient air and can be accepted as inverse of the corresponding resistances (Yerrapragada et al., 1996; Gauri and Bandyopadhyay, 1999).

SO_2 and NO_2 calcite reaction was very fast and the reaction was kinetically controlled in the early stages. After product formation on the surface, reaction slows down and diffusion through the product layer dominates the control of reaction rate (Kulshreshtha et al., 1989; Yerrapragada et al., 1994; Gauri and Bandyopadhyay, 1999). The ambient air assumptions for the model are turbulent flow and bulk concentrations of the gaseous reactants as ambient air concentrations. In addition, the mass transfer coefficient can be assumed as infinitely and could be neglected for the outdoor conditions (Yerrapragada et al., 1994; Gauri and Bandyopadhyay, 1999).

Table 6.6 presents calculated rate constant and effective diffusivity values of SUCM in ambient air The k_s and D_e values were higher than the available literature values which was belong to Carrara marble. The type of marble and meteorological condition could be reasons for these differences. The lowest values (D_e, k_s) were obtained for PLA/MMT5 composite coated surfaces

Table 6.6. The calculated k_s and D_e values for Marmara marble at ambient air for SCUM

Samples	**Experimental***		**Literature****	
	D_e (cm^2/h)	**k_s (cm/h)**	**D_e (cm^2/h)**	**k_s (cm/h)**
Uncoated	0.13	394.7	0.11	375
PLA	0.013	118.4	--	--
PLA/MMT2	0.0003	23.7	--	--
PLA/MMT5	0.0002	19.7	--	--
PLA/MMT7	0.0006	59.2	--	--

*(SUCM)-Gauri and Bandyopadhyay, 1999, **(SUCM)-Yerrapragada et al., 1996 (10 ppb SO_2 and 25 ppb NO_2)

6.4.3. Surface Properties after Outdoor Exposures

6.4.3.1. Color Alteration

Color variation or optical appearance of the coated and uncoated marbles just only related with the esthetic perspective. Before the outdoor exposure ΔE values for PLA, PLA/MMT2 and PLA/MMT5 coated marbles were found as clinically acceptable ($1<\Delta E<3.3$). However, the values of ΔE were calculated as higher than 3.3 which referred as clinically were not accepted for the PLA/MMT7 coating before reaction. The color variations of the bio-nano composites under outdoor conditions were also investigated. The ΔE values for the uncoated, PLA, PLA/MMT2, PLA/MMT5 and PLA/MMT7 bio-nano composite coated marbles were calculated after 20 months outdoor exposures and represented in the Figure 6.34. The ΔE values were defined as 20.51±1.32 for uncoated, 26.09±1.50 for neat PLA, 22.59±0.98 for PLA/MMT2, 22.39±0.73 for PLA/MMT5 and 21.04±1.36 for PLA/MMT7 bio-nano composites coatings. These higher color variation results showed that all coatings lost their aesthetic properties after 20 months. However, high color variation value of uncoated marbles after 20 months showed that coatings did not remarkably lost their transparency.

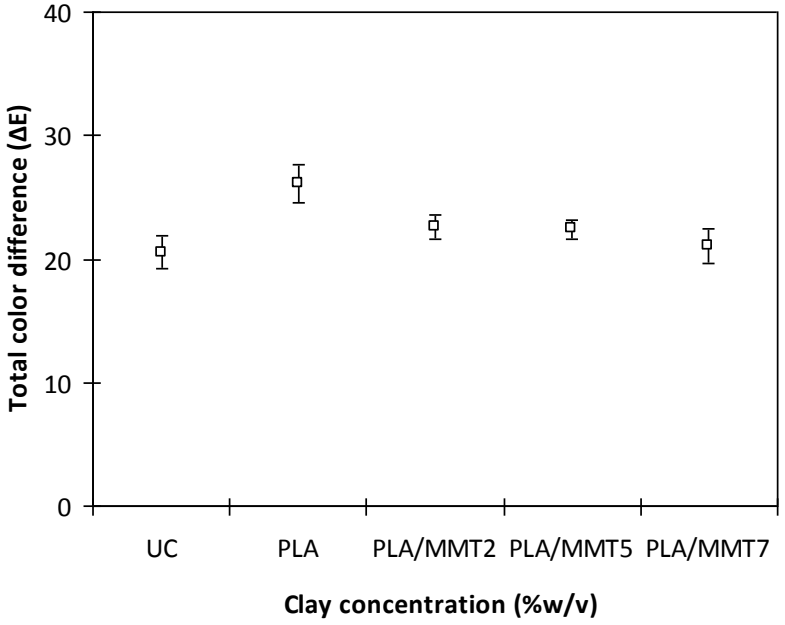

Figure 6.34. Total color variation (ΔE) of the uncoated, PLA, PLA/MMT2, PLA/MMT5 and PLA/MMT7 coated marbles after 20 months outdoor exposures. Error bars represent one standard deviation.

6.4.3.2. Water Contact Angle

Hydrophobicity is the significant parameter which shows the tendency of water being repelled of water from surface of coating materials. Before the outdoor exposures, marble surfaces were characterized as hydrophilic materials. Neat PLA, PLA/MMT2, PLA/MMT5 and PLA/MMT7 bio-nano composites coating increased the contact angle value of the marble surfaces and coated marble surfaces behaves as hydrophobic before the outdoor exposures. Additionally, increase of the nano particles in the polymer matrix enhanced the surface hydrophobicity up to 5%. The water contact angle values were measured after the 20 months outdoor exposures and obtained values were given in the Figure 6.35. The contact angle values were as 36±3.82 for uncoated marble, 9.25±2.05 for neat PLA polymer, 38.25±5.75 for PLA/MMT2, 40.75±4.13 for PLA/MMT5 and 38±5.23 for PLA/MMT7 bio-nano composites coated marbles referring 20 months outdoor exposures changed the surfaces extremely to hydrophilic. These significant reductions on contact angle could be resulted from the formed gypsum and nitrocalcite crystals on the coating materials and loose of protection efficiency of the coating material due to polymeric degradation. Since, gypsum and nitro-calcite crystals can be classified as deliquescent salts and these crystals may increase the water content or water contact angle values of the stones.

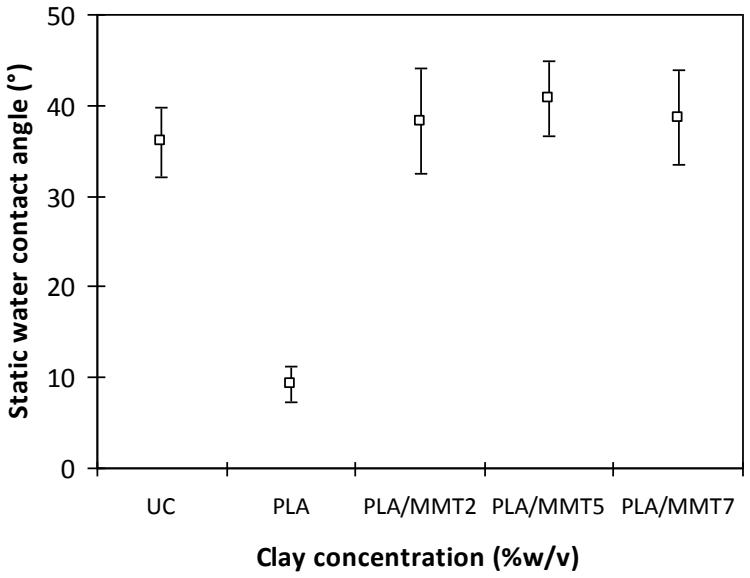

Figure 6.35. Water contact angle values of the uncoated, PLA, PLA/MMT2, PLA/MMT5 and PLA/MMT7 coated marbles after 20 months outdoor exposures. Error bars represent one standard deviation.

6.4.3.3. FTIR Analysis of the Composite Coatings

The chemical changes on the surfaces of coated marbles exposed to ambient air were characterized by using FTIR (Figure 6.36-37). Pure calcium carbonate showed a strong band centered around 1453 cm^{-1} and characteristics of the C-O stretching mode of carbonate together with a narrow band around 873 cm^{-1} of the bending mode (Böke et al., 1999). These defined strong bands were observed on the FTIR spectra of the uncoated and neat PLA, PLA/MMT2, PLA/MMT5 and PLA/MMT7 composites coated marbles before outdoor exposures (Figure 6.36).

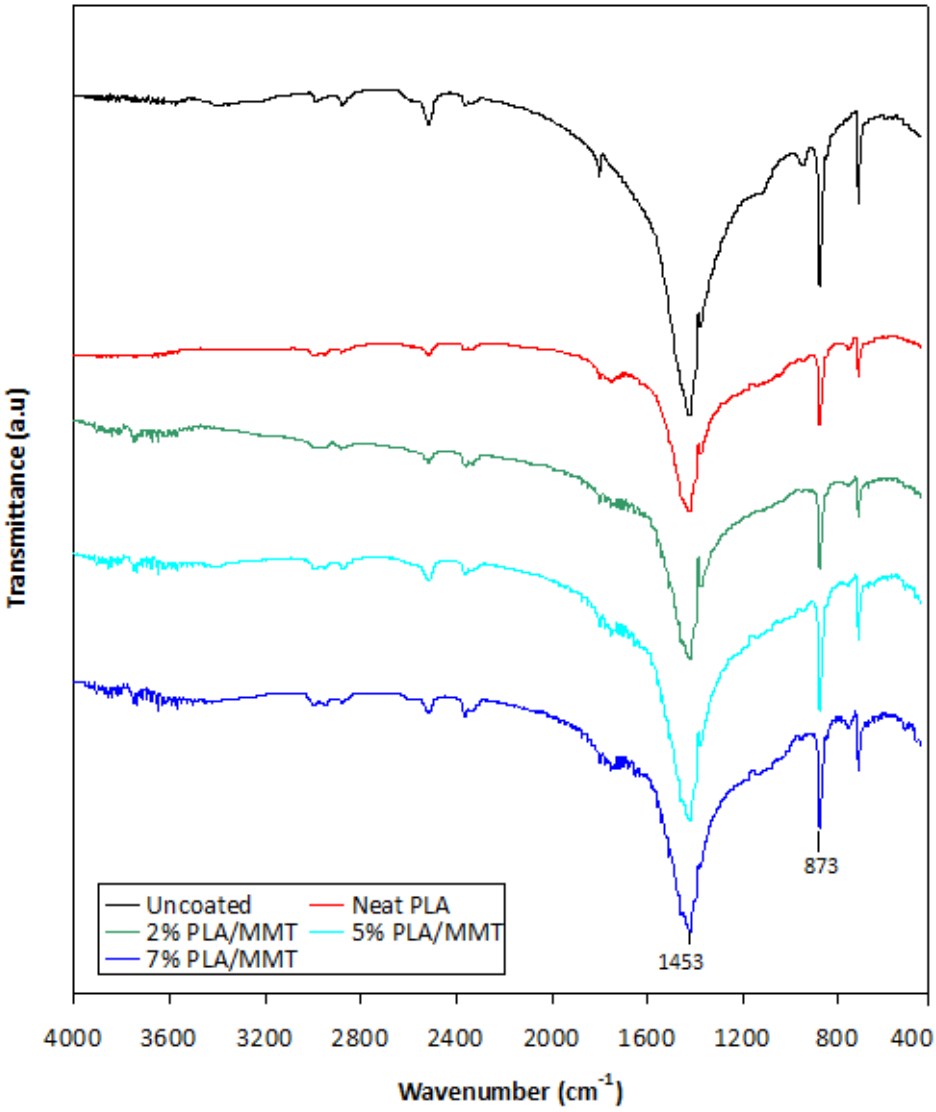

Figure 6.36. FTIR spectra of the uncoated and neat PLA, PLA/MMT2, PLA/MMT5 and PLA/MMT7 composites coated marbles before outdoor exposures.

The calcite strong band centered around 1453 cm^{-1} was observed on the all FTIR spectra of the coated and uncoated marbles after 20 months exposure in ambient city atmosphere. The other observed strong bands centered at the 1146 and 980 cm^{-1} implying that the gypsum and calcium sulfite hemihydrate formations on the coated and uncoated marble surfaces were present. The nitrocalcite peaks also observed on the FTIR spectra of the coated and uncoated marble surfaces at 1051 cm^{-1}.

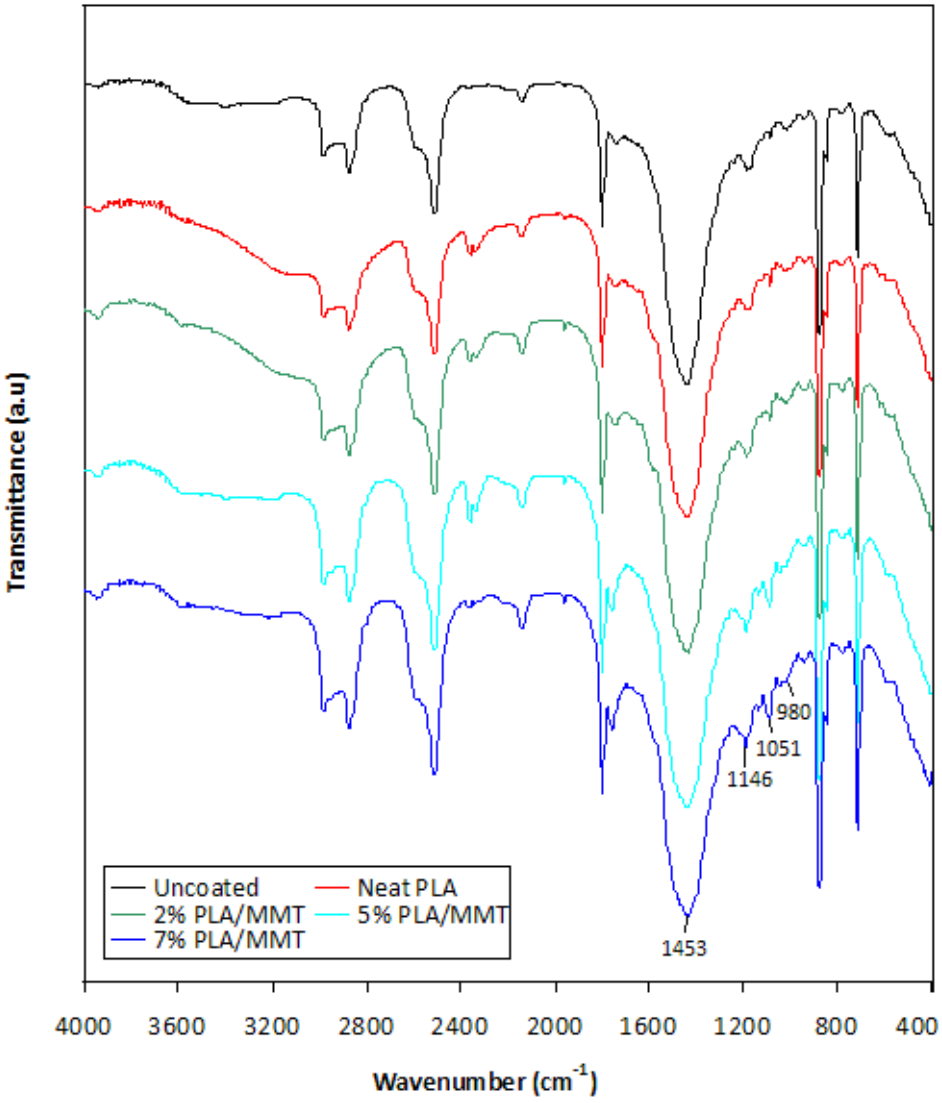

Figure 6.37. FTIR spectra of the uncoated and neat PLA, PLA/MMT2, PLA/MMT5 and PLA/MMT7 composites coated marbles after 20 months outdoor exposures.

CHAPTER 7

CONCLUSION

The protection efficiency of the nanocomposite coatings from acid deposition on marble was investigated in this thesis. The nanoparticle addition increased the protection ability of the coating materials up to optimum amount. The layered silicate clay platelets in the polymer matrix effectively delaminated in PLA/MMT2 and PLA/MMT5. Nanocomposite structure evaluated as exfoliated/highly intercalated according to structural characterizations. Highest stacked layer silicate aspect ratios and more homogenous dispersion were observed on the PLA/MMT5 coated surfaces.

Addition of nanoclays to polymer coatings improved the surface hydrophobicity. Water vapor permeability and water capillary absorption reduced significantly especially for PLA/MMT5 composite in accordance with the increased surface hydrophobicity.

Most of the surfaces kept their original color and defined as clinically acceptable as a result of color alteration test, except for the PLA/MMT7 coatings.

PLA polymer and PLA/MMT2, PLA/MMT5 and PLA/MMT7 bio-nano composites' protection efficiency in a reactor chamber at 8 ppm SO_2 and almost 100 % water vapor presence resulted in a significant reduction of gypsum formation. Neat PLA coating inhibited the gypsum formation of SO_2-calcite reaction approximately 2-3 times in 180 days of exposure. The best protection was obtained on the PLA/MMT5 nanocomposite coated surfaces marble surface in the reaction chamber for the 180 days exposure duration of uncoated and coated marbles. In conjunction with this result before exposure PLA/MMT5 showed good barrier properties for water vapor permeability, and capillary water absorption. PLA/MMT coated surfaces showed significant reductions in crust formation compared to uncoated marble (~5 times). The use of the coatings decreased the kinetic parameters such as kinetic rate constants (k_s) and the internal diffusion (D_e) on the marble surfaces compared to uncoated marbles which showed some extra resistance was created for the surface.

The coating was also showed a good performance, the decrease on the crust thicknesses on coated surfaces were approximately 2-3 times lower for the neat PLA

coated while it was 9-10 times lower for PLA/MMT5 bio-nano composites coated surfaces at the end of 20 months of exposure to ambient air. Similar decreases in the k_s and D_e values were also observed.

PLA/MMT bio-nano composites were observed to be more effective than PLA biodegradable polymer, MMT (Cloisite 10A) nanoparticle addition up to the 5% wt improved protection capabilities of the coatings. Finally, results showed that biodegradable PLA/MMT nanocomposites are promising coating agents, and can be used for the protection of monumental marble surfaces against the detrimental effects of polluted air.

FUTURE RECCOMENDATIONS

Further investigations are needed to analyze the surface morphology of coatings with respect to time for the determination under ageing. Eventhough the degrability of polymer has been researched, In the presence of nanoclay particles in polymer matrix could change the degradation mechanism. Therefore the degradation mechanism under the effect of nanoparticles should be investigated. This information could be used for the estimation of coatings' renewal time as well.

The additive effect of NO_2 in the presence of water and SO_2 should be investigated under the laboratory conditions to observe the combined effect of acidic deposition precursors on the coating material. In addition to high barrier properties it can also allow new coating application on the marble surfaces due to being biodegradable.

REFERENCES

Aas, W.; Shao, M.; Jin, L.; Larssen, T.; Zhao, D.; Xiang, R.; Zhang, J.; Xiao, J.; Duan, L. Air Concentrations and Wet Deposition of Major Inorganic Ions at Five Non-Urban Sites in Chine, 2001-2003 *Atmospheric Environment* **2007**, 41, 1706-1716.

Alexandre M.; Dubois P. Polymer-Layered Silicate Nanocomposites: Preparation, Properties and Uses of a New Class of Materials *Materials Science and Engineering* **2000**, 28, 1-63

Amaroso, G.; Fassina V. Stone Decay and Conservation Elsevier Science Publishers BC, Amsterdam, Netherlands, 1983.

Atlas, R. M.; Chowdhury, A.N.; Gauri, K. L. Microbial Calcification of Gypsum-Rock and Sulfated Marble *Studies in Conservation* **1988**, 33,149- 153.

Ausset, P.; Crovisier, J.L; Monte, M.D.; Furlan, V.; Girardet, F.; Hammecker, C.; Jeannette, D.L. Experimental Study of Limestone and Sandstone Sulphation in Polluted Realistic Conditions: The Lausanne Atmospheric Simulation Chamber (LASC) *Atmospheric Environment* **1996**, 30, 3197- 3207.

Becker, O.; Varley R.; Simon G.; Morphology, Thermal Relaxations and Mechanical Properties of Layered Silicate Nanocomposites Based Upon High-Functionality Epoxy Resins *Polymer* **2002**, 43, 4365–4373

Bernal, J. L. P.; Bello, M. A. Modeling Sulfur Dioxide Deposition on Calcium Carbonate *American Chemical Society* **2003**, 42, 1028-1034.

Bharadwaj RK. Modeling the Barrier Properties of Polymer-Layered Silicate Nanocomposites *Macromolecules* **2001**, 34, 9189–92.

Bhattacharya S. N.; Kamal M. R.; Gupta R. K. *Polymeric Nanocomposites: Theory and Practice* Hanser Gardner Publicaiton, Inc. Chapter 6, 271-274, 2008.

Bird B. R.; Steaward E. W.; Lightwood E. N. *Transport Phenomena*, John Wiley & Sons (Second adition), 513-725, 2007.

Botkin D. B.; Keller E. A. *Environmental science: Earth as a Living Planet*, John Wiley & Sons, Chapter 22, 448-477, 1995.

Böke, H.; Göktürk, H.; Caner – Saltık E.N.; Demirci S. Effect of Airborne Particles on SO_2 – Calcite Reaction *Applied Surface Science* **1999**, 140, 70- 82.

Böke, H.; Göktürk, H.; Caner – Saltık E.N. Effect of Some Surfactants on SO_2-Marble Reaction *Materials Letters* **2002**, 57, 935-939.

Böke, H.; Gauri K.L. Reducing Marble-SO_2 Reaction Rate by the Application of Certain Surfactants *Water, Air and Soil Pollution* **2003**, 142, 59-70.

Bruno M.; Tavares M. I. B. ; Motta L. M. ; Miguez E. ; Preto M. ; Fernandez A. O. R. Evaluation of PHB/Clay Nanocomposite by Spin-Lattice Relaxation Time *Materials Research* **2008**, 11 (4), 483-485

Calik O.; Tihminlioglu F Barrier properties of corn zein nanocomposite coated polypropylene films for food packaging applications *Journal of Food Engineering* **2013**, 114, 505–513

Camargo P. H. C.; Satyanarayana K. G.; Wypych F. Nanocomposites: Synthesis, Structure, Properties and New Application Opportunities *Materials Research* **2009**, 12 (1), 1-39

Chafidz A.; Ali M. A.; Elleithy R. Morphological, Thermal, Rheological, And Mechanical Properties of Polypropylene-Nanoclay Composites Prepared From Masterbatch in a Twin Screw Extruder *J Mater Sci* **2011**, 46, 6075–6086

Chandra R.; Rusthi R., Biodegradable Polymers *Progress in Polymer Science*, **1998**, 23, 1273–1335

Cheng, J.R.; Hwu, R.; Kim, J.T.; Leu, S.M. Deterioration of Marble Structures *Analytical Chemistry* **1987**, 59,104-106.

Chiellini E.; Solaro R. Biodegradable Polymeric Materials *Advanced Materials* **1996**, 8, 305-313

Chiellini E.; Solaro R. Biodegradable Polymers and Plastics, Kluwer Academics, **2003**, 67-73, 185-211

Choudalakis G.; Gotsis A.D. Permeability of Polymer/Clay Nanocomposites: A Review *European Polymer Journal* **2009**, 45, 967–984

Christopher K. Y.; Leung, M.; Hong-Gang Z.; Jang-Kyo K.; Ricky S. C. W. Use of Polymer/Organoclay Nanocomposite Surface Treatment as Water/Ion Barrier for Concrete *Journal of Materıals In Cıvıl Engıneerıng* **2008**, 20, 484-492.

Ciferri O.; Tiano P.; Mastromei G. *Of Microbes And Art-The Role of Microbial Communities in the Degradation and Protection of Cultural Heritage* Kluwer Academic/Plenum Publisher, New York, 232-235, 2000

Cobourn, W.G.; Gauri, K.L.; Tambe, S.; Li, S.; Saltık, E. Laboratory Measurement of Sulphur Dioxide Deposition Velocity on Marble and Dolomite Stone Surfaces *Atmospheric Environment* **1993**, 27 B (2), 193-201.

Corvo, F.; Reyes, J.; Pérez, T.; Castañeda, A. Role of NOx in Materials Corrosion And Degradation" *Revista CENIC. Ciencias Químicas*, 2010, 41, 1-10

D'Arienzo L.; Scarfato P.; Incarnato L. New Polymeric Nanocomposites For Improving The Protective and Consolidating Efficiency of Tuff Stone" Journal of Cultural Heritage **2008**, 9, 253-260.

Daly, A.; Zannetti P. *An Introduction to Air Pollution – Definitions, Classifications, and History.* Chapter 1 *of AMBIENT AIR*. Published by The Arab School for Science and Technology (ASST), 2007.

Dorgan, J. R.; Lehermeier, H. J.; Palade, L.I.; Cicero, J. Polylactides: Properties and Prospects of an Environmentally Benign Plastic form Renewable Resources *Macromol. Symp.* 2001. 175, 55-66.

Elbir T.; Bayram A.; Kara M.; Altıok H.; Seyfioğlu R.; Ergün P.; Şimşir S. Determination of the Air Pollution From Road Transport In The City Center of Izmir *DEÜ Mühendislik Fakültesi Mühendislik Bilimleri Dergisi* **2010**, 12 (1), 1-17

Elbir T; Muezzinoglu A. Estimation of Emission Strengths of Primary Air Pollutants In the City Of Izmir, Turkey. Atmos Environ **2004**, 38, 1851–7.

Elfving, P.; Johannson, L.G.; Lindquist A Study of the Sulphation of Silane- Treated Sandstone Studies *in Conservation* **1994**, 39, 199-209.

Erk H. F.; Dudukovic M. P. Self-Inhibited Rate in Gas-Solid Noncatalytic Reactions. The Shrinking Core Model *Ind. Eng. Chem. Fundam* **1984**, 23, 49-54.

Ferri L.; Lottici P. P.; Lorenzic A.; Monteneroc A.; Mariani S. Study of Silica Nanoparticles – Polysiloxane Hydrophobic Treatments for Stone-Based Monument Protection *Journal of Cultural Heritage* **2011**, 12, 356–363

Fogler S. H. *Elements of Chemical Reaction Engineering* Prentice Hall; 4th edition, 757-812, 2005.

Finlayson-Pitt B.J.; Pitt Jr. J.N. *Atmospheric Chemistry: Fundamentals and Experimental Techniques* John Wiley and Sons, New York, 1986

Garland, J.A. Dry and Wet Removal of Sulphur from the Atmosphere, *Atmospheric Environment* **1978**, 9, 661-672.

Gauri, K.L.; Doderer, G.C.; Limscomp, N.T.; Sarma, A.C. Reactivity of Treated and Untreated Marble Specimens in SO_2 Atmosphere, *Studies in Conservation* **1973**, 18, 25-35.

Gauri, K.L.; Popli, R.; Sarma, A.C. Effect of Relative Humidity and Grain Size on the Reaction Rates of Marble at High Concentration of SO_2 *Durability of Building Materials* **1982/1983**, 1, 209-216.

Gauri, K.L.; Gwinn, J.A. Deterioration of Marble in Air Containing 5- 10 ppm SO_2 and NO_2 *Durability of Building Materials* **1982/1983**, 1, 217-223.

Gauri, K.L.; Kulshreshtha, N.P.; Punuru, A.R.; Chowdhury, A. Rate of Decay of Marble in Laboratory and Outdoor Exposure *Journal of Materials in Civil Engineering* **1989**, 1, 73-83.

Gauri, K.L.; Bandyopadhyay J.K. *Carbonate Stone, Chemical Behavior, Durability and Conservation*, (JohnWiley & Sons, New York), 125-157, 212- 237, 1999

Gooch J. W. *Encyclopedic Dictionary of Polymers*, 2nd edition, Springer, 563-564, 2010.

Grontorft, T.; Raychaudhuri, M. R. Compilation of tables of surface deposition velocities for O_3, NO_2 and SO_2 to a range of indoor surfaces *Atmospheric Environment* **2004**, 533–544

Grossi, C.M.; Murray M. Characteristic of Carbonate Building Stones That Influence the Dry Deposition of Acidic Gases *Construction and Building Materials* **1999**, 13, 101-108.

Guzman A.; Gnutek N.; Janik H. Biodegradable Polymers For Food Packagıng – Factors Influencıng Theır Degradatıon And Certıfıcatıon Types – A Comprehensıve Revıew *Chemical Technology* **2011**, 5, No. 1, pp: 115-122

Ha S. R.; Ryu S. H.; Park S. J.; Rhee K. Y. Effect of Clay Surface Modification And Concentration of the Tensile Performance of Clay/Epoxy Nanocomposites *Materials Science and Engineering* **2007**, 458, 264-268.

Harintharavimal B.; Azman H.; Mat U. W.; Yussuf A.A.; Shamsul B. A. R. Novel Toughened Polylactic Acid Nanocomposite: Mechanical, Thermal and Morphological Properties *Materials and Design* **2010**, 31, 3289–3298.

Haneef S.J.; Johnson J. B.; Dickinson C.; Thompson G. E.; Wood G.C. Effect of Dry Deposition on NO_x and SO_2 Gaseous Pollutants on the Degradation of Calcareous Building Stones *Atmospheric Environment* **1992**, 26A (16), 2963–2974.

Haugaard K. H.; Udsen A. M.; Mortensen. G.; Hoegh L.; Petersen K.; Monahan F. Potential Food Application of Biobased Materials. An EU-Concerted Action Project *Starch/Starke*, **2001**, 189-200

Incropera F.P.; DeWitt D. P. *Heat and Mass Transfer*. John Wiley & Sons (5th edition). 386-464, 2002.

Izmir Metropolitan Municipality - The Environmental Protection and Control Department (EPCD), 70779648-611.03/461/20556, 2013

Johansson, L.G.; Lindquist, O.; Mangio, R.E. Corrosion of Calcareous Stones in Humid Air Containing SO_2 and NO_2 *Durability of Building Materials* **1988**, 5, 439-449.

Johnson J. B.; Haneef S. J.; Hepburn B. J.; Hutchınson A. J.; Thompson G. E.; Wood G. C. Laboratory Exposure Systems to Simulate Atmospheric Degradation of Building Stone Under Dry and Wet Deposition Conditions *Atmospheric Environment* **1990**, 24A. (10), 2585-2592

Jong-Whan R.; Seok-In H.; Chang-Sik H. Tensile, water vapor barrier and antimicrobial properties of PLA/nanoclay composite film *Food Science and Technology* 2009, 42, 612–617.

Judeikis H. S.; Stewart T. B. 1976. Laboratory Measurement of SO_2 Deposition Velocities on Selected Building Materials and Soils *Atmospherin Environment.* **1976**, 10, 769-116.

Ke Y.C.; Stroeve P. *Polymer-Layered Silicate and Silica Nanocomposites* Elsevier B. V., Chapter 1, 1-67, 2005

Kim, S.; Maeda Y.; Tsujino Y. Assessment of the Effect of Air Pollution on Material Damages in Northeast Asia *Atmospheric Environment*, 2004. 38, 37-48.

Koh H. C.; Park J. S.; Jeong M. A.; Hwang H. Y.; Hong Y. T.; Ha S. Y.; Nam S. Y. Preparation and Gas Permeation Properties of Biodegradable Polymer/Layered Silicate Nanocomposite Membranes *Desalination* **2008**, 233, 201–209

Koo J. H. *Polymer Nanocomposites: Processing, Characterization, and Apllications* McGraw-Hill, New York, 2006

Kreindl J.; Hager W. *Air quality Data in 2010 The Comparison of Cities and Regions in Europe* publisher: MUNICIPALITY OF LINZ Department "Environmental and Technical Center" Report Nr. 2/2011, 2011

Kucera V. Fitz S. Direct and Indirect Air Pollution Effects on Materials Including Cultural Monument *Water, Air and Soil Pollution* **1995**, 85, 153-165

Kulshreshtha N.P.; Punuru A.R.; Gauri K.L. Kinetics of Reaction of SO_2 with Marble *Journal materials in Civil Engineering* 1989, 1, 60-72.

Kumar M. S.; Mohanty S.K.; Nayak S.K.; Rahail P. M. Effect of Glycidyl Methacrylate (Gma) on the Thermal, Mechanical and Morphological Property of Biodegradable Pla/Pbat Blend and Its Nanocomposites *Bioresour. Technology*, **2010**. 101, 8406-8415

Kumar S. K.; Krishnamoorti R. Nanocomposites: Structure, Phase Behavior, and Properties *Annu. Rev. Chem. Biomol. Eng.*, **2009**, 1, 37–58

Lim L. T.; Auras R.; Rubino M. Processing Technologies for Poly(lactic acid) *Progress in Polymer Science* **2008**, 33, 820–852.

Liu T.X.; Liu Z.H.; Ma K.X.; Shen L.; Zeng K.Y.; He C.B. Morphology, Thermal and Mechanical Behavior of Polyamide 6/Layered-Silicate Nanocomposites *Composites Science and Technology* **2003**, 63, 331–337

Luckachan G.; Pillai, C. Biodegradable Polymers- A Review on Recent Trends and Emerging Perspectives *Journal of Polymers and the Environment* **2011**, 19, (3), 637-676

Levenspiel O. *Chemical Reaction Engineering* (3rd Edition), John Wiley & Sons, 1999

Malwela T.; Ray S. S. Study of morphology and crystal growth behaviour of nanoclay-containing biodegradable polymer blend thin films using atomic force microscopy *Polymer* **2012**, 53, 2705-2716

Manoudis P.; Papadopoulou S.; Karapanagiotis I.; Tsakalof A.; Zuburtikudis I.; Panayiotou C. Polymer Silica Nanoparticles Composite Films as Protective Coatings for Stone-Based Monumants *Journal of Physics: Conference Series* **2007**, 61, 1361-1365.

Manoudis P.; Tsakalof A.; Karapanagiotis I.; Zuburtikudis I.; Panayiotou C. Fabrication of super-hydrophobic surfaces for enhanced stone protection *Surface and Coatings Technology*, **2009**, 203, 1322-1328.

McMahon T. A.; Denison P. J. Emprical Atmospheric Deposition Parameters- A Survey *Atmospheric Environment* **1979**, 13, 571-585.

Mittal V. *Optimization of Polymer Nanocomposite Properties* WILEY-VCH Verlag GmbH & Co. 1-418, 2010

Muezzinoglu, A.; Elbir, T.; Bayram, A. Air Quality Management In Izmir Region of Turkey As Required By Clean Air Plans *Water, Air, and Soil Pollution: Focus*, **2003**. 3, 307–323.

Nair L. S.; Laurencin C. T. Polymers as Biomaterials for Tissue Engineering and Controlled Drug Delivery *Adv Biochem Engin/Biotechnol* **2006**, 102, 47–90

Nampoothiri K. M.; Nair N. R.; John R. P. An overview of the recent developments in polylactide (PLA) research *Bioresource Technology* **2010**, 101 (22), 8493–8501

Nho-Kim. E. Y.; Michou M.; Peuch V-H. Parameterization of size-dependent particle drydeposition velocities for global modeling *Atmospheric Environment* **2004**, 38, 1933–1942

Nord A.G.; Holenyi K. Sulphur Deposition and Damage on Limestone and Sandstone in Stockholm City Buildings *Water, air and soil pollution* **1999**, 109, 147-162.

Ocak Y.; Sofuoglu A.; Tihminlioglu F.; Boke H. Protection of marble surfaces by using biodegradable polymers as coating agent, *Progress in Organic Coatings* **2009**, 66, 3, 213-220.

Odabaşı M.; Bayram A.; Müezzinoğlu A.; Sofuoğlu A.; Sofuoğlu C. S.; Duman Y. İzmir Atmosferinde Yüzey Ozon Seviyelerinin İncelenmesi Project Number: 104Y163, TUBITAK, 2008

Ogata N.; Jimenez G.; Kawai H.; Ogihara T. Structure and thermal/mechanical properties of poly(*l*-lactide)-clay blend *Journal of Polymer Science Part B: Polymer Physics* **1997**, 35 (2), 389–396

Olad A. *Polymer/Clay Nanocomposites, Advances in Diverse Industrial Applications of Nanocomposites* 113-138, Dr. Boreddy Reddy (Ed.), 2011 (ISBN: 978-953-307-202-9) InTech, Available from: http://www.intechopen.com/books/advances-in-diverse-industrial-applications-ofnanocomposites/polymerclay-nanocomposites [accessed: 10.05.2013]

Park H. M.; Liang X.; Mohanty A. K.; Misra M.; Drzal L.T. Effect of Compatibilizer on Nanostructure of the Biodegradable Cellulose Acetate/Organoclay Nanocomposites *Macromolecules* **2004,** *37*, 9076-9082

Pavlidou S.; Papaspyrides C. D., A Review on Polymer–Layered Silicate Nanocomposites *Progress in Polymer Science* **2008**, 33, 1119–1198

Pedrazzani P.; Alessandri I.; Bontempi E.; Cappitelli F.; Cianci M.; Pantos E.; Toniolo L.; Depero L. E. Study of sulphation of Candoglia marble by means of micro X-ray diffraction experiments *Appl. Phys*. **2006**, A 83, 689–694

Pérez-Alonso M.; Castro K.; Álvarez M.; Madariaga J.M. Scientific analysis versus restorer's expertise for diagnosis prior to a restoration process: the case of Santa Maria Church (Hermo, Asturias, North of Spain) *Analytica Chimica Acta* **2004**, 524 (1-2), 379-389.

Peruzzi R.; Poli T.; Toniolo L. The Experimental Test for the Evaluation of Protective Treatments: a Critical Survey of the "Capillary Absorption Index" *Journal of Cultural Heritage* **2003**, 4, 251–254

Philip S.; Keshavarz T.; Roy I, Review Polyhydroxyalkanoates: biodegradable polymers with a range of applications *J Chem Technol Biotechnol* **2007**, 82, 233–247

Pope G.A.; Meierding T.C.; Paradise T.R. Geomorphology's Role in the Study of Weathering of Cultural Stone *Geomorphology* **2002**, 47, 211-225.

Ray S. S.; Okamato M. Polymer-layered silicate nanocomposites a review from preparation *Prog. Polym. Sci.* **2003**, 28, 1539–1641

Ray S. S.; Yamada K.; Okamato M.; Ueda K. Polylactide-Layered Silicate Nanocomposite: A Novel Biodegradable Material *Nano Letters* **2002**, 2 (10), 1093-1096

Rhim J. W.; Hong S. I.; Ha C. S. Tensile, water vapor barrier and antimicrobial properties of PLA/nanoclay composite films *LWT - Food Science and Technology* **2009** 42, 612–617

Scarfato P.; Maio L. D.; Fariello M. L.; Russo P.; Incarnato L. Preparation and evaluation of polymer/clay nanocomposite surface treatments for concrete durability enhancement *Cement & Concrete Composites* **2012**, 34, 297–305

Sehmel G. A. Partıcle and Gas Dry Deposıtıon: A Review *Atmospheric Environment*, **1980**, 14, 983-1011.

Seinfeld J. H. *Atmospheric Chemistry and Physics of Air Pollution* John Wiley and Sons, New York, 1986

Sharma S.K.; Nayak S.K. Surface Modified Clay/Polypropylene (PP) Nanocomposites: Effect on Physico-Mechanical, Thermal and Morphological Properties *Polymer Degradation and Stability* **2009**, 94, 132–138

Shen L.; Haufe J.; Patel M. K. Product overview and market projection of emerging bio-based plastics, PRO-BIP Report 2009, *European Bioplastics* **2009**, 1-191, http://www.plastice.org/fileadmin/files/PROBIP2009_Final_June_2009.pdf [accessed: 10.05.2013]

Shen Z.; Simon G. P.; Cheng Y. B. Comparison of solution intercalation and melt intercalation of polymer-clay nanocomposites *Polymer* **2002**, 43, 4251-4260

Shogren R. Water Vapor Permeability of Biodegradable Polymer Journal of Environmental Polymer Degradation **1997**, 5 (2), 91-95

Siegesmund S.; Snethlage R. *Stone in Architecture Properties Durability* Springer-Verlag Berlin Heidelberg. 4th Edition, pp: 122-126, 2011.

Siracusa V.; Rocculi P.; Romani S.; Rosa M.D. Biodegradable polymers for food packaging: a review *Trends in Food Science & Technology* **2008**, 19, 634-643

Skoulikidis T.N.; Beloyannis N. Inversion of Marble Sulfation – Reconversion of Gypsum Films into Calcite on the Surfaces of Monuments and Statues *Studies in Conservation* **1984**. 29, 1733-1743.

Spiker E.C.; Hosker R.P.; Comer V.J.; White J.R.; Werre R.W.; Harmon F.L.; Gandy G.D.; Sherwood, S.I. Environmental Chamber for Study of the Deposition Flux of Gaseous Pollutants to Material Surfaces *Atmospheric Environment* **1992**. 26 A (16), 2885-2892.

Špírková M.; Pavlic˘evic´ J.; Strachota A.; Poreba R.; Bera O.; Kaprálková L.; Baldrian J.; Šlouf M.; Lazic N.; Budinski-Simendic J. Novel polycarbonate-based polyurethane elastomers: Composition–property relationship *European Polymer Journal* **2011**, 47, 959–972

Södengard A,; Stolt M. Properties of Lactic Acid Based Polymers and Their Correlation with Composition *Progress in Polymer Science* **2002**, 27, 1123- 1163.

Striegel M.F.; Guin E.B.; Hallett K.; Sandoval D.; Swingle R.; Knox K.; Best F.; Fornea S. Coatings, and Cultural Resources *Progress in Organic Coatings* 2003, 48, 281-288.

Su C.; Li J.; Geng H.; Wang Q.; Chen Q. Fabrication of an Optically Transparent Super-Hydrophobic Surface via Embedding Nano-Silica *Applied Surface Science*, **2006**, 253, 2633–2636.

Sperling L. H. *Introduction to Physical Polymer Science* 4th edition, John Wiley & sons, Inc., Hoboken, New Jersey, 1-28, 2006.

Ta W.; Wei C.; Chen, F. Long-term Measurements of SO_2 Dry Deposition over Gansu Province, Chine, *Atmospheric Environment* **2005**, 39, 7095-7105.

Tabatabaei S. H.; Ajji A. Structure-orientation-properties relationships for polypropylene nanoclay composite films *Journal of Plastic Film & Sheeting* **2011**, 27, 87–115

Tambe S.; Gauri K. L.; Li S.; Cobourn W. G. Kinetic Study of SO_2 Reaction with Dolomite *Environ. Sci. Technol* **1991**, 25, 2071-2075.

Tambe S.; Yerrapragada S. S.; Gauri K. L. Kınetıcs of SO_2-Dolomite Reaction: Application of Random Pore Model *Journal of Materials in Civil Engineering* **1994**, 6, (1), 65-77

Thompson M.; Shelley J.; Compton R.G.; Viles H.A. Polymer Coatings to Passivate Calcite from Acid Attack: Polyacrylic Acid and Polyacrylonitrile Jounal *of Colloidal Interface Science* **2003**, 260, 204-210.

Toniolo L.; Poli T.; Castelvetro V.; Manariti A.; Chiantore O.; Lazzari M. tailoring New Fluorinated Acrylic Copolymers as Protective Coatings for Marble *Journal of Cultural Heritage* **2002**, 3, 309–316

Torfs K.; Grieken R.V. Chemical Relations between Atmospheric Aerosols, Deposition and Stone Decay Layers on Historic Buildings at the Mediterranen Coast *Atmospheric Environment* **1997**, 31 (15), 2179-2192.

Turkiye İstatistik Kurumu (TUIK), Çevre İstatistikleri Sorularla Resmi İstaitistikler Dizisi-8, **2009**, Yayın no: 3257, ISBN: 978-975-19-4508-2. Available: http://www.tuik.gov.tr/Kitap.do?metod=KitapDetay&KT_ID=18&KITAP_ID=203 [accessed: 10.05.2013]

Türkiye Çevre Durum Raporu (TCDR) / **2011**, Yayın no: 11, ISBN: 978-605-5294-01-4. Available: http://www.csb.gov.tr/turkce/dosya/ced/TCDR_2011.pdf [accessed: 10.05.2013]

U. S. Environmental Protection Agency, Air Quality Index, A Guide to Air Quality and Your Health, 2000. Available: http://www.miamidade.gov/development/library/brochures/air-quality-index.pdf [accessed: 10.05.2013]

Ulery B. D.; Nair L. S.; Laurencin C. T. Biomedical Applications of Biodegradable Polymers *Journal Of Polymer Science Part B: Polymer Physics* **2011** 49, 832–864

Yerrapragada S. S.; Jaynes J. H.; Chirra S. R.; Gauri K. L. Rate of Weathering of Marble due to Dry Deposition of Ambient Sulfur and Nitrogen Dioxide *Anal. Chem.* **1994**, 66, 655-659

Yerrapragada S. S.; Chirra S. R.; Jaynes J. H.; Bandyopadhyay J. K.; Gauri K. L. Weathering Rates of Marble In Laboratory and Outdoor Conditions Journal of Environmental Engineering, **1996**, 122, 856-863.

Zanetti M.; Lomakin S.; Camino G. Polymer Layered Silicate Nanocomposites, *Macromolecular Material and Engineering* **2000**, 279, 1-9.

Żenkiewicza, M.; Richert, J. Permeability of Polylactide Nanocomposite Films for Water Vapour, Oxygen and Carbon Dioxide, *Polymer Testing*, **2008**, 27:7, 835-840

Zhang S.; Sun D.; Fu Y.; Du H. Recent advances of superhard nanocomposite coatings: a review *Surface and Coatings Technology*, **2003**, 167, 113–119

Zielecka M.; Bujnowska E. Silicone-containing polymer matrices as protective coatings: Properties and applications *Progress in Organic Coatings*, **2006**, 55, 160-167

Xie S.; Qi L.; Zhou D. Investigation of the Effects of Acid rain on the Deterioration of Cement Concrete Using Accelerated Tests Established in Laboratory *Atmospheric Environment* **2004**, 38, 4457-4466.

Xu L. C.; Siedlecki C. A. Effects of Surface Wettability and Contact Time on Protein Adhesion to Biomaterial Surfaces *Biomaterials* **2007**, 28(22), 3273-3283

Vichi A.; Ferraria M.; Davidson C. L. Color and Opacity Variations in Three Different Resin-Based Composite Products after Water Aging *Dental Materials* **2004**, 20, 530–534

Wanga J.; Li L., Liu Z.; Wang R. Nano-Composite Materials Studied by CTEM and STEM *Solid State Phenomena* **2007**, 121-12, 991-994

Weber J.C. Biobased Packaging Materials for the Food Industry: Status and Prospectives (KVL). **2000**, pp. 1-136.

Weber C.J.; Haugaard V.; Festersen R.; Bertelsen G. Production and Applications of Biobased Packaging Materials for the Food Industry *Food Additives and Contaminants*. **2002**. 19, 172-177.

Wesely M. L.; Hicks B. B. A Review of the Current Status of Knowledge on Dry Deposition *Atmospheric Environment* **2000** 34, 2261-2282

VITA

YILMAZ OCAK

Date of Birth: 20.03.1980

Place of Birth: Turkey

Citizenship: Turkish

EDUCATION

[1998-2002] B.Sc. (Environmental Engineering)

Süleyman Demirel University

Department of Environmental Engineering, Isparta, Turkey

Dissertation: Principles, modeling and design of the biological wastewater treatment systems

[2004-2007] M.Sc. (Environmental Engineering)

İzmir Institute of Technology

Department of Environmental Engineering, Izmir, Turkey

Dissertation: Protection of the Marble Monument Surfaces by Using Biodegradable Polymers

[2007-2013] Ph.D. (Chemical engineering)

İzmir Institute of Technology

Department of Chemical Engineering, Izmir, Turkey

Dissertation: Use of Bio-Nano Composites as Protective Coating on Natural Stone Surfaces

PUBLICATIONS

Ocak Y.; Kılıçvuran A.; Eren A. B.; Sofuoglu A.; Sofuoglu S. C. Exposure to Particulate Matter in a Mosque *Atmospheric Environment* **2012**, 56, 169-176.

Ocak Y.; Sofuoglu A.; Tihminlioglu F.; Böke H. Protection of marble surfaces by using biodegradable polymers as coating agent *Progress in Organic Coatings* **2009**, 66, 213-220.

Cansever B.; Seyhan A.T.; **Ocak Y.**; Tanoğlu M.; Balköse D.; Ülkü S. Cure Kinetics of Epoxy Resin-Natural Zeolite Composites *Journal of Thermal analysis and Calorimetry* 2008, 94, 43-747.